A MOVING BOUNDARY APPROACH FOR CYLINDERS SUBJECTED TO HIGH INTERNAL PRESSURE

WEI ZHAO

A MOVING BOUNDARY APPROACH FOR CYLINDERS SUBJECTED TO HIGH INTERNAL PRESSURE

BY

WEI ZHAO, B. ENG. M. ENG.

A DISSERTATION SUBMITTED TO THE SCHOOL OF GRADUATE STUDIES IN PARTIAL FULFILLMENT OF THE REQUIREMENTS FOR THE DEGREE OF DOCTOR OF PHILOSOPHY

FACULTY OF ENGINEERING AND APPLIED SCIENCE

MEMORIAL UNIVERSITY OF NEWFOUNDLAND

ST. JOHN'S, NEWFOUNDLAND, CANADA,

AUGUST 2003

ABSTRACT

This dissertation proposes a novel analytical approach for elastic plastic analysis of thick wall cylinders under internal pressure. It involves two parametric functions and piecewise linearization of the stress strain curve. A deformation type of relationship is combined with Hooke's law in such a way that stress strain law has the same form in all linear segments of the material curve, but each segment involves different material parameters.

This approach incorporates the deformed geometry in elastic plastic analysis of thick wall cylinders. Using an iterative procedure based on the principle of virtual work, this approach accounts for the effect of deformed geometry due to high internal pressure. The resulting analytical formulation is capable of predicting stress, strain, displacement, and energy on a moving boundary basis.

The analytical formulation for autofrettaged cylinders obeying work hardening material behavior has also been presented. An iterative implementation procedure for shakedown pressure calculation has been developed. Shakedown pressures have been calculated for both undeformed geometry and deformed geometry. The proposed formulation has also been applied to plastic collapse load estimation. Calculations indicate that the moving boundary approach provides conservative plastic collapse load estimation compared with the traditional small deformation theory.

This moving boundary approach is appropriate for inelastic analysis including autofrettage, shakedown, and limit analysis on thick wall cylinders. The comparison of the analytical formulation with the ANSYS inelastic finite element analysis is favorable.

The effect of deformed geometry on inelastic analysis has been assessed on thick wall cylinders subject to high internal pressure. The discrepancy of results between the proposed method and small deformation theory has been analyzed. Calculation indicates that the difference of energy is significant for high internal pressures.

The J integral of thick wall cylinders with circumferential flaw has been evaluated using the ANSYS finite element program. The result indicates a significant difference between the analysis using large deformation and small deformation theories. This difference depends on the magnitudes of the internal pressure, and is dependent on the material behavior. It indicates that neglecting the difference can be unconservative when evaluating the inelastic fracture parameter, J integral. Therefore the proposed approach is appropriate for representing energy of deformation in the energy approach in fracture mechanics, as it incorporates the effect of geometric change due to high internal pressures.

As the analytical approach can be implemented by MAPLE program, this method represents an alternative assessment tool that can be used for inelastic analysis of thick wall cylinders, which is usually performed by the more expensive and elaborate nonlinear finite element analysis.

ACKNOWLEDGEMENT

First, the author wishes to express his sincere gratitude to his supervisor, Dr. R. Seshadri, for the source of knowledge, guidance and support in the course of his doctoral program. This dissertation would not have been possible without his expertise and insights.

The author is especially grateful to Dr. R. N. Dubey of University of Waterloo, for the extensive and insightful discussion and direction, hospitality, and conference travel sponsoring.

The author would also acknowledge the members of his supervisory committee, Dr. S. Adluri and Dr. K. Munaswamy, for their helpful comments and advice.

The financial support provided by Memorial University of Newfoundland, Faculty of Engineering and Applied Science, School of Graduate Studies, and Dr. Seshadri's research grant, is gratefully acknowledged.

Finally, the author wants to thank his wife, Jianping Cui, who has raised their child alone while the author could focus on this research work. Deep appreciation goes to her, for her love, support, and patience.

DEDICATION

This dissertation is dedicated to

my wife

Jianping Cui

and my son

Dylan Boyang Zhao

TABLE OF CONTENTS

LIST OF FIGURES

LIST OF TABLES

NOMENCLATURE

A	Crack area
E	Young's modulus
E_k	Tangent modulus in domain k
E_p	Plastic modulus
f, g	Parametric functions
G	Energy release rate
J	J integral
P_n	Internal pressure
P_S	Shakedown pressure
r	Radius of deformed geometry
R	Radius of initial geometry
r_1	Radius of elastic plastic interface
r_{k-1}	Radius of interface of domains k and k-1
r_n	Inside radius of cylinder
r_o	Outside radius of cylinder
U	Strain energy

U_0	Strain energy density
W	Work done by external force
W_S	Surface energy of the material
ε	Uniaxial strain
ε_{ij}	Total strain tensor
$\varepsilon_{ij}^{k\,oe}$	Tensor of overestimated strain in *kth* domain
ε_{ij}^{oe}	Total overestimated strain tensor
ν	Poisson's ratio
ν_k	Poisson's ratio of domain *k*
ν_p	Poisson's ratio of plastic region
σ	Uniaxial stress
σ_{ij}	Stress tensor
σ'_{ij}	Deviatoric stress tensor
$\sigma_{r,res}$	Residual radial stress
$\sigma_{\theta,res}$	Residual hoop stress
σ_Y	Yield stress
Π	Potential energy

1. INTRODUCTION

Advances in high pressure technology were largely based on the theoretical understanding of the behavior of a pressurized thick wall cylinder since an obvious structural shape to contain high pressure is the thick wall cylinder.

For several centuries, the military cannon was the only significant application of high pressure technology in which pressure is contained by a cylindrical vessel. Little was known of the stress analysis in cylindrical vessels until 1833, when Lame derived the elastic stress distribution in a thick wall cylinder, and made it possible to understand the strength of high pressure vessels. Since then, efforts have been continually made to increase the analysis sophistication and accuracy of high pressure cylindrical vessels, which are now being extensively used in chemical, petrochemical, and food sterilizing industries.

The design of high pressure cylindrical vessels usually requires elastic plastic analysis. For example, the pre-loads induced residual stress needs to be determined by elastic plastic analysis. Compressive residual stresses in many applications such as autofrettage, not only increase the pressure or load bearing capacity of the component, but also enhance the component's fatigue life. The presence of these beneficial residual stresses reduces the probability of crack initiation and retards the growth of fatigue cracks. Reliable prediction of the influence of residual stresses on the critical crack length and fatigue life of the components requires an accurate prediction of the actual residual stress

field in the component. It is therefore essential to develop accurate and reliable methods to calculate residual stresses induced by pre-loads. Inelastic analyses, which are less sophisticated, more understandable, and easy to implement but still accurate, have been realized by more and more practicing engineers and researchers (Seshadri 1994, Jahed and Dubey 1997).

1.1 INELASTIC ANALYSIS BASED ON LINEAR ELASTIC SOLUTIONS

The traditional method of analyzing the structural integrity of high pressure vessels is the use of closed form solutions, which are typically valid for the elastic materials. To describe the elastic plastic behavior, however, theory of plasticity is required. In general, the theory of plasticity has not been completely exploited by practicing engineers. Usually it takes considerable effort to understand and implement the analytical techniques for plastic analysis (Jahed 1997).

Numerical method provides an alternative technique to perform plastic analysis. Among various numerical techniques, the nonlinear finite element method is an inelastic analysis technique that has been well developed and widely used. Nonlinear finite element analysis (NLFEA) is an incremental or iterative computational method to solve nonlinear problems by relating small changes of load with small changes of displacements. However, the iterative process of nonlinear FEA requires high-end computer resources to handle relatively large load and sub-load increments, thus makes the procedure often elaborate, expensive, and time consuming. Besides, the merit of applying detailed

nonlinear FEA for a given problem is sometimes questionable due to convergence problems and requirement of results interpretation knowledge.

In view of the limitations of the prevailing methods, it has increasingly attracted research attentions to develop alternative or simplified methods of inelastic analysis based on linear elastic analysis. These methods provide simpler techniques to approximate the elastic plastic behavior of components and therefore are attractive to practicing engineers. In recent years, considerable research efforts have been directed to this direction and a number of methods have been well established and applied successfully to a wide range of engineering problems (Seshadri 1991, Mackenzie and Boyle 1993).

1.2 MOTIVATIONS AND OBJECTIVES

In general, current simplified inelastic methods rely on the supplement of numerical procedures, which are typically implemented by linear FEA to simulate nonlinear FEA. It has been noticed that inadequate research effort has been directed to the analytical perspective for simplified inelastic method without recourse to FEA based methods. Actually, simplified inelastic method in the analytical form can be more convenient to provide insights into some aspects of the behavior than numerical methods. Therefore, the major motivation of this research is to develop a simplified inelastic method in the analytical perspective, which will largely reduce the excessive dependence on extensive and expensive computer resources and commercial FEA software. Another motivation for this research is that the current analytical inelastic approaches rarely account for the

effect of geometric change for cylindrical vessels subject to high pressure, which may make pronounced difference in inelastic analysis.

Firstly, the objective of this dissertation is to establish a simplified inelastic method for high pressure cylindrical vessels in an analytical perspective. This method should be appropriate for inelastic analysis by predicting the stress, strain and displacement based on linear elastic solutions. It should also be capable of predicting mechanically induced residual stress, strain and displacement fields. Unlike conventional methods, this method should be able to employ the concept of piecewise linearization to approximate the actual material stress strain curve. The proposed method will then be applied to problems involving autofrettage, shakedown, and collapse load estimation.

Secondly, the proposed method accounts for the effect of moving boundary. The boundary value problems are formulated in terms of deformed geometry. A procedure is developed that helps evaluate the deformed geometry as an integral part of the solutions. The effect of deformed geometry to inelastic solutions is investigated.

1.3 OUTLINE AND CONTRIBUTIONS

The dissertation consists of eight chapters. The current chapter discusses the problem definition, motivation, and objectives. The fundamental concepts and theories that are related to the proposed research are reviewed in chapter 2. The literature related to simplified inelastic method based on linear elastic solutions is reviewed in chapter 3. A

general introduction in the topic of high pressure technology including various theories of elastic plastic analysis for pressurized thick wall cylinders is also given in chapter 3.

The moving boundary approach for elastic plastic analysis, which is an analytical method for carrying out inelastic analysis based on elastic solutions, is proposed in chapter 4. A generalized method for axisymmetric analysis on thick wall cylinders subjected to high internal pressure is formulated based on the piecewise linearization concept. The deformed geometry is incorporated in the formulation by using an iterative procedure based on the virtual work principle. Then the proposed formulation is applied to cylinders for various dimensions in the evaluations of stress, strain, displacement, and energy of deformation. Results are obtained to assess the effects of geometric change and compared with finite element analysis implemented by the ANSYS finite element program.

An analytical formulation for autofrettage cylinders obeying work hardening stress strain law is proposed in chapter 5. The Bauschinger effect is included in the analysis for kinematic work hardening material. Analytical solutions based on deformed geometry are obtained and compared with the ANSYS nonlinear finite element analysis. An iterative calculation procedure for shakedown pressure estimation is also given in this chapter. For cylinders of various end conditions, shakedown pressures are calculated on both the moving boundary basis and the fixed boundary basis. The effects of geometric changes and end conditions on shakedown pressure estimations are also examined.

In chapter 6, the proposed method is used to estimate plastic collapse loads of thick wall cylinders for material exhibiting work hardening behavior. Results for different end conditions are calculated to assess the effect of end conditions. Plastic collapse loads calculated by deformed geometry theory are compared with those by undeformed geometry theory in order to evaluate the effect of geometric change. The ANSYS nonlinear finite element program is used for the purpose of comparison.

In chapter 7, the effect of geometric changes is further assessed in terms of the difference of the energy required for deformation using large deformation and small deformation theories, respectively. Using the ANSYS finite element analysis, the effect of large deformation on the fracture parameter, J integral, is examined for inelastic materials. The numerical examples include a range of diameter-ratio cylindrical pressure vessels with a circumferential flaw. The nonlinear energy release rates are calculated and compared for small deformation and large deformation theories.

The major contributions of this research are:

1. The effect of the moving pressure boundary on inelastic analyses for thick wall cylinders being incorporated into the proposed analytical approach;
2. the development of a generalized formulation in terms of parametric functions for inelastic analyses on thick wall cylinders using piecewise linearization of actual stress strain curves;

3. the development of iterative calculation programs for inelastic solutions and shakedown pressures on moving boundary basis without recourse to FEA based methods; and lastly
4. the assessment of effects of deformed geometry on inelastic analyses and the fracture parameter, J integral.

Firstly, the significance of the research lies in the generalized formulation in terms of accommodating different stress strain relationships, which is mathematically simpler to use than the incremental theory of plasticity. As an analytical method, it provides practitioners an alternative assessment and benchmarking tool that can be used for inelastic analysis, which is usually performed by the elaborate and time-consuming nonlinear finite element analysis.

The significance also includes the effect of deformed geometry, which is incorporated into the proposed method of inelastic analysis for thick wall cylinders, which was rarely considered in known prior research. Due to high internal pressure, cylindrical vessels could experience large deformations. Neglecting the effect of geometric changes can be unconservative in the context of integrity and reliability assessment of vessels subject to high pressures. The development of the proposed method can also provide insights into the effects of geometric change on inelastic analysis and the fracture parameter (J integral).

2. THEORETICAL BACKGROUND

2.1 INTRODUCTION

Two tasks are generally involved in structural design and analysis: the determination of the internal force field acting on the structural material, and the determination of the response of the material to that force field. The determination of the internal force involves an analysis of the stresses acting within the structures and materials due to the application of externally applied mechanical and/or thermal loads. The determination of the response often requires a constitutive model or knowledge of the stress strain relationship. The linear relationship that exists between stress and strain in an idealized material forms the basis of infinitesimal theory of elasticity, which has been applied widely in practice to estimate stresses or strains in the real life materials and structural components under stipulated load conditions. The design codes for pressure vessels, which have evolved by reliance upon the engineering practice of decades and centuries, restrict the stresses to be less than a specified allowable stress level that is chosen as some fraction of the yield strength of the material or its ultimate strength (Fryer and Harvey, 1998).

Theory of plasticity, on the other hand, provides an adequate understanding of the behavior of actual materials in which linear relationship of stress and strain is no longer valid. It represents a necessary extension of the theory of elasticity, because it furnishes more realistic estimates of load-carrying capacities of structures and provides a complete

theory for structural analysis in both plastic and elastic ranges. Theory of plasticity endeavors to quantify and predict the behavior of solids, generally metals, undergoing permanent (irreversible) deformation. There are four major components for the prediction of elastic plastic deformation, which are:

1. A stress strain relationship, which describes the uniaxial loading behavior of material;
2. a yield criterion, which defines the limits of elasticity under combined state of multiaxial stresses;
3. a flow or deformation rule, which relates the stresses to the corresponding strains or strain increments; and lastly
4. a hardening rule, which describes the subsequent increase of yield stress in plastic deformation.

First, a brief introduction of the constitutive relationships, yield criteria, flow or deformation rules, and hardening rules is given in this chapter. As well, equilibrium equations, compatibility equations, and constitutive equations, which are basically the three major components of boundary value problems, are discussed. Then a brief introduction of the virtual work principle is given at the end of this chapter.

2.2 INELASTIC BEHAVIOR IN SIMPLE TENSION TEST

A material's response to uniaxial loading is assessed most often by means of tension and compression test. Standard test procedures and size specimens are used to determine the

physical properties of material for pressure vessels and structural steels. Of these, the simplest and most widely used is the tension test. This consists of pulling a 0.5 *in.* (1.27 *cm*) diameter, 2 *in.* (5.08 *cm*) gage length specimen and then estimate the proportional limit, yield strength, ultimate strength, elongation in the gage length, and the reduction in the cross-sectional area at failure. Figure 2.1 shows such a stress strain curve. The well-known uniaxial stress strain diagram affords a useful representation of the plastic as well as the elastic behavior.

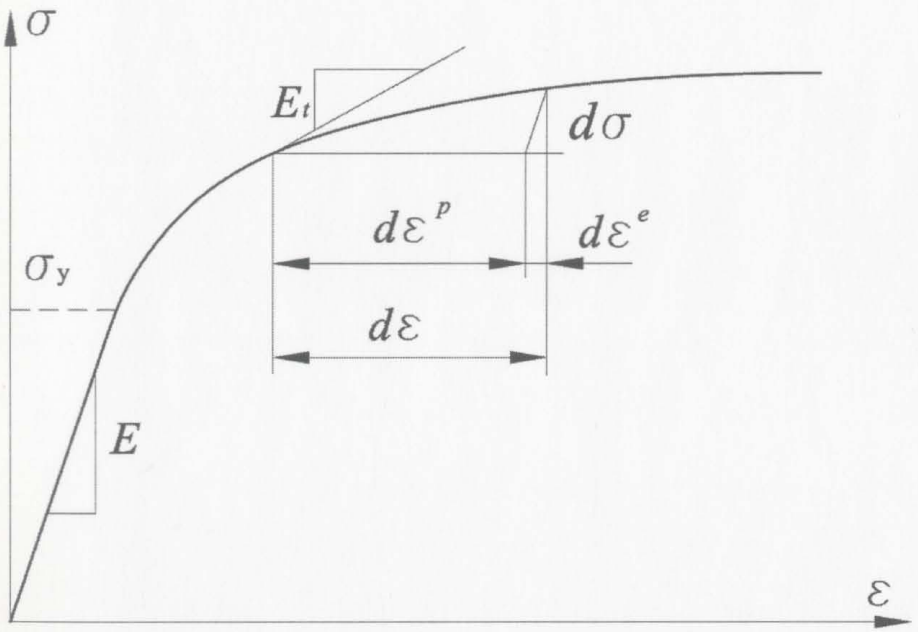

Fig. 2.1 Stress strain curve in simple tension test

2.2.1 Stress Strain Curve in Simple Tension Test

Fig. 2.1 shows a typical uniaxial stress strain curve for a strain-hardening material. The yield point is a most important characteristic since it represents the point at which plastic flow commences. Ductility is measured as the elongation of the test specimen gage length, and uniform elongation and reduction in area occur up to the ultimate strength, at which time necking begins and further elongation becomes localized. The area under the stress strain curve represents the amount of work required to produce elastic plastic deformation. It can describe the characteristic of a material, since it depends on both its strength and ductility.

2.2.2 Material Properties of Inelastic Behavior

Material properties, such as the modulus of elasticity, tangent modulus, plastic modulus, and Poisson's ratio are obtained from a uniaxial stress strain experimental data curve. Fig. 2.1 shows the definition of elastic, tangent, and plastic moduli. For material with linear elastic behavior, the modulus of elasticity is simply expressed as:

$$E = \frac{\sigma}{\varepsilon} \tag{2.1}$$

However, because the elastic plastic stress strain curve of the material is nonlinear in nature, an incremental procedure is often adopted. The increment of strain in elastic

plastic deformation consists of two parts: the elastic strain increment, $d\varepsilon^e$, and the plastic strain increment, $d\varepsilon^p$, such that

$$d\varepsilon = d\varepsilon^e + d\varepsilon^p \tag{2.2}$$

The infinitesimal stress increment, $d\sigma$, is related to the infinitesimal strain increment, $d\varepsilon$, by

$$d\sigma = E_t d\varepsilon \tag{2.3}$$

where E_t is the tangent modulus that varies during plastic deformation. In Fig. 2.1, E_t is the instantaneous slope of the nonlinear stress strain curve. If the plastic strain, ε^p is separated from the total strain, ε, then the plastic strain increment and stress increment are related by

$$d\sigma = E_p d\varepsilon^p \tag{2.4}$$

where E_p is referred to as the plastic modulus, which in the case of uniaxial loading is the slope of the $\sigma - \varepsilon^p$ curve. The elastic strain increment $d\varepsilon^e$, is related to the increment stress by the modulus of elasticity E:

$$d\sigma = E d\varepsilon^e \tag{2.5}$$

Substitution of $d\varepsilon$ in Eq. 2.3, $d\varepsilon^p$ in Eq. 2.4, and $d\varepsilon^e$ in Eq. 2.5 into Eq. (2.2) leads to the relationship between the three moduli E_t, E, and E_p

$$\frac{1}{E_t} = \frac{1}{E} + \frac{1}{E_p} \tag{2.6}$$

Besides the modulus of elasticity, Poisson's ratio is also an important material parameter, which describes the lateral behavior of materials under axial load. Poisson's ratio is defined as

$$\nu = -\frac{\varepsilon_{lateral}}{\varepsilon_{axial}} \tag{2.7}$$

Although Poisson's ratio is not explicitly defined by the stress strain curve, it is often measured and calculated by the same simple unaxial loading test.

2.3 MODELING OF UNIAXIAL BEHAVIOR IN PLASTICITY

Experimental stress strain curves of material are often idealized to obtain elastic plastic solution (Chen and Han, 1987). Four types of idealized stress strain curve are discussed herein.

2.3.1 Elastic Perfectly Plastic Model

In some cases, it is permissible and convenient to neglect the effect of work hardening and assume that the plastic flow occurs as the stress has reached the yield stress, σ_y.

Thus, the uniaxial stress strain relation may be expressed as

$$\varepsilon = \frac{\sigma}{E} \qquad \text{for } \sigma < \sigma_y \qquad (2.8a)$$

$$\varepsilon = \frac{\sigma}{E} + \varepsilon^p \qquad \text{for } \sigma = \sigma_y \qquad (2.8b)$$

This material behavior model is shown in Fig. 2.2a.

2.3.2 Elastic-Linear Work-Hardening Model

For material with work hardening behavior, the experimental stress strain curve can be approximated by two straight lines, thus replacing the smooth transition curve by a sharp breaking point, the ordinate of which is taken to be the elastic limit stress or the yield strength. The first linear branch of the diagram has a slope of modulus of elasticity, E. The second linear branch, representing the work hardening range in an idealized fashion, has a slope of $E_t < E$ (Fig. 2.2.b). The stress strain relation has the following form:

$$\varepsilon = \frac{\sigma}{E} \qquad \text{for } \sigma \leq \sigma_y \qquad (2.9a)$$

$$\varepsilon = \frac{\sigma_y}{E} + \frac{1}{E_t}\left(\sigma - \sigma_y\right) \qquad \text{for } \sigma > \sigma_y \qquad (2.9b)$$

2.3.3 Elastic-Exponential Hardening Model

For work hardening material, stress strain relations can be approximated in the following power expression:

$$\sigma = E\varepsilon \qquad \text{for } \sigma \le \sigma_y \qquad (2.10a)$$

$$\sigma = k\varepsilon^n \qquad \text{for } \sigma > \sigma_y \qquad (2.10b)$$

where k and n are two characteristic constants of the material to be determined to best fit the experimentally obtained curve. Clearly, the power expression is only applicable to the work hardening range, as shown in Fig. 2.2c.

2.3.4 Ramberg-Osgood Model

Ramberg and Osgood (1943) proposed a relation of representing the nonlinear stress strain behavior (Fig. 2.2d) in the following expression:

$$\varepsilon = \frac{\sigma}{E} + \alpha\frac{\sigma}{E}\left(\frac{\sigma}{\sigma_y}\right)^{m-1} \qquad (2.11)$$

where material constants α and m are the yield offset and the hardening exponent, respectively. The initial slope of the curve takes the value of elastic modulus at $\sigma = 0$,

and decreases monotonically with increasing load. Since this model has three parameters, it allows for a close fit of real stress strain curves. This method of idealization is usually utilized in the deformation theory of plasticity.

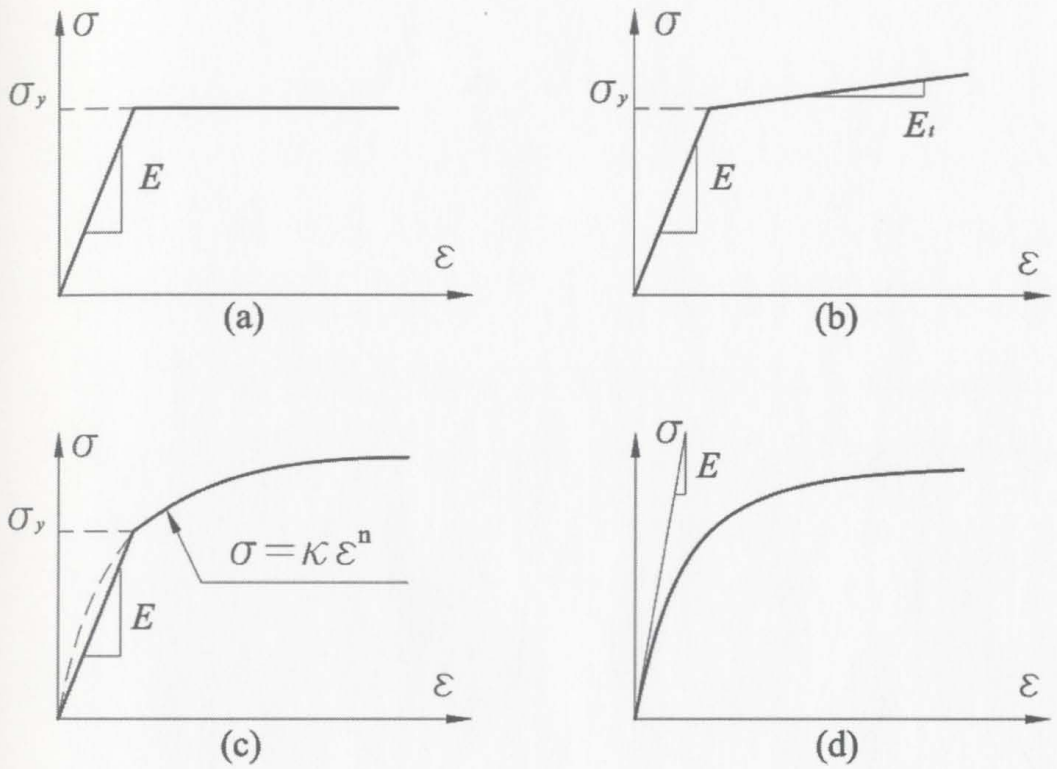

Fig. 2.2 Idealized stress strain curves

(a) Elastic perfectly plastic model

(b) Elastic-linear work-hardening model

(c) Elastic-exponential hardening model

(d) Ramberg-Osgood model

2.4 YIELD CRITERIA

The yield criterion defines the elastic limits of a material under combined states of stress. For structural elements with multiaxial stresses, a yield criterion describes how each stress component contributes to yielding due to a complicated set of loads.

Depending on which type of material, yield criteria can be dependent or independent of hydrostatic pressure. However, it is generally agreed that most of ductile metals is hydrostatic pressure independent. Although many yield criteria have been proposed, the maximum shear stress criterion, also know as Tresca yield condition, and the maximum distortion energy criterion, also referred to as the von Mises yield condition, best represent actual material behavior while preserving mathematical tractability (Chen and Han, 1987).

2.4.1 The Maximum Shear Stress Criterion

In 1864, Tresca historically proposed the first yield criterion for a combined state of stress of metals. According to his theory, yielding would occur when the maximum shear stress at a point reaches a critical value. Tresca yield criterion can be expressed as

$$\left|\sigma_{\max} - \sigma_{\min}\right| = \sigma_y \tag{2.12}$$

where σ_{max} and σ_{min} are the maximum and minimum principal stresses, and σ_y is the yield stress in tension. For a biaxial state of stress, the yield locus is obtained as a hexagon, shown in Fig. 2.3.

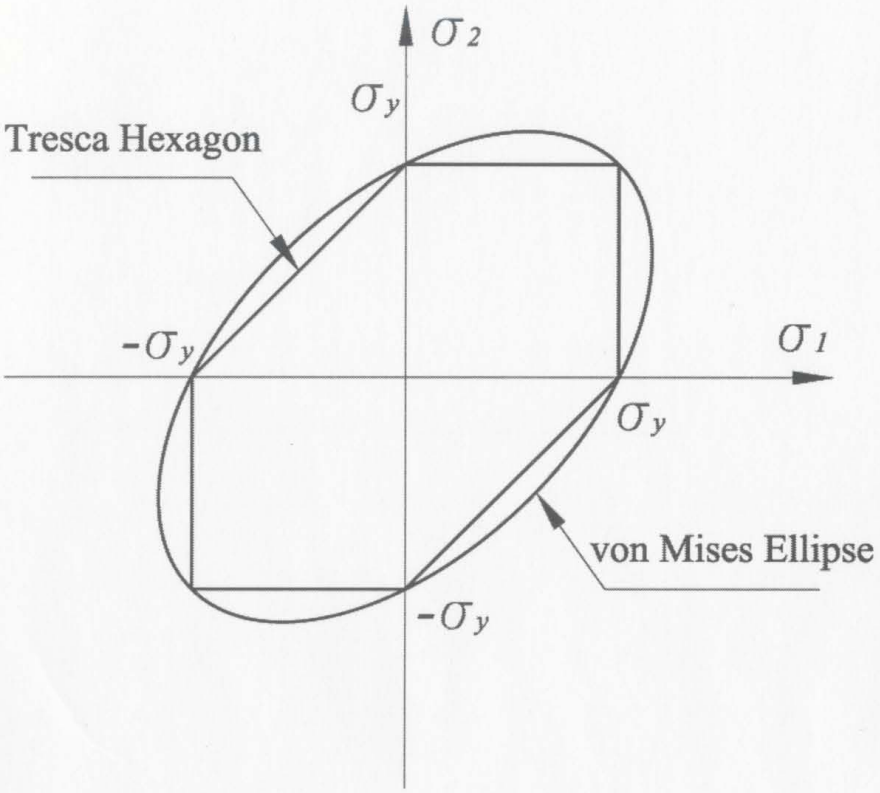

Fig. 2.3 Yield locus for a biaxial stress state

Tresca's equivalent stress, σ_{eq}^{T}, may be defined in the following form:

$$\sigma_{eq}^{T} = |\sigma_{max} - \sigma_{min}| \tag{2.13}$$

The definition comes from Eq. (2.12), where the left hand side of it is taken as a representation of the state of equivalent stress at a given material point. The definition of equivalent stress is essential when working with hardening materials as initial yielding is not the only concern.

2.4.2 The Maximum Distortion Energy Criterion

The maximum shear stress criterion is simple, however it does not reflect any influence of the intermediate principal stress. The maximum distortion energy criterion, which was developed in 1913, is based on an alternative theory that yielding begins when the distortion energy for a complex stress state is equal to the distortion energy at yield in a simple tension test. The maximum distortion energy criterion is also known as von Mises criterion. von Mises criterion is represented using the deviatoric stress tensor, σ'_{ij}, and the yield stress σ_y, which can be expressed

$$\sigma'_{ij} = \sigma_{ij} - \frac{\sigma_{kk}}{3}\delta_{ij} \tag{2.14}$$

and

$$\sigma_y^2 = \frac{3}{2}\sigma'_{ij}\sigma'_{ij} \tag{2.15}$$

where δ_{ij} is the Kronecker delta. The von Mises criterion in terms of principal stresses is

$$\sqrt{\frac{1}{2}\left[(\sigma_1-\sigma_2)^2+(\sigma_1-\sigma_3)^2+(\sigma_2-\sigma_3)^2\right]}=\sigma_y \tag{2.16}$$

where σ_1, σ_2, and σ_3 are the principal stresses. For the case of a biaxial state of stress ($\sigma_3 = 0$), the yield locus is an ellipse as shown in Fig. 2.3.

The von Mises criterion takes the intermediate principal stress into consideration. The von Mises equivalent stress is defined by

$$\sigma_{eq}=\sqrt{\frac{1}{2}\left[(\sigma_1-\sigma_2)^2+(\sigma_1-\sigma_3)^2+(\sigma_2-\sigma_3)^2\right]} \tag{2.17}$$

The Tresca and von Mises yield criteria never give dramatically different prediction of the yield behavior under combined stress. The experimental work (Osgood 1947) shows that the yield points fall between the Tresca hexagon and the von Mises ellipse, though closer to the latter. The maximum distances from the origin to the Mises ellipse and the Tresca hexagon in Fig. 2.3 have the ratio of 1.155. Hill (1950) suggested that solutions obtained using the Tresca criterion may be scaled by this factor to give estimations based on the von Mises criterion.

2.5 STRESS STRAIN RELATIONS

Generalized Hooke's law describes the linear elastic response of materials during multiaxial elastic and plastic deformation. Two other basic approaches describe the plastic response. The first type of formulation is the deformation theory in the form of the total stress strain relation. Another type of formulation is the incremental theory or flow theory. This type of formulation relates the increment of plastic strain components to the state of stress.

2.5.1 Linear Elastic – Generalized Hooke's Law

The generalized Hooke's law constitutes the linear elastic relationship

$$\varepsilon_{ij}^{e} = \frac{1}{2G}\sigma_{ij} - \frac{\nu}{E}\sigma_{kk}\delta_{ij} \tag{2.18}$$

where G, E and ν are the shear modulus, elastic modulus and Poisson's ratio, respectively.

This relationship applies not only prior to yielding but also after yielding, except that in the latter case it gives only the elastic portions of the strains. The total strains are obtained by adding the plastic portion to the elastic portion:

$$\varepsilon_{ij} = \varepsilon_{ij}^{e} + \varepsilon_{ij}^{p} \tag{2.19}$$

2.5.2 Deformation Theory of Plasticity

In 1924, Hencky formulated a theory to describe the relationship between total plastic strains and stresses. Assuming small strains, the formulation may be written as

$$\varepsilon_{ij}^{p} = \phi \sigma_{ij}' \tag{2.20}$$

where ϕ is a scalar valued function determined by experiments. To calibrate this scalar, a strain variable called the equivalent plastic strain is introduced and defined as

$$\varepsilon_{eq}^{p} = \sqrt{\frac{2}{3}\varepsilon_{ij}^{p}\varepsilon_{ij}^{p}} \tag{2.21}$$

Using the definition of equivalent stress σ_{eq} (e.g. Mises equivalent stress) and equivalent strain ε_{eq}^{p} leads to an expression for the parameter function ϕ:

$$\phi = \frac{3}{2}\frac{\varepsilon_{eq}^{p}}{\sigma_{eq}} \tag{2.22}$$

2.5.3 Incremental Theory of Plasticity

Levy (1871) and von Mises (1913) independently proposed a relationship between strain increments and the current state of stress. Prandtl (1924) extended the earlier Levy-von

Mises theory to plane strain case for an elastic perfectly plastic material. Reuss (1930) extended the Prandtl equations to the three-dimensional case and gave the general form of

$$d\varepsilon_{ij}^{p} = d\lambda \sigma'_{ij} \tag{2.23}$$

or in terms of the components of the strain increments and stresses as

$$\frac{d\varepsilon_{11}^{p}}{\sigma'_{11}} = \frac{d\varepsilon_{22}^{p}}{\sigma'_{22}} = \frac{d\varepsilon_{33}^{p}}{\sigma'_{33}} = \frac{d\varepsilon_{12}^{p}}{\sigma'_{12}} = \frac{d\varepsilon_{13}^{p}}{\sigma'_{13}} = \frac{d\varepsilon_{23}^{p}}{\sigma'_{23}} = d\lambda \tag{2.24}$$

where $d\lambda$ is a factor of proportionality, which may be found by considering plastic work increments. Hill (1950) suggested that the increment of plastic work per unit volume for the von Mises yield criterion is

$$dW^{p} = \sigma'_{ij} d\varepsilon_{ij}^{p} = \sigma_{eq} d\varepsilon_{eq}^{p} \tag{2.25}$$

where the equivalent plastic strain increment is defined as

$$d\varepsilon_{eq}^{p} = \sqrt{\frac{2}{3} d\varepsilon_{ij}^{p} d\varepsilon_{ij}^{p}} \tag{2.26}$$

Therefore, $d\lambda$ can be determined by the following equation:

$$d\lambda = \frac{3}{2}\frac{d\varepsilon_{eq}^{p}}{\sigma_{eq}} \tag{2.27}$$

Both deformation theory and incremental theory have been used for plastic analysis of materials. There have been many studies, especially during the 1950's and 1960's, comparing the two theories. Many of these studies emphasized that deformation theory cannot adequately describe the phenomena associated with plastic deformation due to the assumption of loading-path-independent behavior, while some (Hodge and White 1952, Budiansky 1959, Chen 1973) have pointed out the applicability of deformation theory. Experimental results (Mroz and Olszak, 1963) show that the Prandtl-Reuss equation, which is path dependent, is the most accurate relationship. However, due to the mathematical complexity arising from the incremental formulation, deformation theory is preferred for many applications and has been used extensively in practice for the solution of elastic plastic problems because of its comparative simplicity, less computational time and reasonable accuracy. These applications can be found in notch analysis (Seeger 1985), cyclic plasticity (Dowling 1993), and fracture mechanics (Chen 1996).

2.6 HARDENING RULES

Engineering material usually exhibits a work hardening behavior. The rule that specifies the post yield response of the material is called the hardening rule. Hardening rules describe how the yielding criterion changes during the course of plastic deformation. For unloading situations, they also describe the onset of reversed yielding. For a material

element under a reversed loading condition, the subsequent yield stress is usually determined by the following hardening rules: 1) isotropic hardening and 2) kinematic hardening.

Although it is necessary to work with a hardening rule for complex loading and unloading problems, neither isotropic hardening rule nor kinematic hardening rule is able to capture all features of material behavior. For example, an experimental stress strain curve of the material AISI 4333 has a minor work hardening behavior in loading while showing a significant hardening effect upon unloading. The Bauschinger effect is not captured even by the kinematic hardening rule because the curve is close to perfectly plastic response in loading. Unlike during loading, the material transition from elastic unloading to reversed yielding is smooth in the actual stress strain curve. Therefore utilizing the actual stress strain curve can lead to accurate estimation of material response, where it is applicable.

2.6.1 Isotropic Hardening Rule

The isotropic hardening rule is based on the assumption that the initial yield surface expands uniformly without distortion and translation as plastic flow occurs. The center of the yield surface remains fixed. Such behavior is shown schematically in Fig 2.4. The diagram is drawn in two dimensions, but the basic geometric ideas are readily extended to three-dimensional spaces. Using the von Mises yield criterion, the yield surface is described by

$$\sigma_{eq}^2 - \frac{3}{2}\sigma'_{ij}\sigma'_{ij} = 0 \tag{2.28}$$

Isotropic hardening rule cannot account for the Bauschinger effect that has been experimentally observed for many metals (Milligan et. al. 1966). Isotropic hardening model is considered to best describe material behavior for large strains. Therefore, this rule is applied more in metal forming problems.

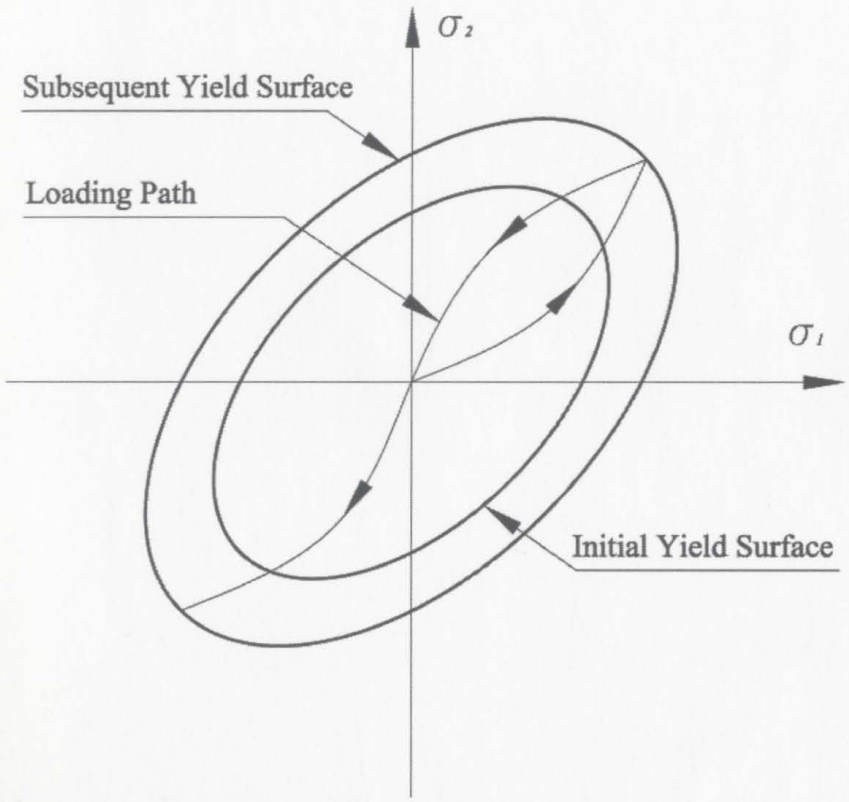

Fig. 2.4 Yield surface for isotropic hardening material

2.6.2 Kinematic Hardening Rule

The kinematic hardening rule is based on the assumption that during plastic deformation, the loading surface translates as a rigid body in stress space, maintaining the size, shape, and orientation of the initial yield surface. This hardening rule was first proposed by Prager (1957) as a way to model the Bauschinger effect. This rule is illustrated schematically in Fig. 2.5.

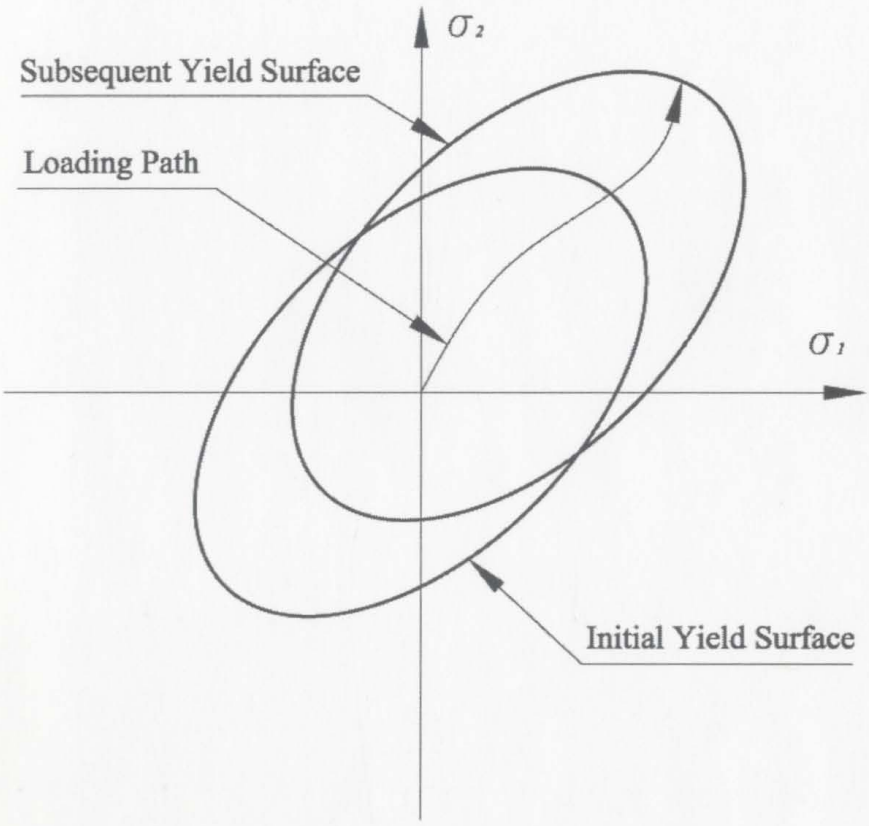

Fig. 2.5 Yield surface for kinematic hardening material

For von Mises material, the yield surface equation is expressed as

$$\sigma_y^2 - \frac{3}{2}\left(\sigma'_{ij} - \alpha_{ij}\right)\left(\sigma'_{ij} - \alpha_{ij}\right) = 0 \tag{2.29}$$

where α_{ij} is the shift tensor that accommodates translation. Different relations for the shift tensor increment have been proposed. Ziegler (1959) modified Prager's rule by proposing the following evolution form for the shift tensor

$$d\alpha_{ij} = d\mu\left(\sigma'_{ij} - \alpha_{ij}\right) \tag{2.30}$$

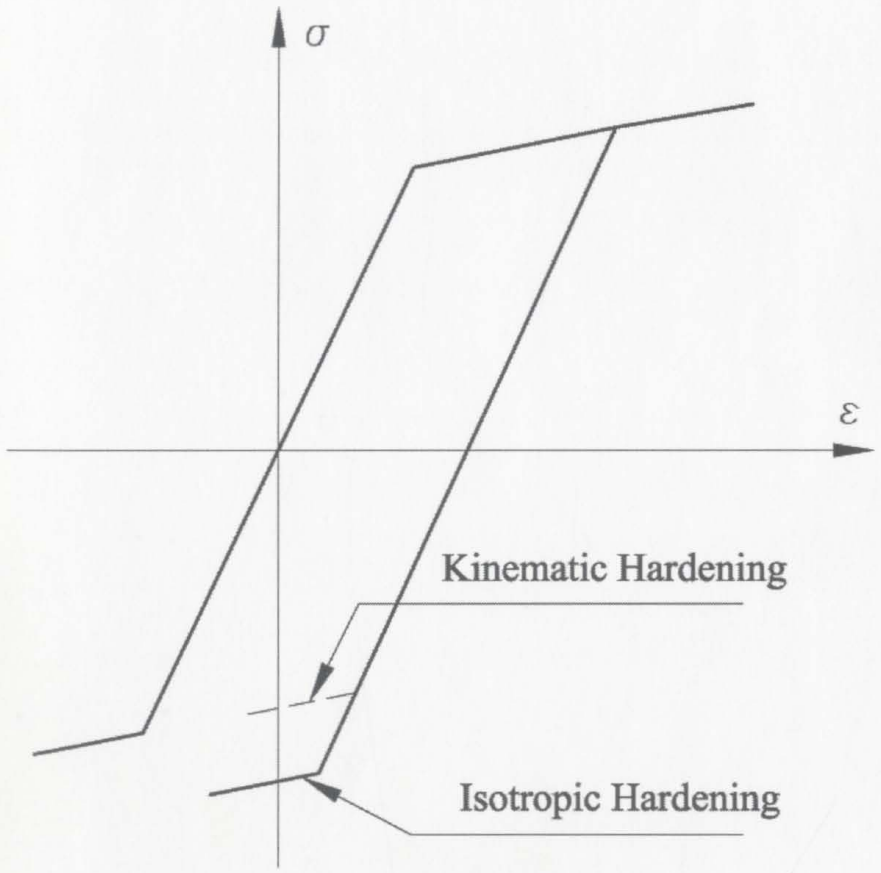

Fig. 2.6 Isotropic and kinematic hardening

Kinematic hardening rule provides a simple means of accounting for the Bauschinger effect. This hardening rule is used mostly in fatigue analysis and cyclic plasticity. Fig. 2.6 shows the possible unloading paths of isotropic hardening and kinematic hardening materials on the uniaxial stress strain curve.

2.7 BOUNDARY VALUE PROBLEMS

Formulation of boundary value problems requires considerations of: 1) the equilibrium equation, 2) the compatibility condition, and 3) the constitutive equation. It is essential to understand and enforce these considerations in analytical or numerical formulations of solid mechanics because complete and reliable solutions are achieved only if equilibrium and compatibility are maintained, and the correct constitutive relation is employed.

2.7.1 Equilibrium Equations

The state of stress at a point in a body is completely determined by the components of the Cartesian stress tensor σ_{ij}. Naturally, the stresses vary within the body. The equations governing the distribution of stresses are known as the equations of equilibrium and are derived from the application of the fundamental physical principles of linear and angular momentum.

Consider a body of volume V enclosed within surface Γ. The body is in equilibrium if the stress tensor satisfies the following equation

$$\sigma_{ij,j} + F_i = 0 \tag{2.31}$$

where F_i is the body force.

The equilibrium equation (Eq. 2.31) ensures the equilibrium of stresses of the material interior to Γ. The stress and displacement fields must be such as to conform to the conditions of loading imposed at the boundaries. If the prescribed boundary condition consists of tractions, T_i, and displacements, u_i^*, then the following two conditions must be satisfied to ensure the equilibrium and compatibility on the boundary:

$$\sigma_{ij} n_j = T_i\big|_{\Gamma_1} \tag{2.32}$$

for traction T_i over the boundary Γ_1 and

$$u_i = u_i^*\big|_{\Gamma_2} \tag{2.33}$$

for displacement u_i^* over the boundary Γ_2. The surface consists two parts

$$\Gamma = \Gamma_1 + \Gamma_2 \tag{2.34}$$

2.7.2 Compatibility Equations

The Lagrangian strain tensor ε_{ij}^{L} is defined by

$$\varepsilon_{ij}^{L} = \frac{1}{2}\left(u_{i,j} + u_{j,i} + u_{k,i}u_{k,j}\right) \tag{2.35}$$

In small strain theory, the displacement gradients $u_{k,i}$ are small in comparison to unity, then products of such term are negligible in Eq. (2.35) and they may be dropped. For such case, the definition of small or infinitesimal strain tensor ε_{ij} is introduced:

$$\varepsilon_{ij} = \frac{1}{2}\left(u_{i,j} + u_{j,i}\right) \tag{2.36}$$

Note that no restriction is placed on the magnitude of the u_i terms but only the gradients. It is thus theoretically possible at this point to describe relatively large deformation by infinitesimal strains (Gould 1983).

In the analysis of stress, equilibrium equation ensures the body is always in equilibrium state. In the analysis of strain, the compatibility condition must be imposed on the strain components so that the deformed body remains continuous, which are illustrated in the following equation:

$$\varepsilon_{ij,kl} + \varepsilon_{kl,ij} - \varepsilon_{ik,jl} - \varepsilon_{jl,ik} = 0 \tag{2.37}$$

The compatibility equation is the necessary and sufficient condition required to ensure that the strain components give single-valued continuous displacements (Chen and Han, 1987).

2.7.3 Constitutive Laws

The equilibrium equation that involves only stresses is independent of the compatibility condition that involves only strains. The constitutive laws connect the stress and strain through the mechanical properties of materials. Therefore, knowledge and understanding of the material behavior is necessary and important.

Throughout this work, only homogeneous and isotropic materials are considered. A homogeneous material displays identical properties throughout the body and the properties are identical in all directions at a point for an isotropic material. Hencky's relation and Prandtl-Reuss equation, which have been discussed earlier, are two examples of constitutive laws. In chapter 4, a set of constitutive relations analogous to the generalized Hooke's law is established and applied to describe elastic plastic behavior of boundary value problems.

2.8 PRINCIPLE OF VIRTUAL WORK

Analysis of stress and deformation can be accomplished through the use of energy methods, which provides an alternative to the methods based upon analytical solutions of

differential equations. Applications of energy methods, such as the principle of virtual work, have been proved effective in situations including various solid mechanics problems and offering concise and relatively simple approaches for structure and structural elements. In particular, the principle of virtual work, which is developed from the law of conservation of energy, has proved very powerful as a technique in solving problems with both elastic and inelastic material behavior.

The equation of virtual work principle connects two separate and unrelated sets: the equilibrium set and the compatible set, as shown in Fig. 2.7. The equilibrium set and the compatible set, which are independent to each other, are brought together in the equation of virtual work principle:

$$\int_A T_i u_i^* dA + \int_V F_i u_i^* dV = \int_V \sigma_{ij} \varepsilon_{ij}^* dV \tag{2.38}$$

where A and V are the whole area and volume of the body, respectively. The quantity T_i is external surface force and F_i is body force. In Eq. 2.38, the equilibrium set consists of T_i, F_i, and σ_{ij} while the compatible set consists of u_i^* and ε_{ij}^*. The stress field σ_{ij} is any set of stresses, real or virtual, in equilibrium with body forces F_i within the body and with surface forces T_i on the surface where they are prescribed. Similarly, the strain field ε_{ij}^* represents any set of strains compatible with the real or virtual displacements u_i^* of the points of application of the external forces T_i and F_i.

An essential point of virtual work principle is that neither the equilibrium set nor the compatible set need be the actual state, nor need the equilibrium and compatible sets be related in any way to each other (Chen and Han, 1987).

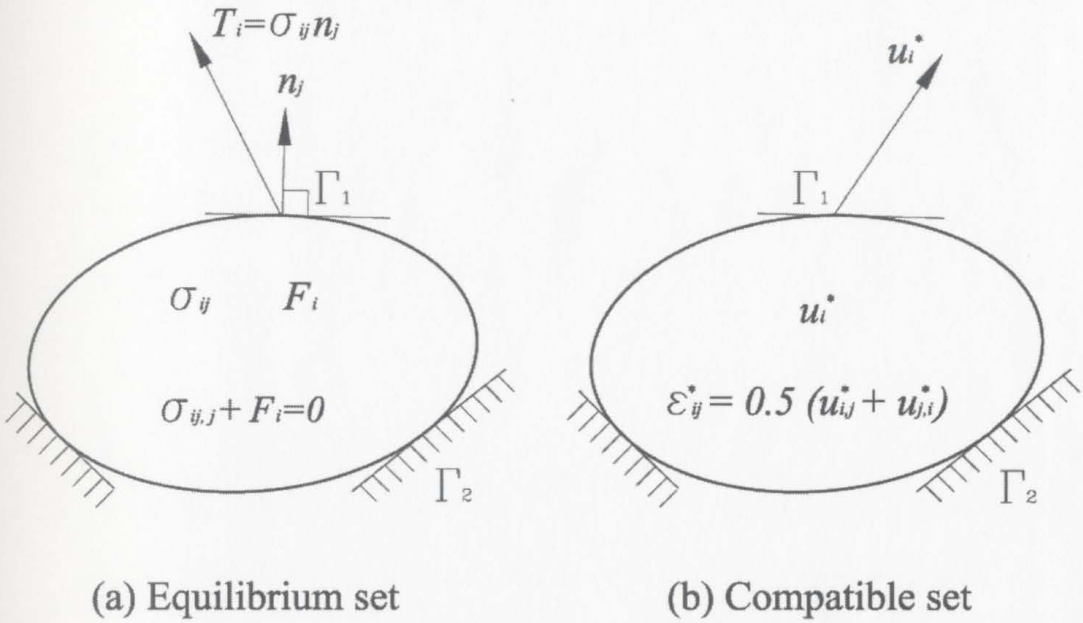

(a) Equilibrium set (b) Compatible set

Fig. 2.7 Two independent sets in the equation of virtual work

2.8.1 Principle of Virtual Displacement

In the case of that virtual displacements δu_i^* are applied to a system in equilibrium under a set of real surface tractions and body forces, the principle of virtual work is expressed as:

$$\int_A T_i \delta u_i^* dA + \int_V F_i \delta u_i^* dV = \int_V \sigma_{ij} \delta \varepsilon_{ij}^* dV \tag{2.39}$$

This is the principle of virtual displacements, which can be used to determine the external reactive forces on the body or the unknown internal loading in the body (Gould 1983).

2.8.2 Principle of Virtual Force

Similarly, when virtual forces are applied to a system in equilibrium, the principle of virtual work is expressed as:

$$\int_A \delta T_i u_i^* dA + \int_V \delta F_i u_i^* dV = \int_V \delta \sigma_{ij} \varepsilon_{ij}^* dV \tag{2.40}$$

This is the principle of virtual force, which describes compatibility between internal deformation and external displacements. The principle of virtual force is usually helpful to calculate external displacements (Gould 1983).

3. REVIEW OF LITERATURE

In this chapter, a general review of literature starts from the topic of elastic plastic analysis based on linear elastic solutions, as the proposed method is an analytical method for inelastic analysis based on elastic solutions. The piecewise linearization of nonlinear stress strain law, which is one of the main features of the proposed formulation, employs the concept of reduced modulus to describe the inelastic behavior. A general introduction of the topic of high pressure technology is given including various theories of elastic plastic analysis for thick walled cylinders, and related design aspects.

3.1 ELASTIC PLASTIC ANALYSIS BASED ON ELASTIC SOLUTIONS

Linear elastic behavior of materials is a well-established branch of solid mechanics. Unified understanding of the linear elastic response of materials has been achieved. Linear elastic formulations of problems are mathematically simple and their solutions are, for the most part, readily attainable. Most practical problems in this field possess either analytical or numerical solutions that are in good agreement with experimental observation.

Plasticity, however, is much more complicated. Although a unified theory of plasticity began to emerge after 1950's, the understandings of plastic behavior are diversified even today. In practice, plasticity theory, which has been formulated from some experimental observations and conjecture, needs to be further justified by more experiments. Besides,

theoretical plasticity with complex mathematics is a matter of debate itself. Therefore, simplified methods of elastic plastic analysis have attracted increasing attention amongst researchers in the practical field of plasticity. The simplicity of linear elasticity and difficulties with nonlinear plasticity has made way for researchers to attempt solving elastic plastic problems by adapting a modified form of available elastic solutions. The idea of estimating the elastic plastic behavior by using elastic analysis can be traced back to Nadai (1930) who carried out a plastic analysis of a thin wide plate with a circular hole using a linear elastic method.

3.1.1 Method of Successive Elastic Solution

Ilyushin (1946) proposed a method of using successive elastic solutions to perform plastic analysis on a thin shell. This method uses the following constitutive relation

$$\varepsilon_{ij} = \frac{1}{2G}\sigma_{ij} - \frac{\nu}{E}\sigma_{kk}\delta_{ij} + \varepsilon_{ij}^{p} + \Delta\varepsilon_{ij}^{p} \tag{3.1}$$

where ε_{ij}^{p} is the total accumulated plastic strain up to, but not including the current increment of loading $\Delta\varepsilon_{ij}^{p}$. The method allows the plastic strain increment to be related to the stresses through any yield criterion and the associated flow rule, but the Prandtl-Ruess relations are preferred. The loading path is divided into a number of increments. For the first increment of load, a distribution is assumed for the components of plastic strain increments $\Delta\varepsilon_{ij}^{p}$. The components of total plastic strain ε_{ij}^{p} are zero. Therefore, the

boundary value problem formed by the above constitutive equation can be solved as for any elastic problem to give a first approximation for the stresses and total strains. The assumed values for $\Delta\varepsilon_{ij}^{p}$ give an equivalent plastic increment $\Delta\varepsilon^{p}$. From the uniaxial stress strain curve, the corresponding value of equivalent stress is obtained and new sets of $\Delta\varepsilon_{ij}^{p}$ are calculated from the Prandtl-Reuss relation. Using the new plastic strain increments, the boundary value problem is solved again as a new elastic problem. This process is continued until convergence is obtained. Mendelson (1968) records a collection of work on different plastic problems using this method.

3.1.2 Reduced Modulus Method

Plastic analysis investigates components and structures both at global and local level. At global level, limit load that results in plastic collapse needs to be determined. There are a number of techniques to calculate structural limit load, the state of art analysis technique is the incremental finite element analysis implemented by specialist nonlinear programs such as ANSYS, ABAQUS and I-DEAS, etc. However, calculation of limit loads by detailed inelastic analysis can be difficult and computationally expensive. In practice, limit load analysis for design considerations is often performed using simplified methods, most commonly based on elastic analysis. Jones and Dhalla (1981) investigated the inelastic response, rather than performing an elastic analyses, using iterative linear elastic analyses in which highly stressed regions of the structure were systematically weakened by reduction of the local modulus of elasticity in order to simulate the effect of local inelasticity. First an elastic analysis is performed and the equivalent stress and strain at

the most highly loaded location noted. A rough estimate of the inelastic strain corresponding to the elastically calculated stress is then made. The minimum secant modulus is defined as the ratio of the effective elastic stress to the estimated inelastic strain:

$$E_s^{\min} = \frac{\sigma_A}{\varepsilon^P} \tag{3.2}$$

where A is the most highly loaded location. Once the minimum secant modulus is defined, three values of reduced moduli between the minimum secant modulus and Young's modulus are defined. Next, an elastic analysis is performed in which these reduced modulus values are assigned to the most highly stressed local regions of the component.

Marriott (1988) proposed a method that adopted a truly iterative elastic procedure. An initial elastic analysis is performed and all elements with a maximum difference in principal stress greater than stress S_m, which is to be defined by pressure vessel design code, are identified. The elastic moduli of these elements are then individually reduced on an element-by-element basis, obeying the following equation

$$E_R = E_o \frac{S_m}{SI} \tag{3.3}$$

where E_R and E_o are the reduced and previous values of modulus, respectively. S_m is the code allowable stress and SI is the element stress (i.e., the maximum difference in the principal stresses). Then a second elastic analysis is carried out to obtain a reduced modulus analysis solution. The modulus reduction procedure is then repeated in an iterative manner until the maximum element stress, SI, is less than S_m. The stress field obtained satisfies all the conditions of being statically admissible. The applied load of the solution implies a lower bound on the exact limit load.

Seshadri (1990 and 1991) developed the generalized local stress strain analysis (GLOSS). It is a systematic method for inelastic evaluation on components and structures using two linear elastic FEA. Seshadri calculated the reduced modulus on an element-by-element basis. The reduced modulus required for perfectly plastic behavior is calculated by the following equation:

$$E_S = E_o \frac{\sigma_y}{\sigma_e} \tag{3.4}$$

where E_s is the reduced elastic modulus, E_o is original elastic modulus, σ_y is yield stress and σ_e is theoretical equivalent stress. This theory was developed on the basis of a comparison between multiaxial and uniaxial stress relaxation process, which was presented by Seshadri and Mikulcik (1989). It was postulated that multiaxiality either "speed up" or "slow down" the uniaxial stress relaxation process. Multiaxial stress relaxation and uniaxial behavior are related by the constraint parameter $\overline{\lambda}$, which

characterizes the effect of multiaxiality. The multiaxial stress relaxation model is expressed as

$$\frac{d\sigma_e}{dt} + \overline{\lambda} BE\sigma_e^n = 0 \tag{3.5}$$

where σ_e is the von Mises equivalent stress, B and n are creep parameters. Therefore, when $\overline{\lambda}$ is known, the multiaxial stress relaxation can be determined.

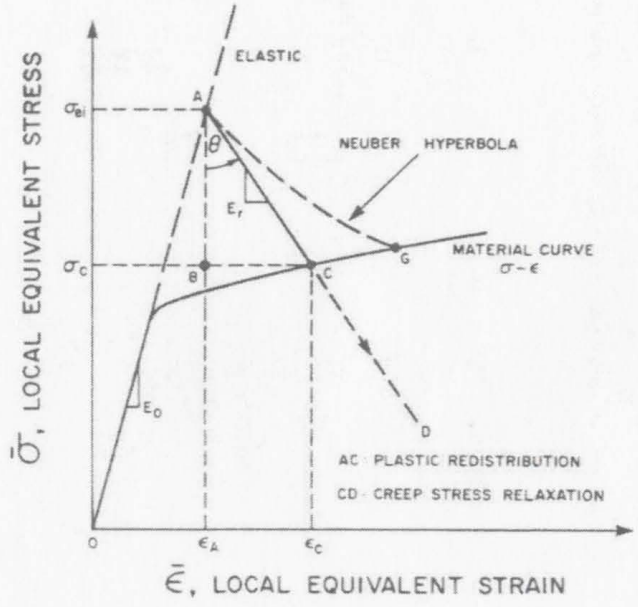

Fig. 3.1. Local system relaxation response on the GLOSS diagram

Seshadri et al. (1992) laid out a procedure for determining limit loads based on two elastic FEA. This method is to identify load controlled locations in the cross section of a structure at which the stress did not change as the solution progressed from the initial elastic solution to the final stationary solution. The aim of this method is to find these points called redistribution nodes or r-nodes. In this method, a linear elastic solution is

first obtained. A location j is then arbitrarily chosen. The moduli of all other elements are then modified according to the following equation:

$$(E_s)_j = E_o\left(\frac{\sigma_{arb}}{\sigma^o_{ej}}\right) \tag{3.6}$$

where σ_{arb} is an arbitrary non-zero stress value. The second linear elastic FEA is performed. Based on the two linear elastic analyses, the r-node element is identified and by interpolation, the exact location of the r-node is obtained. Since r-nodes are statically determinate locations, the effective stresses at the r-nodes are linearly proportional to externally applied loads as a consequence of equilibrium. This method has been successfully applied to a wide range of structures.

Mackenzie and Boyle (1993) developed an elastic compensation method that uses conventional elastic finite element analysis to determine limit loads for bounding theorems of classical plasticity. The elastic compensation method requires only a few linear elastic finite element analyses of a structure. After each iteration, the elastic modulus of each element is modified according to the equation

$$E_i = E_{(i-1)}\frac{\sigma_n}{\sigma_{(i-1)}} \tag{3.7}$$

where subscript i is the present iteration number, σ_n is a nominal stress value and $\sigma_{(i-1)}$ is the maximum nodal equivalent stress associated with the element from the previous solution. After a few iterations, an estimate of the limit load is calculated.

Seshadri and Mangalaramanan (1997) proposed a method for improved lower bound limit load: m_α-multiplier method using a modulus adjustment scheme. This method extended Mura's variational formulation to include local plastic collapse mechanisms. A multiplier, m_α, is obtained on the basis of two linear elastic FEA. The limit loads obtained by this theory are lower bound estimates. Further research discussion and assessment about the variational concepts in limit analysis and improved lower-bound limit load estimate were presented by Seshadri (2000), Reinhardt and Seshadri (2003).

3.2 HIGH PRESSURE TECHNOLOGY

The origin of high pressure technology can be traced back to fourteenth century when the first known cannon was invented. Today, the high pressure technology has been developed from the early basic science to the major applications that have driven the technology. An obvious structural shape to contain high pressure, which may be in the range from 10,000 *psi* (0.690×10^2 *MPa*) to approximately 200,000 *psi* (1.379×10^3 *MPa*), is the thick wall cylinder. The advances of high pressure technology were based on the theoretical understanding of thick wall cylinder subject to internal pressure. Thick wall cylinders subjected to high internal pressure are widely used in various industries, such as petrochemical, gun barrels, and hydrostatic extrusion, etc. In general, vessels under high

pressure require a strict analysis for an optimum design for reliable and secure operational performance. Efforts have been continually made to obtain a thorough understanding of the behavior of the pressurized thick wall cylinder and to increase reliability of design. Solutions have been obtained either in analytical form or with numerical implementations.

3.2.1 Thick Wall Cylinders Subject To High Internal Pressure

In 1833, Lame proposed equations for an elastic stress distribution in a thick wall cylinder, which made it possible to understand the strength of high pressure vessels. This theory also made possible an understanding of the differences between high pressure technology and low pressure technology.

For a cylinder with the inside radius r_i and outside radius r_o, subjected to internal pressure of p_i and external pressure of p_o, Lame's solution can be expressed as:

$$\sigma_r = C_1 - \frac{C_2}{r^2}$$
$$\sigma_\theta = C_1 + \frac{C_2}{r^2} \qquad (3.8)$$

where C_1 and C_2 are constants, given by

$$C_1 = \frac{p_i r_i^2 - p_o r_o^2}{r_o^2 - r_i^2} \tag{3.9}$$

$$C_2 = \frac{(p_i - p_o) r_i^2 r_o^2}{r_o^2 - r_i^2} \tag{3.10}$$

For cylinder under internal pressure only, C_1 and C_2 are

$$C_1 = \frac{p_i r_i^2}{r_o^2 - r_i^2} \tag{3.11}$$

$$C_2 = \frac{p_i r_i^2 r_o^2}{r_o^2 - r_i^2} \quad . \tag{3.12}$$

Hill et al. (1951) developed a numerical solution to solve partially plastic closed-end tube under internal pressure. Hill et al. assumed there was no work hardening, and the plastic behavior obeyed Prandtl-Reuss rule. Mendelson (1968) proposed a numerical method for cylinders under internal pressure and thermal stress. It worked for both incremental theory and Hencky theory. The material behavior followed the actual material loading curve. Durban (1979) developed a closed form method based on deformation theory. The material behavior obeyed Ramberg-Osgood model with no elastic part. Chen (1992) proposed a numerical method with the following assumptions: a) Tresca yield criterion, b) deformation theory, c) linear hardening behavior, and d) plane stress condition. This method was used to determine stress, strain and displacement. Durban and Kubi (1992) suggested an analytical method for solving pressurized elastic plastic tubes in plane strain

based on deformation theory. It applied to cylinders in plane strain condition that is described by the Ramberg-Osgood model.

Jahed and Dubey (1996 and 1997) proposed a numerical method for solution of a boundary value problem for elastic-plastic thick wall cylinders using deformation theory of plasticity. In his theory, the constitutive relations are written in a form that is analogous to elastic relations, but allow material parameters to vary in a systematic way. For instance, the effective Young's modulus was reduced on the basis of approximating actual stress and strain curve. Based on this formulation, numerical implementation on a thick wall cylinder was made to get the complete elastic plastic solution on the basis of equivalent elastic solution.

In their theory, Jahed and Dubey assumed that plastic behavior is given by Hencky's total deformation theory

$$\varepsilon_{ij}^{p} = \phi s_{ij} \tag{3.13}$$

where s_{ij} is the deviatoric stress, and ϕ is scalar valued function given by

$$\phi = \frac{3}{2}\frac{\varepsilon_{eq}^{p}}{\sigma_{eq}} \tag{3.14}$$

where ε_{eq}^{p} is the equivalent plastic strain and σ_{eq} is the equivalent stress, as defined below:

$$\varepsilon_{eq}^{p} = \sqrt{\frac{2}{3}\varepsilon_{ij}^{p}\varepsilon_{ij}^{p}} \quad \text{and} \quad \sigma_{eq} = \sqrt{\frac{3}{2}s_{ij}s_{ij}} \tag{3.15}$$

The constitutive equation can be expressed as:

$$\varepsilon_{ij} = \frac{1+\nu_{eff}}{E_{eff}}\sigma_{ij} - \frac{\nu_{eff}}{E_{eff}}\sigma_{kk}\delta_{ij} \tag{3.16}$$

where E_{eff} and ν_{eff} are the effective Young's modulus and Poisson ratio, respectively, where:

$$E_{eff} = \frac{3E}{3+2E\phi} \tag{3.17}$$

$$\nu_{eff} = \frac{3\nu + E\phi}{3+2E\phi} \tag{3.18}$$

These effective parameters depend on the values of stresses, ν, and E at a point. The constitutive equation employed in this theory is used to describe inelastic behavior. The forms of effective moduli are discussed and expressed:

$$\frac{1}{E_{eff}} = \frac{1}{E} + \frac{\varepsilon^p}{\sigma_o} \tag{3.19}$$

$$v_{eff} = \frac{2v\frac{\sigma_o}{E} + \varepsilon^p}{2\frac{\sigma_o}{E} + 2\varepsilon^p} \tag{3.20}$$

for elastic-perfectly plastic behavior, and

$$\frac{1}{E_{eff}} = \frac{1}{E} + \frac{\alpha}{E}\left(\frac{\sigma}{\sigma_o}\right)^{n-1} \tag{3.21}$$

$$v_{eff} = E_{eff}\left[\frac{2v + \alpha\left(\frac{\sigma}{\sigma_o}\right)^{n-1}}{2 + \alpha\left(\frac{\sigma}{\sigma_o}\right)^{n-1}}\right] \tag{3.22}$$

for a uniaxial stress strain curve obeying Ramberg-Osgood model, where σ_o and ε_o are stress and strain at initial yield, respectively.

To implement a procedure for determination of effective moduli, three numerical moduli adjustment scheme were used and discussed in their research, which are projection method, arc-length method, and energy method.

Dubey and Seshadri (2000) presented a concept of analytical method for a pressurized thick wall cylinder using parametric functions. For a bilinear work hardening material,

the stress distribution can be expressed in terms of two chosen parametric functions, $g(r)$ and $f(r)$, which satisfy

$$\sigma_r = g - f \tag{3.23}$$

$$\sigma_\theta = g + f \tag{3.24}$$

$$r^2 \frac{\partial g}{\partial r} = \frac{\partial}{\partial r}\left(r^2 f\right) \tag{3.25}$$

Dubey and Seshadri assigned a constant value for $g = A$ for the elastic or Lame's solution. Eq. (3.25) was then solved to obtain $f = B/r^2$, which involves the coordinate function $1/r^2$. As a consequence, the general expressions for stresses in the elastic solution are $A \pm B/r^2$. In the case of perfectly plastic solid, f is assigned a constant C. Eq. (3.25) then yields a solution $g = A + 2C\ln r$, which involves the coordinate function $\ln r$. Dubey and Seshadri showed that a general solution of the boundary value problem involves both two coordinate functions $1/r^2$ and $\ln r$. Supposing that the solution is continuous across the elastic plastic boundary, the choice of

$$g = g_1 + 2g_2 \ln\left(\frac{r}{r_1}\right) \tag{3.26}$$

$$f = g_2 + \frac{g_1 r_0^2 - g_2 r_1^2}{r^2} \tag{3.27}$$

satisfies the equilibrium as well as the continuity condition, where r_1 is the elastic plastic boundary. The elastic perfectly plastic solution can be obtained by choosing $g_1 r_0^2 - g_2 r_1^2 = 0$. These choices make the boundary value problem statically determinate.

The generalized Hooke's law for linear isotropic elastic behavior is split in volumetric and deviatoric parts:

$$\varepsilon_{kk} = \frac{1-2\nu}{E}\sigma_{kk} \tag{3.28}$$

$$\varepsilon'_{ij} = \frac{1+\nu}{E}\sigma'_{ij} \tag{3.29}$$

In the plastic region, the respective relationships are of the form

$$\varepsilon_{kk} = \frac{1-2\nu}{E}\sigma_{kk} = \frac{1-2\nu_2}{E_2}\sigma_{kk} \tag{3.30}$$

$$\varepsilon'_{ij} = \left(\frac{1+\nu}{E} + \frac{1+\nu_p}{E_p}\frac{\sigma-\sigma_y}{\sigma}\right)\sigma'_{ij} \tag{3.31}$$

This method provides a unified solution for the thick wall cylinder problems, and it has been applied to a sample problem and results were encouraging.

3.2.2 Autofrettage

The application of autofrettage originates in the gun barrel industry of the nineteenth century. With the development of high pressure technology, the application of autofrettage is not limited to the armament industry, but is widely used in industries utilizing high pressure cylindrical vessels, such as chemical reactors and hydrostatic extrusion chambers. The purpose of autofrettage is to obtain a favorable initial stress pattern, by applying a sufficiently high internal pressure to produce plastic flow in the inner portion of pressure vessel as a means of increasing the maximum allowable pressure that the vessel can withstand. This process of autofrettage is carried out by means of hydraulic pressurization, or by pushing an oversized mandrel, or swage through the forging, etc. Once the required permanent deformation is reached, the pressure is released. While the outer layers tend to return to their original dimensions, the inner layers, having been considerably expanded due to plastic deformation, tend to maintain their enlarged diameter. Thus, a residual stress field is introduced in the cylinder's wall. This residual stress is compressive at inner layers and tensile at outer ones. Apart from increasing the pressure bearing capacity of the vessel, the residual stress induced by autofrettage enhances the vessel's fatigue life. The presence of compressive stresses at the bore reduces the probability of crack initiation and slows the growth of fatigue cracks. This enhancement may result in an extension of fatigue life by a factor of up to three (Perl and Arone, 1988).

A reliable prediction of the influence of the autofrettage on the critical crack length and fatigue life of a thick wall cylinder under high pressure requires an accurate prediction of

the actual residual stress field. Therefore it is essential to develop accurate and reliable methods to calculate the residual stress field induced by autofrettage.

Adapting the assumption that the shear strain is inversely proportional to the square of the cylinder radius, Franklin and Morrison (1960) proposed a method of residual stress calculation. Their method requires full knowledge of the shear stress strain properties of the material in pure torsion. In their two-step method, the cylinder is first divided into an even number of equal layers and successive values of strain at the external boundary are assumed. By using the basic assumption that the total shear strain is inversely proportional to the square of the cylinder radius, the shear strain in different layers is calculated. Based on this calculation and using the shear stress-strain curve, the corresponding stress value is read from the torsion curve. With the plane strain state assumed, this method gave reasonable estimate to the residual hoop stress field when compared with experimental measurements of residual stress. However, the axial strain predicted from this method did not agree with experimental results, especially in the proximity of the bore.

Chen (1986) presented a method that incorporated both the Bauschinger effect and the hardening effect due to unloading. From experimental observations of high strength steel behavior, the Bauschinger effect factor is found to be important in determining the range of elastic unloading. After reversed yielding occurs, a very large degree of strain hardening will develop, even when the initial tensile test exhibits very little strain hardening. Chen argued that any discrepancy between the different solutions and the

experimental results was due to two factors: 1) the Bauschinger effect factor dependency on the value of reversed yielding, and 2) the linear hardening response during elastic-plastic unloading. Chen's solution is a two step closed form solution. The first step involves loading of the cylinder. During loading the material is assumed to be elastic-perfectly plastic, obeying Tresca's yield criterion and associated flow theory. In the second step, if the pressure is not sufficient to cause reversed yielding, the unloading is purely elastic. However, if the pressure is high enough to cause reversed yielding, by introducing a Bauschinger factor and a hardening factor, elastic-plastic unloading is analyzed. This method is capable of using a better model of the unloading curve, once the Bauschinger factor and hardening parameter are selected based on actual unloading curve. However, this method is restricted to the elastic-perfectly plastic behavior and Tresca's yield criterion.

Perl and Arone (1994) proposed an axisymmetric stress release method for measuring the autofrettage level in thick wall cylinders. The experimental method is based on measuring the hoop strain while axisymmetrically releasing the residual stress field prevailing in the cylinder's wall. The proposed method was studied numerically by performing finite element simulations of the process for some relevant cylinders with wall thickness ratios from 1.6 to 2.2 and the autofrettage level 50-100 percent. Their study yielded a simple empirical relation that readily enables the determination of the level of autofrettage from released strain measurements.

Seshadri (1994) presented a method for estimating residual stresses and assessing shakedown on the basis of two linear finite element analysis (GLOSS method). Practical pressure components exhibit some local elastic follow-up, and thereby induce smaller residual stresses than those estimated by uniaxial models. GLOSS analysis of sample thick wall cylinders has indicated that the effectiveness of autofrettage can be affected by local follow-up action.

Jahed and Dubey (1997) performed numerical investigation on autofrettaged tubes using a variable material property approach. In their work, three different examples for predicting residual stress field were examined. The first one is the residual stress field based on actual material behavior curve. The other two are based on idealized models, which are isotropic hardening and kinematic hardening models. The residual hoop stress predicted by this method using the actual material curve agrees very well with the experimental measurements near the bore. The authors argued that a closer result to the experimental results could be achieved by using von Mises yield criterion.

Perl (2000) developed an analytical model for predicting the level of autofrettage following either inner, outer, or combined machining of gun barrel based on Hill's solution (1950) for the autofrettage residual stress field. The analysis resulted in simple algebraic expressions for the post-machining level of autofrettage in terms of the original level induced in the blank tube and the geometrical changes the barrel underwent. A finite element analysis of the machining process is performed in which the residual stress

field is simulated by an equivalent thermal load. The numerical results are found to be in excellent agreement with the analytical ones.

Parker (2001) employed a numerical procedure, which generally followed that proposed by Jahed and Dubey (1997), to calculate a wide range of autofrettage pressures and a limited number of hoop and axial residual stress fields for tubes under open end covering tube diameter ratios up to 3.0 and all possible levels of overstrain from 0% to 100%. By focusing upon the value of residual hoop stress at the bore, Parker formulated a design procedure that provides accurate representation over a range of overstrains and of tube diameter ratios. The numerical procedure was also used to compare residual hoop stress values with the relevant section of the ASME Code. The code is shown generally to be modestly conservative, albeit limited to a maximum of 40 percent overstrain for design based upon a specific pressure. This work also extended Jahed and Dubey's numerical procedure (1997) to calculate autofrettage hoop strains at ID and OD for a tube of radius ratio 2 under open end, closed end, and plane strain conditions using von Mises criterion.

4. MOVING BOUNDARY APPROACH

4.1 INTRODUCTION

The moving boundary approach is an analytical method to calculate nonlinear plastic response for cylinders under internal pressure. It incorporates the moving boundary in elastic plastic analysis of thick walled cylinders. Using an iterative procedure based on the principle of virtual work, this approach accounts for the effect of deformed geometry due to high internal pressure.

In this chapter, firstly the constitutive equation is established for elastic plastic analysis based on piecewise linearization concept. It starts from a simple form of bilinear elastic plastic model. Then the concept is extended to actual stress strain curves, which can be modeled as a multi-linear behavior for finite domains of the material. The general form of linearized constitutive equation for finite domains is developed.

Secondly, a generalized method for axisymmetric analysis on thick wall cylinder under high internal pressure is formulated using parametric functions. The formulation provides a generalized solution for thick wall cylinders, which yields Lame's solution and the classical elastic perfectly plastic solution as special cases. As well, it provides elastic plastic solution in closed form for work hardening material using the linearized constitutive equation.

The rules of ASME Pressure Vessels Code, Section VIII, Division 3 constitute general guidance for pressure vessels design with pressure ranging from 10,000 *psi* (0.690×10^2 *MPa*) to approximately 200,000 *psi* (1.379×10^3 *MPa*). Under such high pressure, cylindrical vessels can undergo relatively large deformations and therefore the effect of moving boundary becomes a concern to designers. The proposed method is formulated to take into consideration the deformed geometry. Using the principle of virtual work, an iterative procedure is proposed to obtain elastic plastic solutions on the moving boundary basis. The effects of geometric change on elastic plastic analysis for thick wall cylinder are assessed.

In this research, materials for pressure vessels are assumed homogeneous and isotropic. The components are assumed isothermal.

4.2 PIECEWISE LINEARIZATION OF STRESS STRAIN CURVE

The piecewise linearization approach is a technique to approximate actual stress strain curve for developing a simplified constitutive equation in inelastic analysis. Using this concept, the constitutive equation relates total strains to the current value of stresses in a linear fashion. The nonlinear material behavior of actual stress strain curve is accounted for by dividing the material curve into linear segments, accordingly the material is divided into domains. In each domain, stress and strain relationship is linearized and described by the corresponding constitutive equations. Throughout the material, same form of linearized constitutive equation is adopted, however in each domain different

material parameters are used in the expression of constitutive law. For isotropic materials, the material parameters are E and ν.

4.2.1 Bilinear Model

The generalized Hooke's law for isotropic linear elastic solid can be expressed in the form:

$$\varepsilon_{ij} = \frac{(1+\nu)\sigma_{ij} - \nu\sigma_{kk}\delta_{ij}}{E} \tag{4.1}$$

Although the stress strain behavior for plastic deformation is nonlinear, it can be linearized for analysis. For instance, the incremental theory is an example of a linear relationship between stress and strain increments. Given a bilinear stress strain curve with work hardening behavior, as shown in Fig. 4.1, the constitutive equation for an axisymmetric component can be expressed in a form that resembles the generalized Hooke's law:

$$\varepsilon_{ij} = \frac{(1+\nu_2)\sigma_{ij} - \nu_2\sigma_{kk}\delta_{ij}}{E_2} - \left.\frac{(1+\nu_2)\sigma_{ij} - \nu_2\sigma_{kk}\delta_{ij}}{E_2}\right|_{r=r_1} + \left.\frac{(1+\nu_1)\sigma_{ij} - \nu_1\sigma_{kk}\delta_{ij}}{E_1}\right|_{r=r_1} \tag{4.2}$$

where $E_1 = E$ and $\nu_1 = \nu$ in the elastic segment, E_2 and ν_2 are the corresponding modulus and Poisson's ratio in the plastic segment. The stresses reach yield point at the boundary

r_1 between elastic and plastic segments. The mechanical parameters of material, E_2 and ν_2, are related to plastic modulus E_p and ν_p by following equations:

$$\frac{1}{E_2} = \frac{1}{E} + \frac{1}{E_p} \tag{4.3a}$$

$$\frac{\nu_2}{E_2} = \frac{\nu}{E} + \frac{\nu_p}{E_p} \tag{4.3b}$$

The second and third terms are included in Eq. (4.2) for correction to the plastic strain, which is overestimated by the linearization of stress strain curve in plastic domain. The overestimated strain, ε^{oe} shown in Fig. 4.1, has to be subtracted from the total strain.

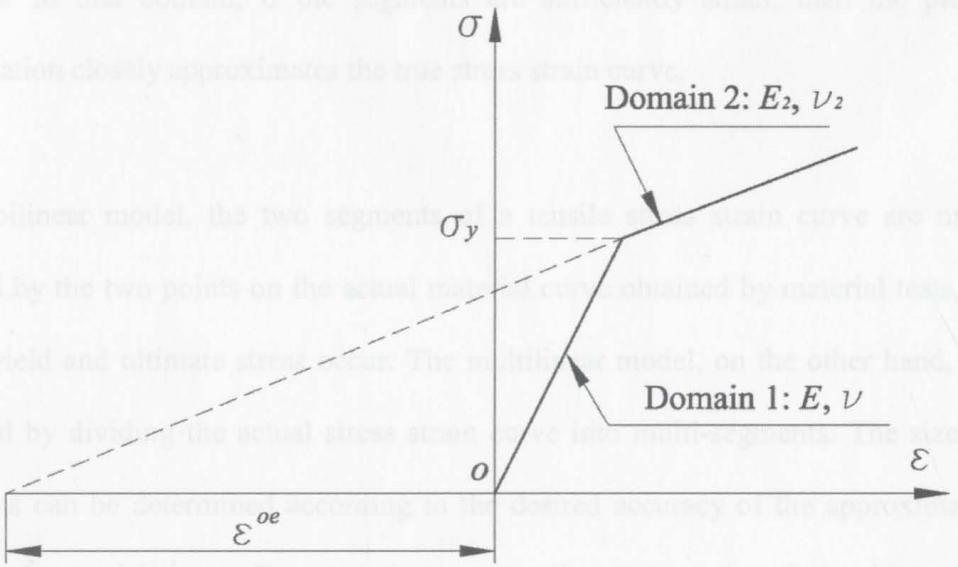

Fig. 4.1 Bilinear stress strain behavior

dividing the after yield region into $k-1$ equal segments, which start from initial yield point to ultimate stress point.

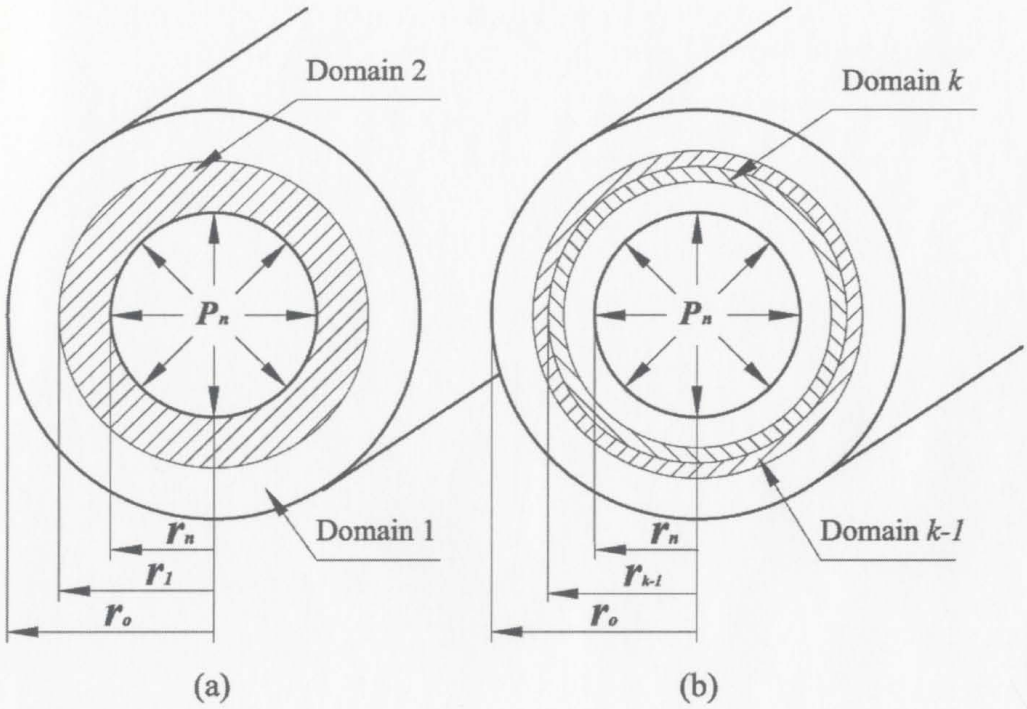

Fig. 4.2 Cylinder geometry and load condition

(a) Two domains model

(b) Finite domains model

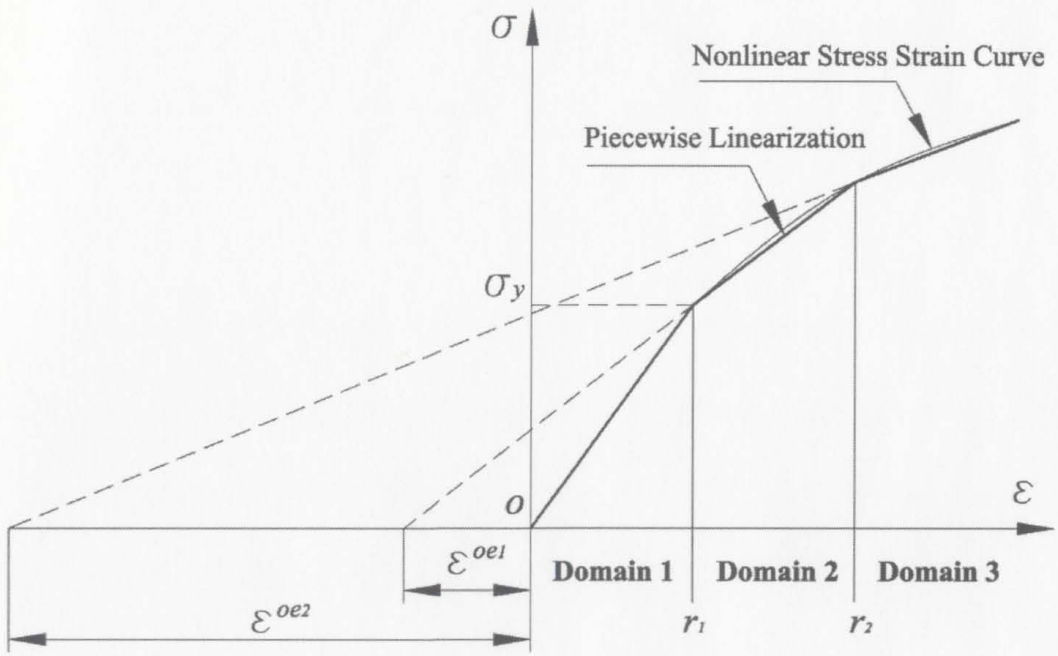

Fig. 4.3 Three domains piecewise linearization of stress strain curve

To derive the generalized formulation of k domains in elastic plastic solid, first consider the case of three domains shown in Fig.4.3. It indicates that strains in domains 2 and 3 are over estimated if it is based entirely on the respective linear stress strain curve. To find the true strain, it is necessary to apply a correction for each crossing from one domain to the next. For example, linear stress strain law of domain 2 overestimates the true strain by ε^{oe1}. This value must be subtracted from the strain of the constitutive equation to obtain actual strain in this domain. Similarly, a crossing from domain 2 to domain 3 would require a correction of ε^{oe2}. In this example, the plastic region consists of two domains. The concept can be readily extended to 'k' domains.

Fig.4.2 (b) illustrates that cylinders can be divided into finite domains in the cross section plane. The $k-1^{th}$ domain and the k^{th} domain share the common boundary at r_{k-1}. In the case of a high strength low-alloy steel 30 Cr Mo 4 (0.3 C, 0.95 Cr and 0.2 Mo) used for cylindrical vessel construction, the experimental stress strain curve of the material can be approximated by a finite number of segments, as shown in Fig. 4.4.

Strain obtained from Eq. (4.1) overestimates the value in k^{th} domain by an amount

$$\varepsilon_{ij}^{k\,oe} = \left\{ \left(\frac{1+\nu_k}{E_k} - \frac{1+\nu_{k-1}}{E_{k-1}} \right) \sigma_{ij} - \left(\frac{\nu_k}{E_k} - \frac{\nu_{k-1}}{E_{k-1}} \right) \sigma_{pp} \delta_{ij} \right\}_{r=r_{k-1}} \tag{4.4}$$

The material parameters of this domain can be expressed in terms of plastic modulus because of

$$\frac{1+\nu_k}{E_k}=\frac{1+\nu}{E}+\frac{1+\nu_p}{E_{pk}}$$

$$\frac{1+\nu_{k-1}}{E_{k-1}}=\frac{1+\nu}{E}+\frac{1+\nu_p}{E_{pk-1}} \tag{4.5}$$

When the material is incompressible in plastic deformation, $\nu_p=1/2$, and strain overestimated due to crossing of the boundary $r=r_{k-1}$ is:

$$\varepsilon_{ij}^{k\,oe}=\left\{\frac{3}{2}\left(\frac{1}{E_{pk}}-\frac{1}{E_{pk-1}}\right)\sigma_{ij}-\frac{1}{2}\left(\frac{1}{E_{pk}}-\frac{1}{E_{pk-1}}\right)\sigma_{pp}\delta_{ij}\right\}_{r=r_{k-1}} \tag{4.6}$$

or

$$\varepsilon_{ij}^{k\,oe}=\frac{3}{2}\left(\frac{1}{E_{pk}}-\frac{1}{E_{pk-1}}\right)\sigma'_{ij}\Big|_{r=r_{k-1}}. \tag{4.7}$$

Therefore, the total overestimated strain including all the previous domains is

$$\varepsilon_{ij}^{oe}=\frac{3}{2}\sum_{m=2}^{k}\left\{\left(\frac{1}{E_{pm}}-\frac{1}{E_{pm-1}}\right)\sigma'_{ij}\right\}_{r=r_{m-1}} \tag{4.8}$$

In summary, the strain in the k^{th} segment can be expressed as:

$$\varepsilon_{ij} = \frac{(1+\nu_k)\sigma_{ij} - \nu_k \sigma_{pp}\delta_{ij}}{E_k} - \frac{3}{2}\sum_{m=2}^{k}\left\{\left(\frac{1}{E_{pm}} - \frac{1}{E_{pm-1}}\right)\sigma'_{ij}\right\}_{r=r_{m-1}} \tag{4.9}$$

Eq. (4.9) is a deformation type of stress strain relationship, which is combined with Hooke's law in such a way that stress-strain law has the same form in all segments, while each segment involves different material parameters. For axisymmetric problems, Eq. (4.9) provides a constitutive equation to conduct elastic plastic analysis for materials exhibiting work hardening behavior.

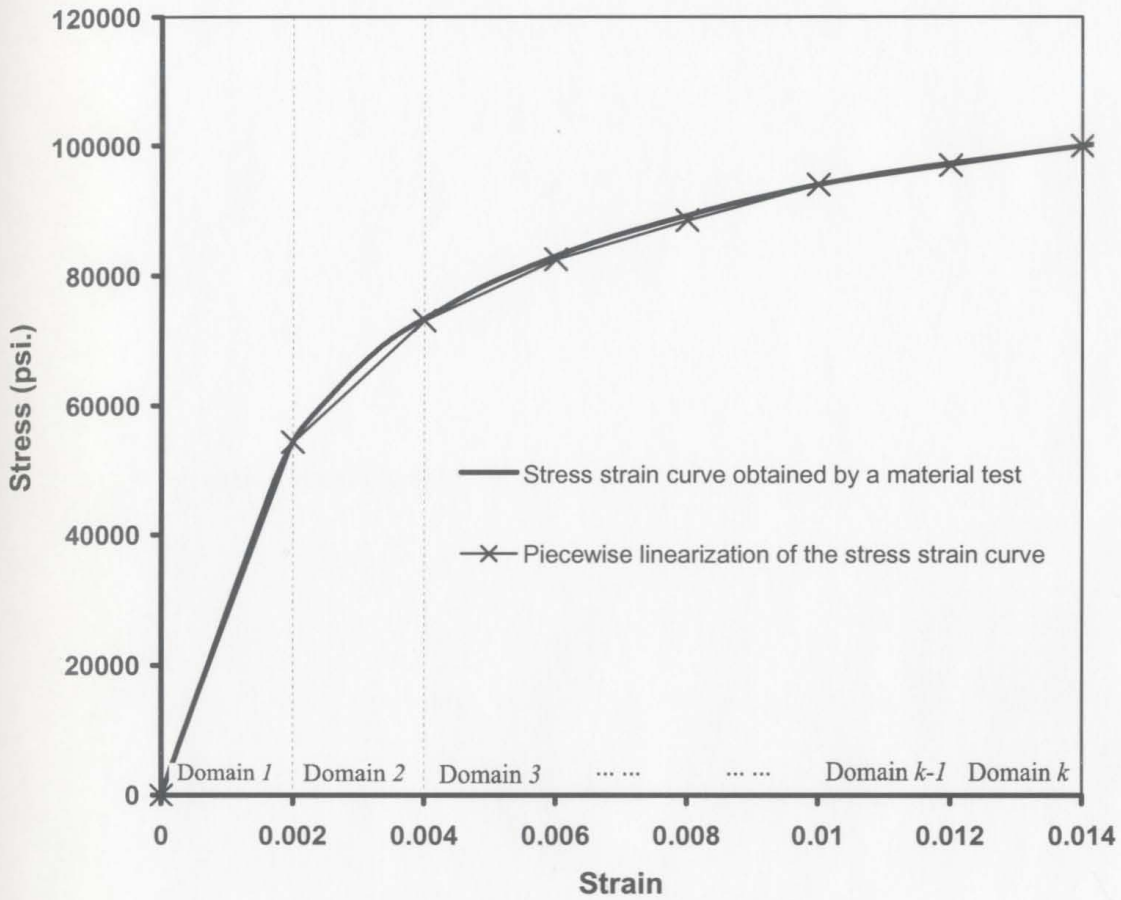

Fig. 4.4 Finite domain piecewise linearization of stress strain curve

4.3 GENERALIZED METHOD OF INELASTIC ANALYSIS FOR CYLINDERS

4.3.1 Introduction

For the most general case, the problem is static indeterminate nonlinear nature. One would need to solve concurrently the equation of equilibrium, strain displacement equation, and constitutive equation along with the appropriate boundary conditions. Further, the general problem will be non-symmetric, and will require arbitrary loading and unloading sequence (Lubliner 1990).

The proposed method provides a generalized solution of inelastic analysis for thick wall cylinders. Solution of the problem is expressed in terms of two parametric functions. The parametric functions satisfy the equilibrium condition, boundary conditions and continuity at the interface between elastic and plastic domains. These two parametric functions involve several constants to describe material behaviors. The relationship between them suggests that Lame's elastic solution and solution for perfectly plastic material depend on special choices for these parameters.

The piecewise linearization of stress strain curve provides a linearized constitutive equation for nonlinear plastic analysis for materials exhibiting work hardening behavior. One important restriction in the selection of parametric functions is that stress strain field associated with each set must be consistent with the chosen segment of the stress strain curve. The restriction is imposed to allow for unloading and reloading, if necessary. This requirement leads to another feature used in the analysis. It involves stress strain law in

plastic deformation. The deformation type of relationship is combined with Hooke's law in such a way that the constitutive equation has the same form in all segments, but each segment involves different material parameters.

Using an iterative procedure based on the principle of virtual work, this method accounts for the effect of deformed geometry due to high internal pressure. The resulting analytical formulation is capable of predicting stress, strain, displacement distribution, and energy for deformation on a moving boundary basis. The formulation is applicable to the analysis of inelastic thick wall cylinders, autofrettage, shakedown and limit analysis.

4.3.2 Thick Wall Cylinders subject to Internal Pressure

4.3.2.1 Formulation

Consider a long cylinder simultaneously expanded by the internal pressure and closed at both ends either by plugs firmly attached to the cylinder, or by floating pistons which allow it to expand freely. The length of the cylinder is assumed so great in relation to its mean diameter that the distribution of stress and strain sufficiently far from the ends does not vary along the cylinder. It then follows that any originally plane cross section remains plane (Hill, 1950). As illustrated in Fig. 4.2, the boundary condition for a thick wall cylinder under internal pressure can be prescribed in the form:

$\sigma_r = 0$ at the outside boundary $r = r_o$

$\sigma_r = -P_n$ at the inside boundary $r = r_n$ (4.10)

For an elastic solid, the maximum stresses occur at the inside boundary, where it is therefore expected to yield first. Beginning from the internal boundary, the plastic zone spreads in an assumed axisymmetrical pattern as the loading increases. It is possible that for some loading, part of the cylinder including the inside surface becomes plastic while the rest including the outside boundary remains elastic, as shown in Fig. 4.2 (a).

Equilibrium equation for cylinder undergoing axisymmetric deformation can be expressed as:

$$\frac{d\sigma_r}{dr} + \frac{\sigma_r - \sigma_\theta}{r} = 0 \tag{4.11}$$

For a general solution of the equation of equilibrium, introduce two parametric functions $g(r)$ and $f(r)$ such that

$$\sigma_r = g(r) - f(r),\ \sigma_\theta = g(r) + f(r) \tag{4.12}$$

These functions satisfy the equilibrium equation (Eq. 4.11) provided:

$$r^2 \frac{dg}{dr} = \frac{d}{dr}\left(r^2 f(r)\right) \tag{4.13}$$

According to the bilinear stress strain curve, it is possible to divide an axisymmetric component, for instance, a cylinder, into two domains as shown in Fig. 4.2(a), where the proposed stress strain relationships can be applied.

4.2.2 Formulation for Finite Domains

The material curve can be divided into a finite number of segments. A linear stress strain relationship is assumed for each segment, but the slope of the curve differs from segment to segment. Correspondingly the cylinder is divided into sections or domains as shown in Fig. 4.2 (b). Linearized stress strain curve implies constant value for material parameters in each linear segment. Since it is possible to divide the axisymmetric components into circular domains such that the stress strain law of one segment describes the material behavior in that domain, if the segments are sufficiently small, then the piecewise linearization closely approximates the true stress strain curve.

For a bilinear model, the two segments of a tensile stress strain curve are naturally decided by the two points on the actual material curve obtained by material tests, where initial yield and ultimate stress occur. The multilinear model, on the other hand, can be obtained by dividing the actual stress strain curve into multi-segments. The size of the segments can be determined according to the desired accuracy of the approximation to the actual material curve. To approximate a tensile stress strain relationship using a k segments curve, segment one is elastic region, which is from the coordinate origin to the initial yield point of the stress strain curve. Segment two to segment k may be defined by

In the case of elastic or Lame's solution, a constant A is assigned to $g(r)$. The above equation is then solved to obtain $f(r) = B/r^2$, where B is a constant. The coordinates function of $f(r)$ is $1/r^2$ and the general form for stresses in the elastic solution is $A \pm B/r^2$. The Lame's solution is applicable only for elastic or linear elastic materials. In the case of perfectly plastic solid (Hill, 1950 or Chakrabarty, 1987), $f(r)$ is assumed constant as C. The above equation then yields a solution $g(r) = 2C \ln r$ involves the coordinate function $\ln r$. This solution does not include the coordinate function $1/r^2$. A general solution of the boundary value problem may involve both coordinate functions, $1/r^2$ and $\ln r$ (Dubey and Seshadri, 2000). For elastic plastic solids, it can be obtained by choosing

$$g(r) = A + 2C \ln r$$

$$f(r) = C + \frac{B}{r^2} \tag{4.14}$$

The constants of the problem A, B, and C can be determined by the boundary and other relevant conditions.

The above solution is constructed on the basis of known elastic and perfectly plastic solutions that already exist in the literature. Further the equation of strain displacement relationship, equilibrium equation as well as constitutive equation are fully considered in the solutions.

Suppose the solution is continuous across the elastic plastic interface, which is located at $r = r_1$, as illustrated in Fig. 4.2 (a). To maintain continuity of stresses across the elastic plastic boundary, choose the plastic domain parameters such that there is no jump in stresses across the interface. This condition leads to

$$g(r) = A_1 + 2C_2 \ln(r/r_1)$$

$$f(r) = C_2 + \frac{A_1 r_o^2 - C_2 r_1^2}{r^2}, \tag{4.15}$$

where suffix 1 refers to the constants in domain 1 or elastic domain, while suffix 2 is for domain 2 or plastic domain. Choice in the above equation satisfies equilibrium as well as the continuity conditions. As a result, stresses in the plastic domain can be obtained as:

$$\sigma_r = -A_1\left(\frac{r_o^2}{r^2} - 1\right) + C_2\left(\frac{r_1^2}{r^2} - 1 - 2\ln\frac{r_1}{r}\right)$$

$$\sigma_\theta = A_1\left(\frac{r_o^2}{r^2} + 1\right) - C_2\left(\frac{r_1^2}{r^2} - 1 + 2\ln\frac{r_1}{r}\right). \tag{4.16}$$

Both elastic and plastic solutions are embedded in the above general solutions. As a result of the choice $C_2 = 0$, Lame's solution is recovered from the generalized form. The plastic solution discussed by Hill (1950) and Chakrabarty (1987) is for elastic perfectly plastic or non work hardening solid. It can be obtained from the generalized solution by choosing $B_2 = A_1 r_o^2 - C_2 r_1^2 = 0$. Such a choice makes the boundary value problem

statically determinate. In this regard, the choices are useful. However, they put restriction on the generality of solutions for elastic plastic solids.

In order to obtain the generalized solution for elastic plastic solids, it is necessary to find an independent condition to evaluate the constants in Eq. (4.16). For this purpose, consider first the constitutive equation. Strains in the elastic domain are obtained from the generalized Hooke's law,

$$\varepsilon_r = \frac{\sigma_r - \nu\sigma_\theta - \nu\sigma_z}{E}$$

$$\varepsilon_\theta = \frac{\sigma_\theta - \nu\sigma_r - \nu\sigma_z}{E} \tag{4.17}$$

$$\varepsilon_z = \frac{\sigma_z - \nu\sigma_r - \nu\sigma_\theta}{E}$$

The compatibility condition,

$$\frac{d\varepsilon_\theta}{dr} = \frac{1}{r}(\varepsilon_r - \varepsilon_\theta) \tag{4.18}$$

and equilibrium equation (Eq. 4.2) yield

$$\frac{d}{dr}\left(\frac{u}{r} + \frac{1+\nu}{E}\sigma_r\right) = \frac{1}{r}\left(\frac{du}{dr} - \frac{u}{r}\right) - \frac{1+\nu}{E}\frac{\sigma_r - \sigma_\theta}{r} \tag{4.19}$$

In view of the constitutive equation and the expression for stresses, the above equation leads to:

$$\frac{d}{dr}\left(\frac{2A_1-\nu\sigma_z}{E}\right)=\frac{d}{dr}\left(\frac{2A_1(1-\nu^2)}{E}-\nu\varepsilon_z\right)=0 \tag{4.20}$$

Since A_1 is constant, this equation suggests that both axial stress and strain remain constant in the elastic domain. The constant value for axial strain suggests that plane sections normal to the axis remain plane and normal. According to Hill (1950), this assumption is expected to hold away from the two ends of cylinders.

Suppose ε_{z_1} is the axial strain and ε_{r_1} and ε_{θ_1} are the radial and hoop strains at the elastic plastic interface $r=r_1$. Use the following version of the linearized stress strain relation in plastic domain

$$\begin{aligned}
\varepsilon_r &= \frac{\sigma_r-\nu_2\sigma_\theta-\nu_2\sigma_z}{E_2}-\left.\frac{\sigma_r-\nu_2\sigma_\theta-\nu_2\sigma_z}{E_2}\right|_{r=r_1}+\varepsilon_{r_1}\\
\varepsilon_\theta &= \frac{\sigma_\theta-\nu_2\sigma_r-\nu_2\sigma_z}{E_2}-\left.\frac{\sigma_\theta-\nu_2\sigma_r-\nu_2\sigma_z}{E_2}\right|_{r=r_1}+\varepsilon_{\theta_1}\\
\varepsilon_z &= \frac{\sigma_z-\nu_2\sigma_r-\nu_2\sigma_\theta}{E_2}-\left.\frac{\sigma_z-\nu_2\sigma_r-\nu_2\sigma_\theta}{E_2}\right|_{r=r_1}+\varepsilon_{z_1}.
\end{aligned} \tag{4.21}$$

The compatibility condition (Eq. 4.18) and the equation of equilibrium (Eq. 4.2) yield

$$\frac{d}{dr}\left(\frac{u}{r}+\frac{1+\nu_2}{E_2}\sigma_r\right)=\frac{1}{r}\left(\frac{du}{dr}-\frac{u}{r}\right)-\frac{1+\nu_2}{E_2}\frac{\sigma_r-\sigma_\theta}{r} \tag{4.22}$$

Using the piecewise linear constitutive relation, the above equation can be rewritten as follows:

$$\frac{d}{dr}\left(\frac{u}{r}+\frac{1+\nu_2}{E_2}\sigma_r\right)=2A_1\frac{1+\nu_p}{E_p}\frac{r_o^2}{r_1^2}\frac{1}{r} \tag{4.23}$$

The assumption that plane sections normal to the axis remain plane and normal implies ε_z = constant. To satisfy this condition, choose

$$C_2=A_1\frac{1+\nu_p}{2E_p}\frac{E_2}{1-\nu_2^2}\frac{r_o^2}{r_1^2} \tag{4.24}$$

or, if assume plastic incompressibility, $\nu_p=1/2$,

$$C_2=\frac{3A_1}{4E_p}\frac{E_2}{1-\nu_2^2}\frac{r_o^2}{r_1^2}. \tag{4.25}$$

Eq. (4.24) or (4.25) provides the additional equation to solve for constants A_1 and C_2.

Eq. (4.25) and the boundary condition at the inside surface

$$P_n = A_1 \frac{r_o^2 - r_n^2}{r_n^2} - C_2 \left(\frac{r_1^2 - r_n^2}{r_n^2} - 2 \ln \frac{r_1}{r_n} \right) \tag{4.26}$$

along with the yield criterion provide three equations to solve for three constants. Therefore, they make the boundary problem statically determinate.

Tresca yield criterion yields

$$A_1 = \frac{r_1^2}{2r_o^2} \sigma_Y \tag{4.27}$$

where σ_Y is the initial yield stress. For Mises' solid,

$$\sqrt{3\left(A_1 \frac{r_o^2}{r_1^2} \right)^2 + (\sigma_z - A_1)^2} = \sigma_Y \tag{4.28}$$

Besides, three end conditions of cylinders that have been used in the calculation are:

$$\begin{array}{ll} \sigma_z = 0 & \text{open end} \\ \sigma_z = 2\nu A_1 & \text{plane strain} \\ \sigma_z = A_1 & \text{closed end} \end{array} \tag{4.29}$$

The corresponding values for axial strains are:

$$\varepsilon_z = -\frac{2\nu A_1}{E} \qquad \text{open end}$$

$$\varepsilon_z = 0 \qquad \text{plane strain} \tag{4.30}$$

$$\varepsilon_z = \frac{1-2\nu}{E} A_1 \qquad \text{closed end}$$

4.3.2.2 Deformed Geometry and Undeformed Geometry

Deformation due to external load causes the geometry to change. As a result, the load applied to a boundary moves it from its undeformed to deformed position. In the classical theory, displacement is assumed small and hence it is permissible to replace the deformed position of a particle by its initial undeformed position. This argument can be reversed in favor of deformed geometry. That is, it is permissible to use the deformed position of a particle in place of its undeformed position because of small displacement. Further, the consistency of analysis requires the use of deformed geometry if the boundary value problem is formulated in terms of true stress and true traction. Hence, the deformed geometry is incorporated in this research to predict elastic plastic behavior. Thus, the traction boundary conditions are satisfied on the deformed radii.

Suppose the radial displacement

$$u = r - R \tag{4.31}$$

where R and r are respectively the initial and deformed radii. For an axisymmetric component, it is possible to express deformed radius in terms of initial radius and hoop strain:

$$r = (1 + \varepsilon_\theta)R \tag{4.32}$$

The proposed formulation is both admissible for original geometry and deformed geometry.

4.3.3 Application of the Virtual Work Principle

Energy density of deformation can be expressed as:

$$U_0 = \int(\sigma_r d\varepsilon_r + \sigma_\theta d\varepsilon_\theta + \sigma_z d\varepsilon_z) \tag{4.33}$$

The term involving axial stress and strain may drop out because of the constant axial strain. Therefore, this leads to the following expression for energy density:

$$U_0 = \int \frac{(\sigma_\theta + \sigma_r)d(\varepsilon_\theta + \varepsilon_r) + (\sigma_\theta - \sigma_r)d(\varepsilon_\theta - \varepsilon_r)}{2} \tag{4.34}$$

According to its definition, the energy of deformation can be therefore written as

$$U = \iint U_0 r dr d\theta \tag{4.35}$$

In elastic segment of a bilinear solid, the elastic strain energy density is

$$U_{0el} = \frac{1-\nu}{E} A_1^2 + \frac{1+\nu}{E} \frac{r_o^4}{r^4} A_1^2 \qquad \text{open end} \tag{4.36}$$

$$U_{0el} = \frac{\left(1-\nu-2\nu^2\right)}{E} A_1^2 + \frac{\left(1+\nu\right)}{E} \frac{r_o^4}{r^4} A_1^2 \qquad \text{plane strain} \tag{4.37}$$

$$U_{0el} = \frac{\left(1-2\nu\right)}{E} A_1^2 + \frac{\left(1+\nu\right)}{E} \frac{r_o^4}{r^4} A_1^2 \qquad \text{closed end} \tag{4.38}$$

Therefore, the strain energy required for elastic deformation can be obtained from

$$U_{el} = 2\pi \left[-\frac{A_1^2 r_o^2 \nu}{E} + \frac{A_1^2 \left(-r_1^4 + r_1^4 \nu + r_o^4 + r_o^4 \nu\right)}{2E r_1^2} \right] \qquad \text{open end} \tag{4.39}$$

$$U_{el} = 2\pi \left[-\frac{A_1^2 r_o^2 \nu(1+\nu)}{E} + \frac{A_1^2 \left(-r_1^4 + r_1^4 \nu + 2r_1^4 \nu^2 + r_o^4 + r_o^4 \nu\right)}{2E r_1^2} \right] \qquad \text{plane strain} \tag{4.40}$$

$$U_{el} = 2\pi \left[-\frac{3A_1^2 r_o^2 \nu}{2E} + \frac{A_1^2 \left(-r_1^4 + 2r_1^4 \nu + r_o^4 + r_o^4 \nu\right)}{2E r_1^2} \right] \qquad \text{closed end} \tag{4.41}$$

Alternatively, a general form of strain energy density can be derived using the variational method. Virtual strain energy δU can be acquired in a body of volume V as a result of virtual straining,

$$\delta U = \int_{v} \sigma_{ij} \delta \varepsilon_{ij} dV \tag{4.42}$$

Using Eq. (4.1), the virtual strain energy density can be expressed as:

$$\delta U_0 = \frac{(1+\nu)\sigma_{ij}\delta\sigma_{ij} - \nu\delta\sigma_{kk}\delta_{ij}\sigma_{ij}}{E} \tag{4.43}$$

Applying the summation convention, Eq. (4.43) can be written as:

$$\delta U_0 = \frac{(1+\nu)\sigma_{ij}\delta\sigma_{ij} - \nu\delta\sigma_{kk}\sigma_{ii}}{E} \tag{4.44a}$$

or

$$\delta U_0 = \delta\left[\frac{(1+\nu)\sigma_{ij}^2 - \nu\sigma_{kk}^2}{2E}\right] \tag{4.44b}$$

Therefore, a general form of strain energy density for elastic solids can be expressed as:

$$U_{0el} = \frac{(1+\nu)\sigma_{ij}^2 - \nu\sigma_{kk}^2}{2E} \tag{4.45}$$

The general expression of energy density required for elastic plastic deformation, which consists of elastic strain energy and plastic energy dissipation, can be obtained using the piecewise linearized stress strain curve:

$$U_{0pl} = \frac{(1+\nu_2)\sigma_{ij}^2 - \nu_2\sigma_{kk}^2}{2E_2} - \left.\frac{(1+\nu_2)\sigma_{ij}^2 - \nu_2\sigma_{kk}^2}{2E_2}\right|_{r=r_1} + \left.\frac{(1+\nu)\sigma_{ij}^2 - \nu\sigma_{kk}^2}{2E}\right|_{r=r_1} \tag{4.46}$$

The energy required for deformation in plastic zone of the cylinder is therefore

$$U_{pl} = 2\pi \int_{r_n}^{r_1} U_{0pl} r dr \tag{4.47}$$

The work done by the external traction is

$$W = \frac{\pi P_n \left(r_n^2 - R_n^2\right)}{2} \tag{4.48}$$

where R_n and r_n are the initial inside radius and deformed inside radius, respectively.

The principle of work energy balance or $W = U$ can be used to derive the condition

$$\frac{\pi P_n\left(r_n^2 - R_n^2\right)}{2} = 2\pi\left[\int_{r_1}^{r_o} U_{0el} r dr + \int_{r_n}^{r_1} U_{0pl} r dr\right] \tag{4.49}$$

Eq. (4.49) provides the condition to solve boundary value problems on a moving boundary basis. The principle of virtual energy can be used to create an iterative calculation scheme to account for the deformed geometry in elastic plastic analyses since it is applicable for both elastic and plastic materials.

4.4 IMPLEMENTATIONS

4.4.1 Analytical Method

The proposed method is an analytical technique for elastic plastic analysis. To obtain a valid solution of the deformable solid, three basic equations must be satisfied, namely, equilibrium equation, compatibility equation and constitutive equation. For the solid undergoing permanent deformation, a yield criterion is also needed to predict and quantify the plastic behavior.

As discussed earlier in this chapter, equilibrium and compatibility conditions have been formulated in the form of first order differential equations. The constitutive equation is linearized to describe the inelastic material behavior by the piecewise linearization concept.

Considering the axisymmetric boundary conditions and other components of predicting plastic behaviour of solids, the following equations can be obtained to initiate the solving procedure for a thick wall cylinder of materials obeying von Mises criterion:

$$C_2 = A_1 \frac{(1+\nu_p)E_2}{2(1-\nu_2^2)E_p} \frac{r_o^2}{r_1^2} \tag{4.50}$$

$$A_1\left(r_o^2 - r_n^2\right) - C_2\left[\left(r_1^2 - r_n^2\right) - 2r_n^2 \ln\frac{r_1}{r_n}\right] = P_n r_n^2 \tag{4.51}$$

$$A_1 = \frac{r_1^2 \sigma_Y}{\sqrt{3r_o^4 + (1-q)^2 r_1^4}} \tag{4.52}$$

where q is a parameter determined by the assumed end condition. For plane stress condition, $q = 0$; for plane strain condition, $q = 2\nu$; and $q = 1$ for closed end condition.

For material obeying Tresca criterion, Eq. (4.52) is replaced by the following equation to solve the boundary value problem:

$$A_1 = \frac{r_1^2 \sigma_Y}{2r_0^2} \tag{4.53}$$

4.4.2 Iterative Technique for Moving Boundary Solutions

Stress and strain distribution can be expressed in terms of two parametric functions by solving the formulated boundary value problem. The displacement field and energy required for elastic and plastic deformation can also be expressed in terms of the two parametric functions. Solutions obtained in this step are based on the undeformed geometry.

To obtained solutions on a moving boundary basis, the principle of virtual energy can be used to develop a program for calculating plastic response. The program accounts for the deformed geometry using an iterative updating scheme.

The formulation for elastic plastic analysis is implemented by equating work done by external pressure and internal energy required for deformation, which consists of strain energy and plastic energy dissipation. Geometry or boundary of the cylinder is updated using the deformation calculated by the principle of virtual work. Then a successive analysis is carried out, and energy for deformation and work done by external pressure are evaluated on a moving boundary basis. The current solutions are used to update the geometry of the cylinder and the parametric functions in an iterative manner. The final solutions are obtained until the convergence at required accuracy is achieved.

This iterative calculation procedure is illustrated in the following flow chart:

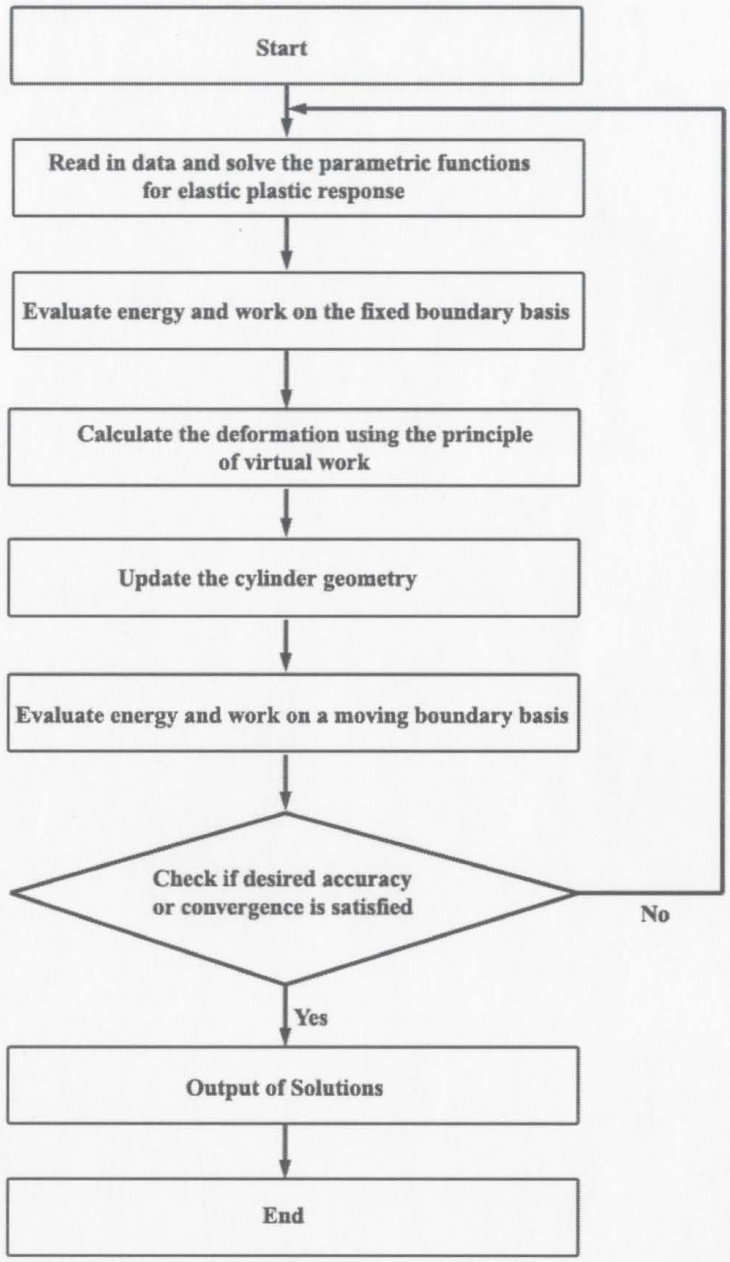

Fig.4.5 Iterative calculation procedure for moving boundary solutions

4.5 EXAMPLES AND CALCULATIONS

The proposed method differs from the conventional analytical method for thick wall cylinders in the following aspects: it is capable of performing elastic plastic analysis on the moving boundary basis; and the generalized solution is expressed in terms of two parametric functions to represent the work hardening behavior.

In this study, thick wall cylindrical pressure vessels are treated as cylinders subjected to internal pressure. Various geometries of cylinders in this study include inside radii, diameter ratios, and various end conditions, such as closed end, open end, and plane strain. The material is assumed to obey linear hardening behavior, as a simple example of the piecewise linearization of the actual stress strain curve. Properties of the material are:

$E = 30 \times 10^6 \ psi \left(2.068 \times 10^5 \ MPa\right)$
$\sigma_Y = 30{,}000 \ psi \left(2.068 \times 10^2 \ MPa\right)$
$\nu = 0.3$
$\nu_p = 0.5$

Maple 6.0 programming language has been used to perform elastic and inelastic analyses on the moving boundary basis. As well, finite element models have been developed. The ANSYS finite element computer program has been used to generate the FEA models and perform linear and nonlinear analysis. The 2-D solid element, Plane 42, is used with axisymmetric option to calculate elastic plastic deformation. Results of finite element analysis (FEA) have been obtained to compare with those of the proposed method.

4.5.1 Internal Pressure

The proposed method can be used to perform analyses on both moving boundary and original boundary basis. When the internal pressure is lower than the initial yielding pressure, the results based on undeformed geometry are the same as Lame's solution. If the internal pressure is increased to the values greater than the initial yielding pressure, plastic deformation initiates at the inside surface and proceeds outward through the cylinder wall. The interface between the plastically deformed region and the elastic region will eventually reach the outer surface at a value of pressure, known as the 'plastic collapse pressure'. The limit pressure that causes yielding throughout the wall thickness can be determined by the proposed approach.

For closed end cylinders, the elastic plastic interface and its corresponding internal pressure are calculated by the moving boundary approach. Results are plotted in Fig. 4.6. The cylinders have a same inside radius of 6 *in.* (0.152 *m*) but with diameter ratios (d_o/d_n) varying from 2 to 3. The material is assumed to follow the linear hardening behavior with the tangent modulus $E_2 = 30\times10^4\ psi.\left(2.068\times10^3\ MPa\right)$. In Fig.4.6, the internal pressure is normalized by yield stress and the elastic plastic interface is normalized by the inside radius.

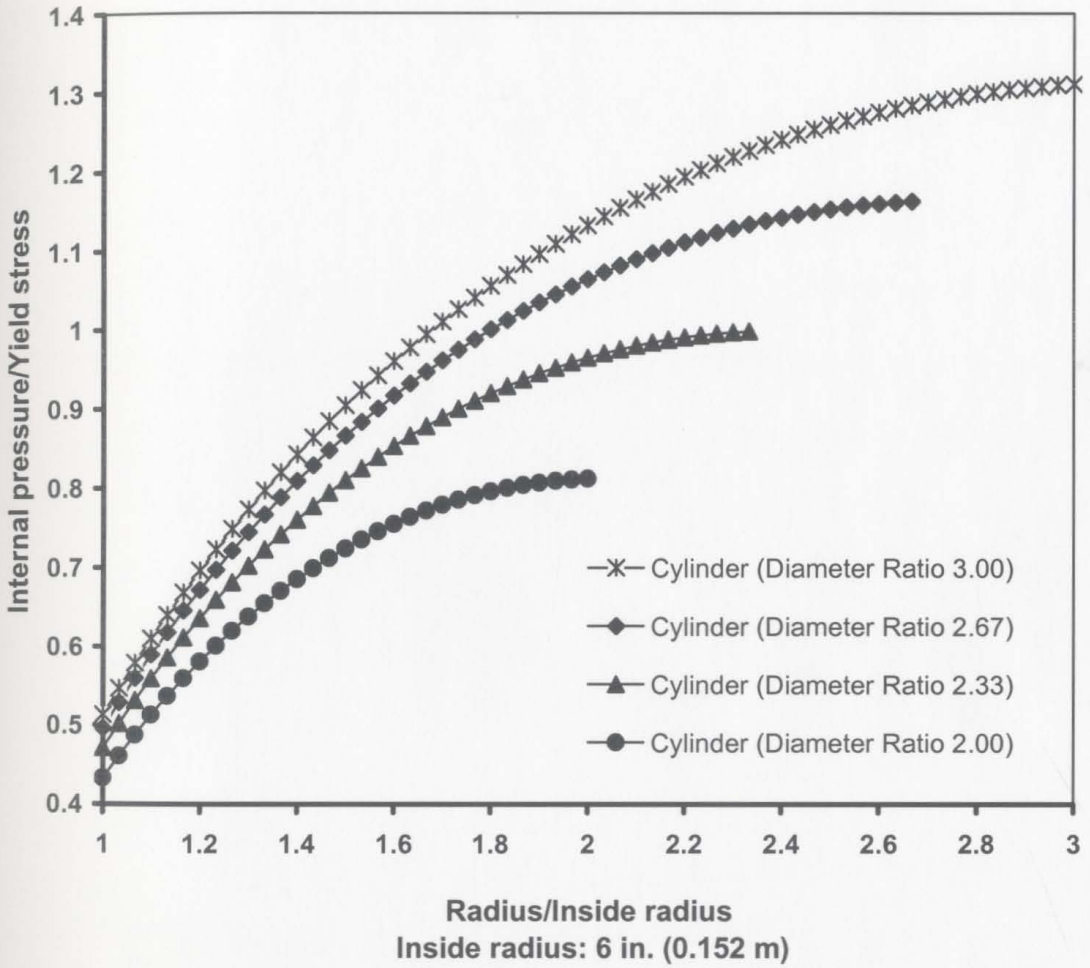

Fig. 4.6 Internal pressures vs. elastic plastic interfaces

The calculation indicates that for a work hardening material, the influence of wall thickness of cylinders on initial yielding and ultimate collapse are different. It may be a common sense that increase of wall thickness can certainly enhance the pressure bearing capability. However, Fig. 4.6 shows that the increase of plastic collapse pressure due to increased wall thickness is much larger than that of initial yield pressure.

4.5.2 Stress and Strain Distributions

Stress and strain distributions have been calculated by the proposed method on the moving boundary basis. For the purpose of comparison, finite element models have been established and detailed linear and nonlinear finite element analyses have been performed using the ANSYS computational program. The element type is PLANE 42 with key option 3 for axisymmetric problem. The analysis type is static on the large deformation basis.

4.5.2.1 Closed End Cylinders

Fig. 4.7 shows the successive distributions of hoop, radial and axial stresses for a thick wall cylinder undergoing plastic deformation. The cylinder under study has a 6 *in.* (0.152 *m*) inside radius and a 12 *in.* (0.305 *m*) outside radius. Results indicate the pattern of stress distributions as the internal pressure increases in magnitude and the plastic region grows from inside surface towards outside surface.

For a closed end cylinder having a 4 *in.* (0.102 *m*) inside radius and a 20 *in.* (0.508 *m*) outside radius, stresses obtained by the proposed method are compared with those of the detailed FEA. The comparison in Fig.4.8 shows the difference between the results using proposed method and finite element analysis with relatively coarse meshing. Fig. 4.8 indicates the difference in terms of hoop and radial stresses mainly occurs in the vicinity of elastic plastic interface. However, as a finer mesh is employed in finite element analyses, the difference is significantly reduced. Eventually the results of these two methods coincide when the size of finite elements is small enough in nonlinear FEA. There is some discrepancy between proposed method and FEA in term of axial stress, mainly in the near bore region. It occurs because the assumption of plane sections remaining plane is involved in the formulation of the proposed method. In general, results of the inelastic analysis using the proposed method and nonlinear finite element analysis are in good agreement.

In the same manner, strain distributions using the proposed method and finite element analysis are plotted in Fig. 4.9. As well, the comparison indicates a general consistency between results using the moving boundary method and nonlinear FEA.

4.5.2.2 Open End Cylinders

Open end condition refers to plane stress of cylindrical tube. Fig. 4.10 shows the stress components and equivalent stress distributions as the internal pressure increases from $0.7\sigma_Y$ to $0.9\sigma_Y$ for an open end cylinder. The inside radius of the cylinder is 4 *in.*

(0.102m). The diameter ratio is 5. Fig. 4.11 shows the patterns of strain distributions when the applied internal pressures are $0.7\sigma_Y$, $1.0\sigma_Y$, $1.3\sigma_Y$, and $1.6\sigma_Y$, respectively. The axisymmetric plastic zone expands from inside surface to outside surface due to increased internal pressure.

4.5.2.3 Plane Strain Cylinders

Fig. 4.12 shows the stress distribution of thick wall cylinders of plane strain condition. The diameter radio of the studied cylinder is 5 and its inside radius is 4 *in*. (0.102 *m*). The internal pressure is 30,000 *psi* (2.068×10^2 *MPa*). The ANSYS nonlinear finite element analysis (NLFEA) has been performed for the purpose of comparison. The FEA model uses 40 plane 42 elements of axisymmetric condition. Analysis type is the static analysis on large deformation basis. This figure shows that the results of radial and hoop stress obtained by the moving boundary approach are in good agreement with those of the large deformation NLFEA.

Strain distribution of the plane strain cylinder has been evaluated by the moving boundary approach. Results are compared with those by nonlinear finite element analysis, as shown in Fig. 4.13. The comparison indicates the results calculated by the proposed method are generally consistent with those by nonlinear finite element analysis.

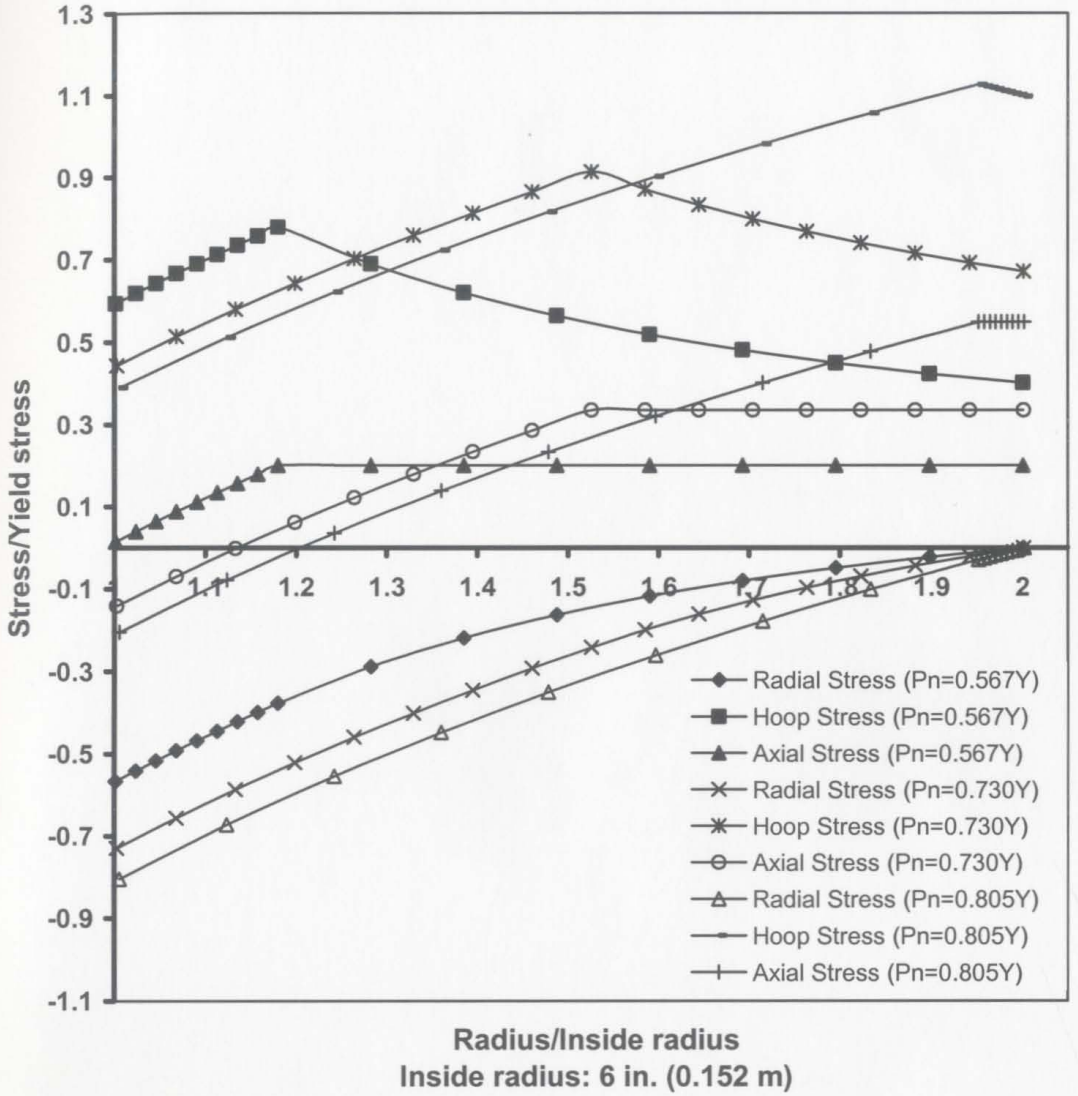

Fig. 4.7 Successive stress distributions in a closed end cylinder

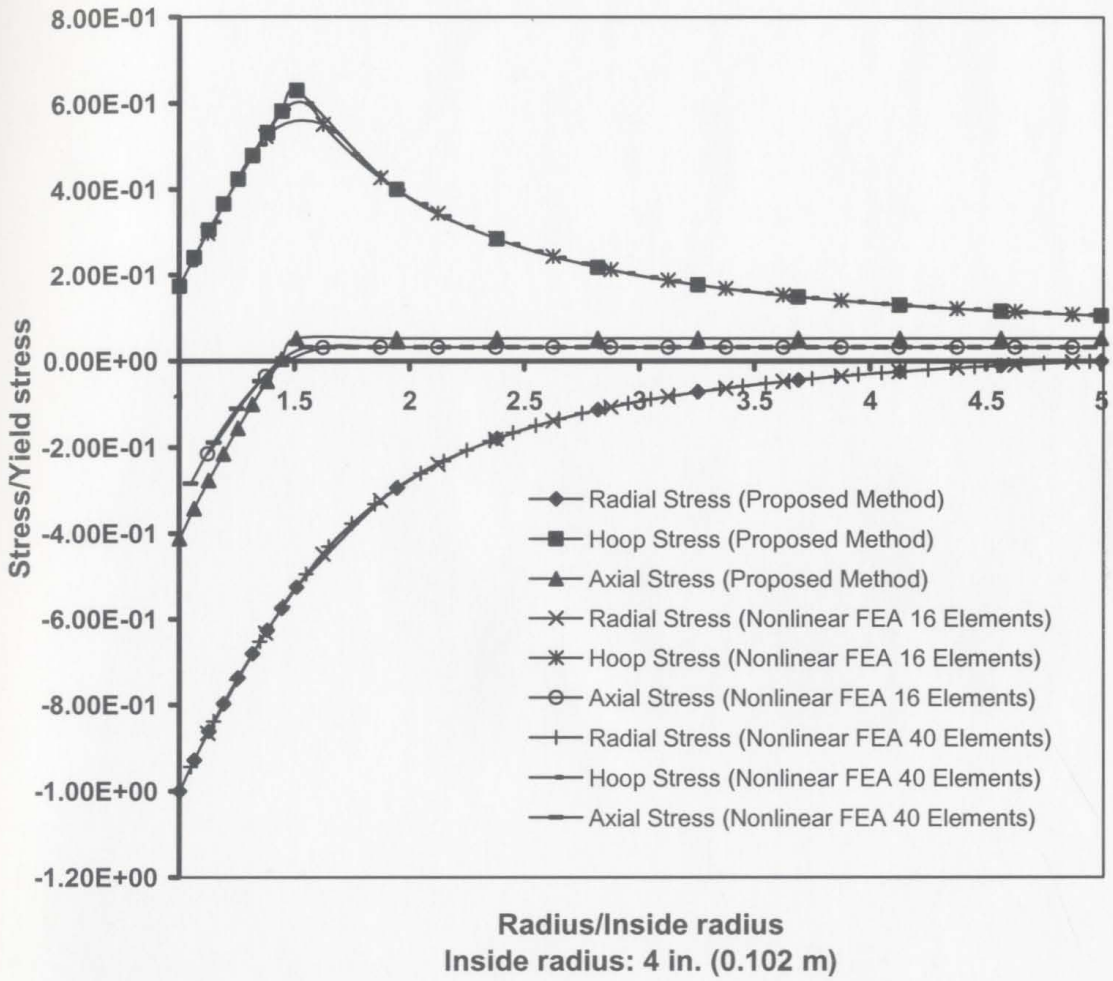

Fig. 4.8 Stress distributions in a closed end cylinder

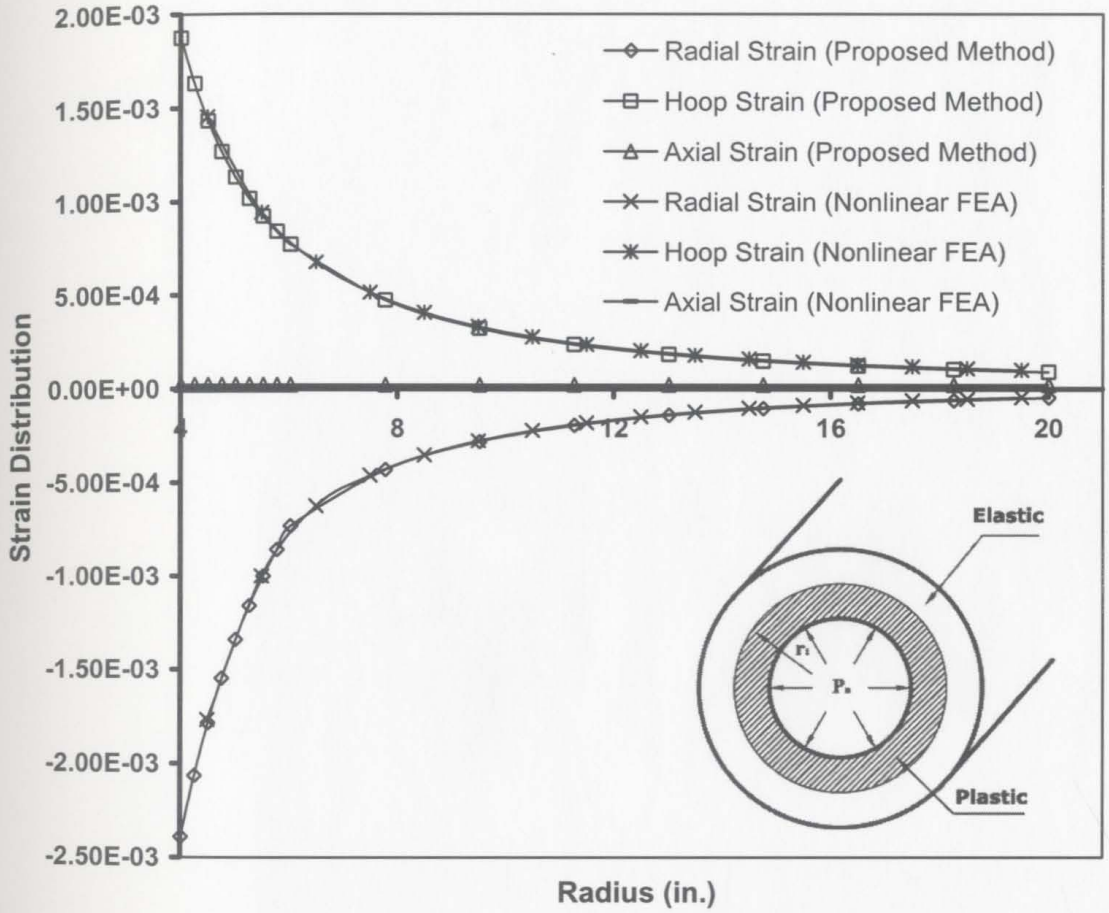

Fig. 4.9 Strain distributions in a closed end cylinder

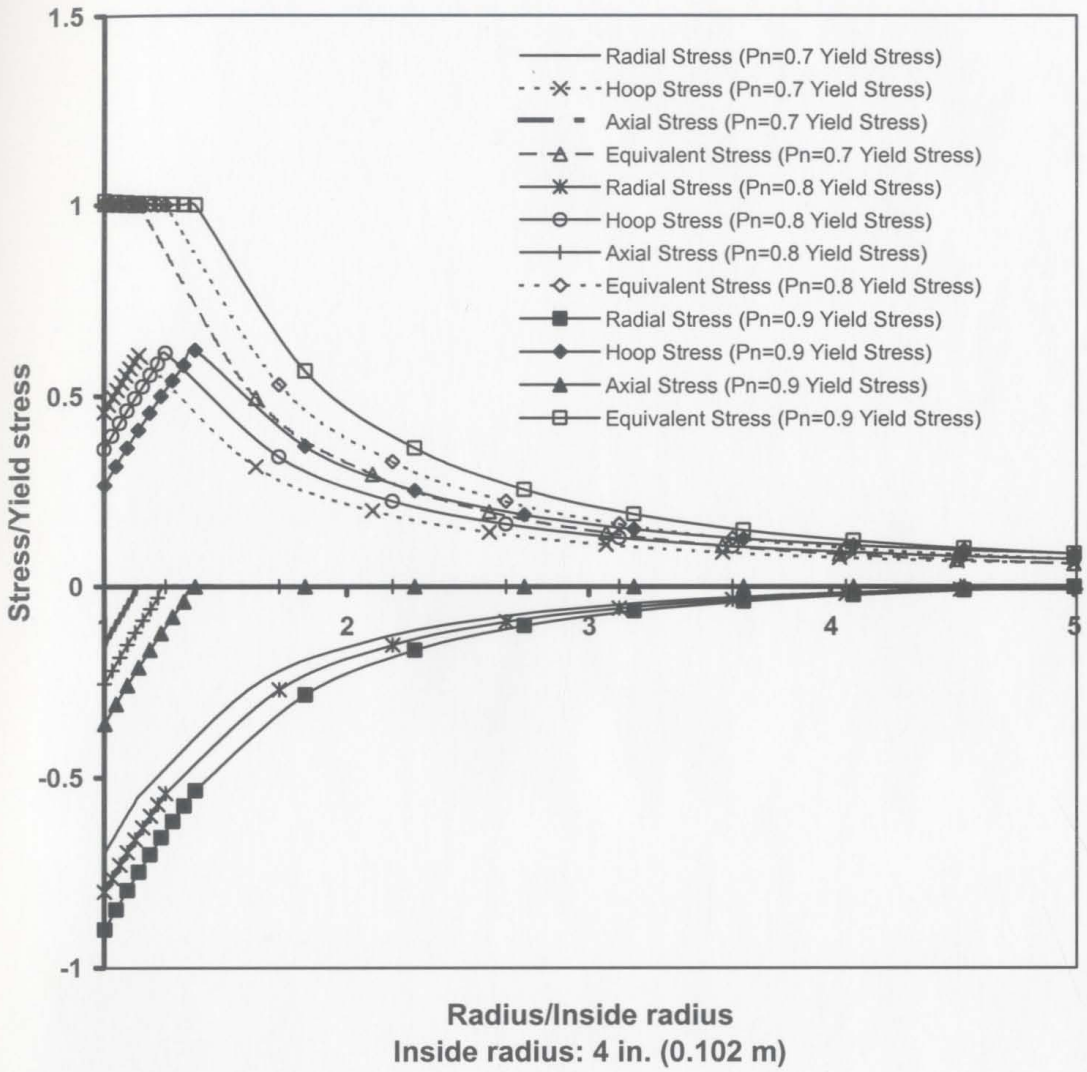

Fig. 4.10 Stress distributions in an open end cylinder

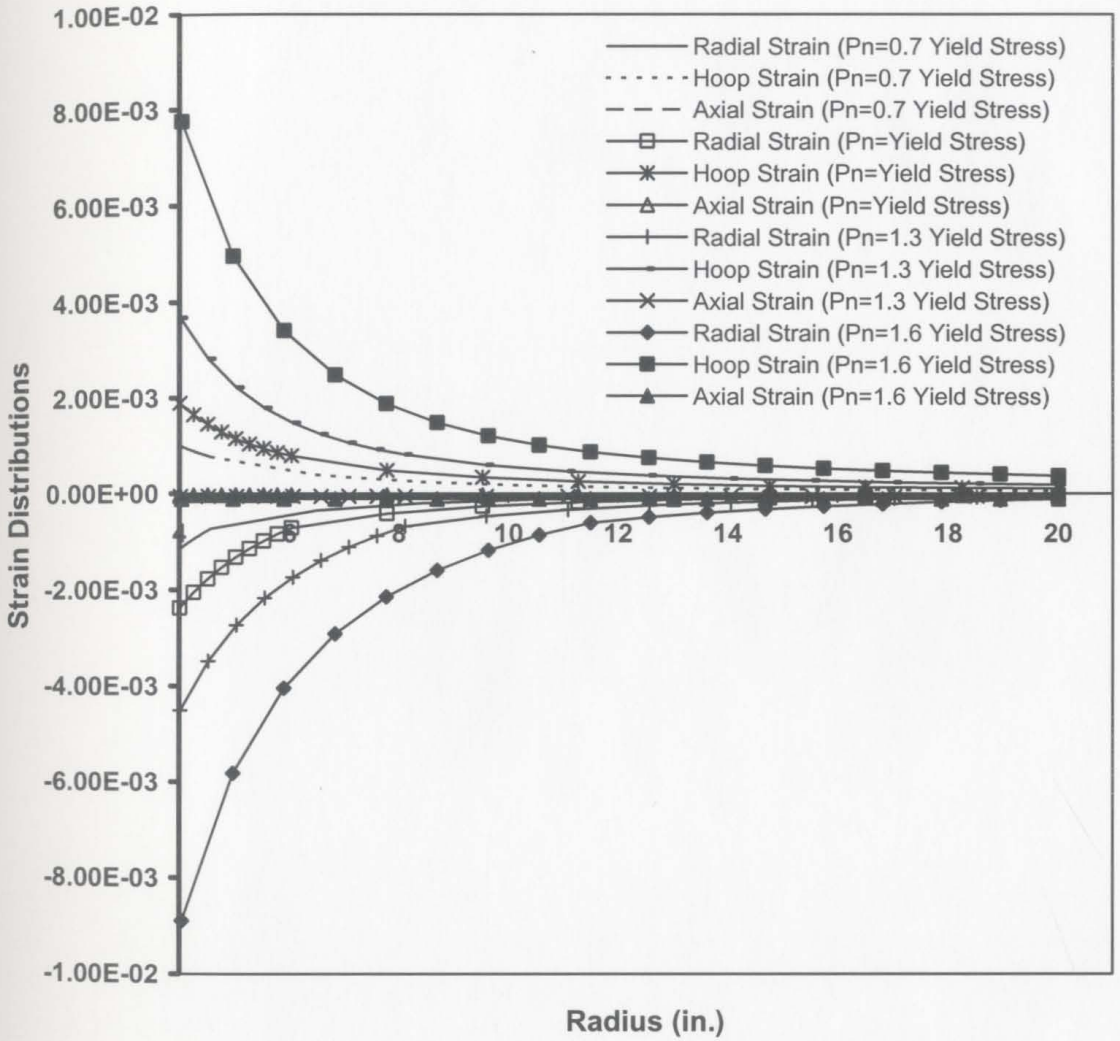

Fig. 4.11 Strains distributions as plastic zone expands in an open end cylinder

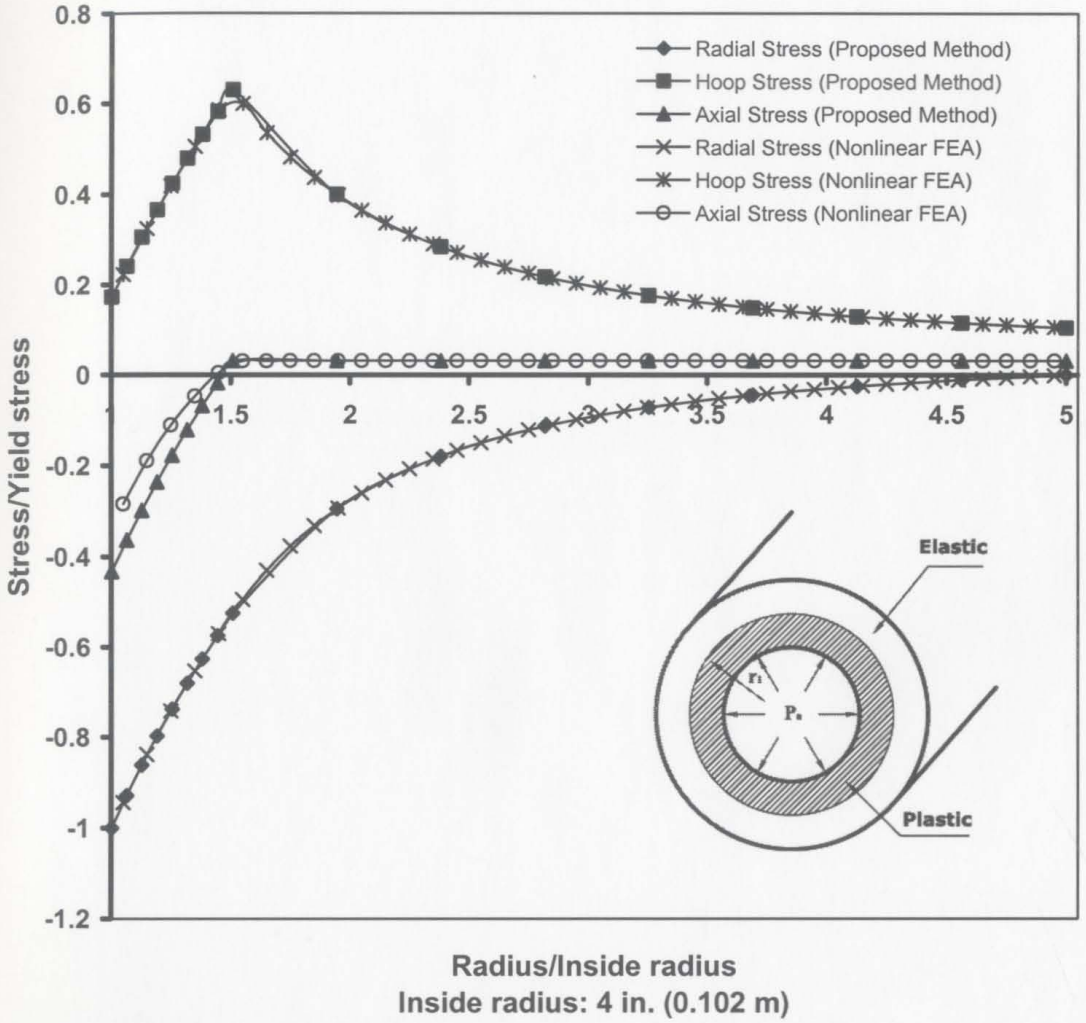

Fig. 4.12 Stress distributions in a plane strain cylinder

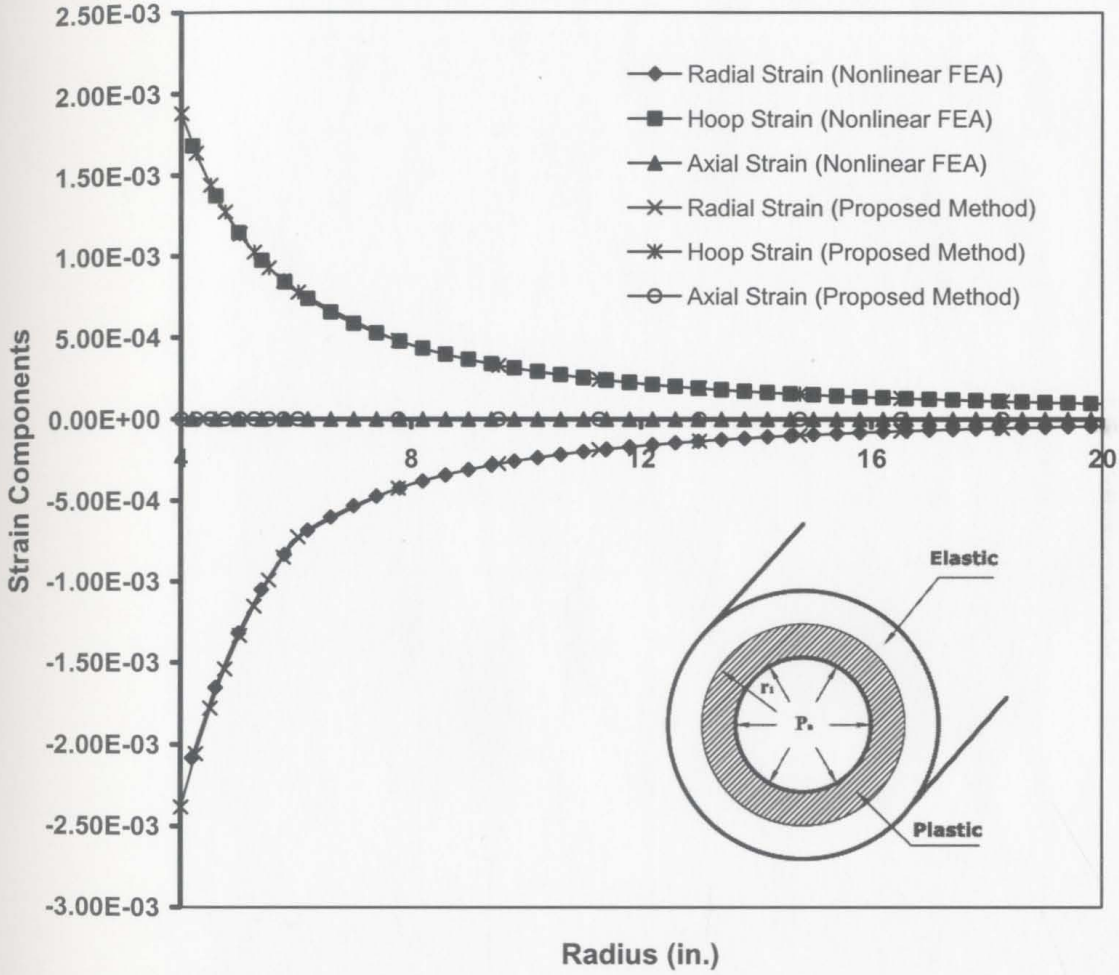

Fig. 4.13 Strain distributions in a plane strain cylinder

4.5.3 Effect of End Conditions

In general, closed end, open end, and plane strain are the three types of end conditions for thick wall cylinders. Plane strain condition is intermediate to closed end and open end conditions. It is nearer to the closed end condition and is strictly equivalent when the material is incompressible. In all three cases, the radial and hoop stresses are the same and only depend on internal pressure. The axial or longitudinal stress has different distribution for different end conditions. Results in Fig. 4.7, Fig. 4.8, Fig. 4.10, and Fig. 4.12 show that axial stress is intermediate to those of radial and hoop stress components.

If Tresca criterion is adopted, the yield pressure depends on yield stress of the material and the diameter ratio of the cylinder. In the case of von Mises criterion, the end condition affects the yield pressure because the axial stress depends on the end condition. Yield pressure can be expressed in the following equation:

$$P_Y = \frac{\sigma_Y\left(t^2 - 1\right)}{\sqrt{(q-1)^2 + 3t^4}} \tag{4.54}$$

where t is diameter ratio $\frac{d_o}{d_n}$ and q is the end condition parameter. For plane stress, plane strain and closed end, q is 0, 2ν, and 1, respectively. Fig 4.14 shows the yield pressure estimate for cylinders under various end conditions. The inside radius of the cylinders under study is 4 *in.* (0.102 *m*). The overall effect of end conditions is trivial because the difference made by various end conditions is less than 1%.

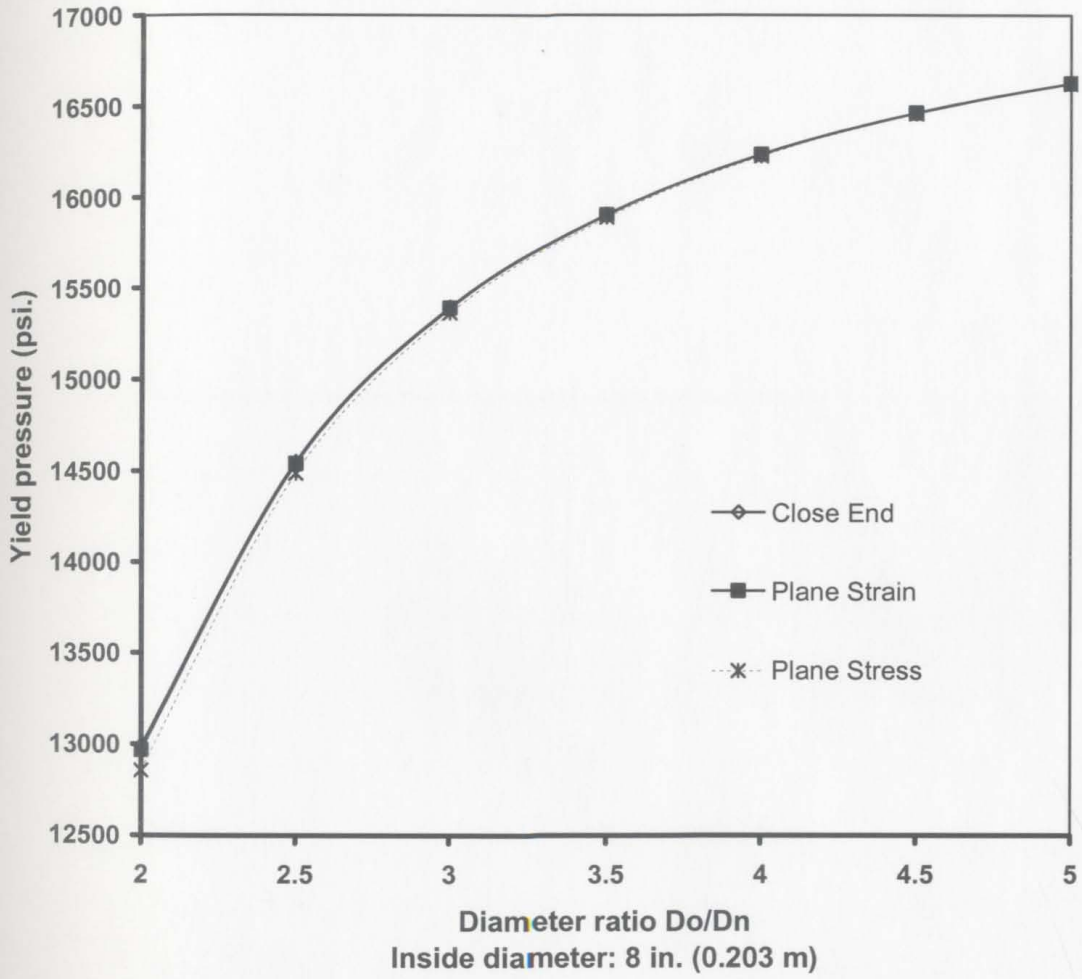

Fig. 4.14 Yield pressure vs. diameter ratio for cylinders under various end conditions

4.5.4 Displacement Calculations

Classical theory of cylinders and ASME Pressure Vessel code are based on the assumption that boundary displacement caused by external load is negligible, therefore fixed or original model is used to investigate the behaviour of solid whose geometry actually has already deformed or the boundary has moved.

The above assumption simplifies the procedure of calculating displacement fields while it can still offer reasonable results in elastic plastic analysis. However, for thick wall cylinders subject to internal pressure from 10,000 *psi* (0.690×10^2 *MPa*) to approximately 200,000 *psi* (1.379×10^3 *MPa*), the geometric change induced by high internal pressure can be an important concern for design and analysis.

The cylinder used in displacement calculations has a dimension of a 4 *in.* (0.102 *m*) inside radius and a 20 *in.* (0.508 *m*) outside radius. The end condition is assumed to be plane strain. In this study, stress distributions do not show significant changes with respect to undeformed geometry and deformed geometry. However, as Fig 4.15 shows, inside surface radial displacements calculated on the moving boundary basis are larger than those of the original boundary theory. The difference is negligible for elastic material behaviour but increases with the internal pressure for plastic material behaviour. For example, the difference is 3.8% when internal pressure is 50,000 *psi* (3.447×10^2 *MPa*) and 10.7% when the pressure is 55,000 *psi* (3.792×10^2 *MPa*). Nonlinear finite element analyses have been performed using the ANSYS software. The two dimensional solid element Plane 42 with axisymmetric option is used for generating the FEA model.

The numerical solutions of nonlinear FEA have demonstrated the same characteristic as the moving boundary approach.

Fig 4.15 also compares the displacements at inside radius calculated by the proposed approach and nonlinear FEA. Both methods yield same results for elastic material behaviour. However, for plastic material behaviour, results obtained by the proposed method are greater in magnitude than those by nonlinear FEA. The difference increases with the internal pressure. In nonlinear finite element analysis, stresses in the surface may couple with the stiffness to generate the effect of stress stiffening. Therefore, the cylinder under high pressure may have an increased stiffness and less radial deformation in the vicinity of bore, owing to the high stress intensity at the inside surface where high internal pressure applies.

Fig 4.16 shows the elastic plastic interface estimation by the proposed method and NLFEA. The results obtained by the two methods are generally consistent with each other. They all show the effect of geometric change on elastic-plastic interface estimation. The difference of results by the moving boundary formulation and original boundary theory increases with the internal pressure. The magnitude of difference, however, is much less than that of the radial displacements at inside radius. As well, similar characteristic is illustrated in the radial displacement calculations at outside radius, as shown in Fig. 4.17.

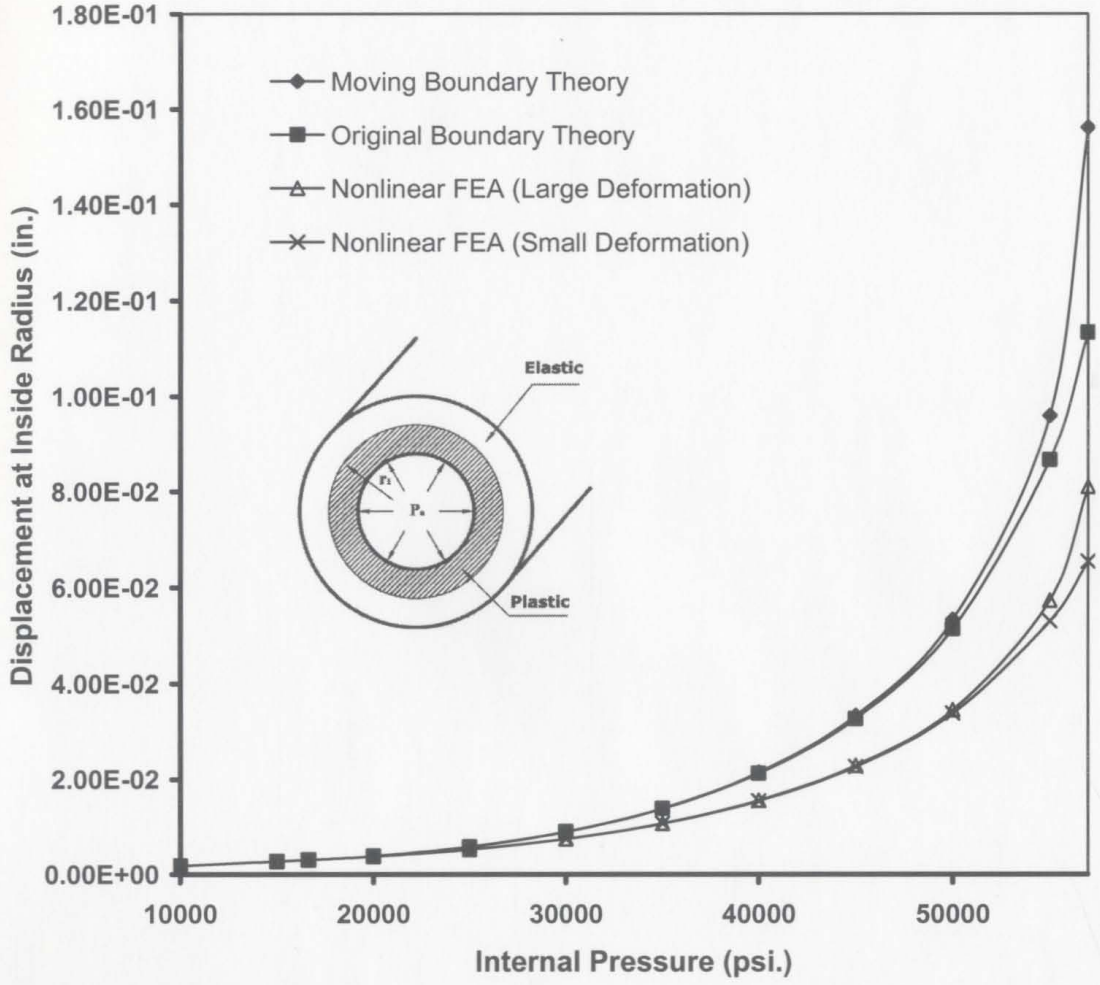

Fig. 4.15 Radial displacement at inside radius

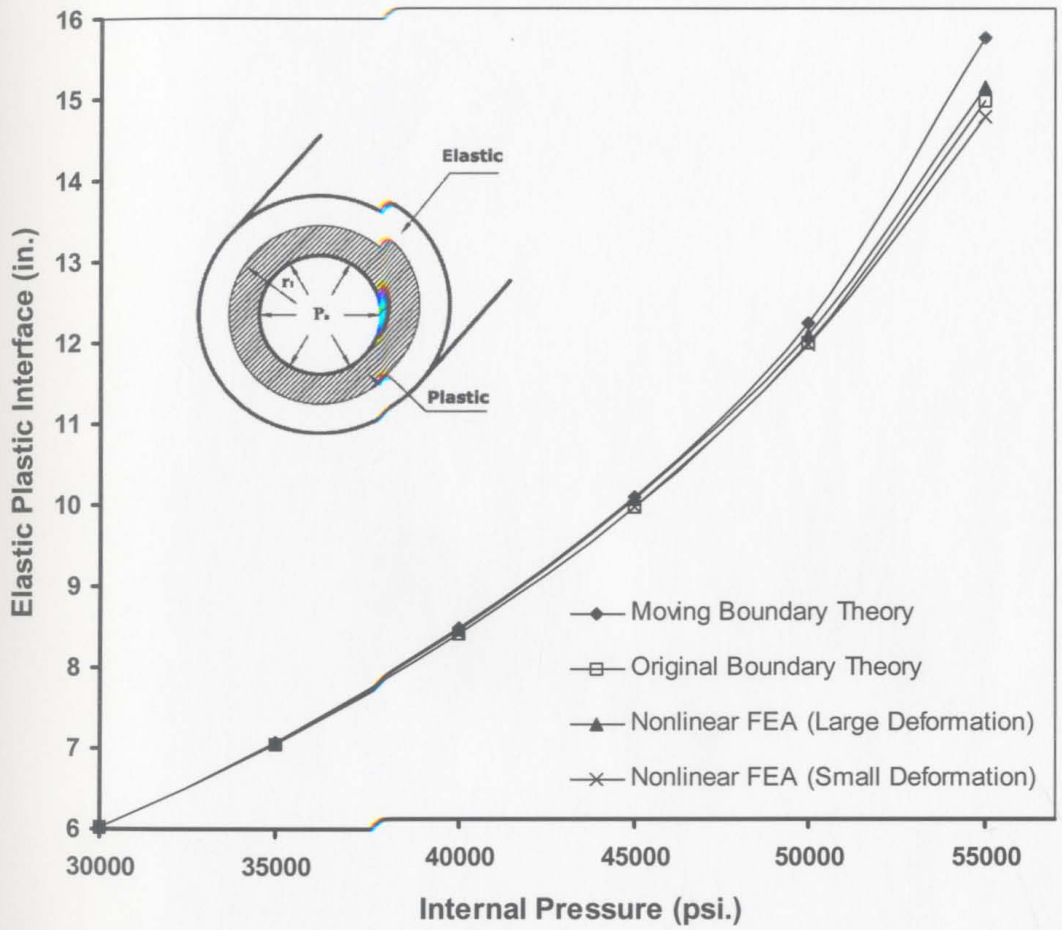

Fig. 4.16 Elastic plastic interface estimation

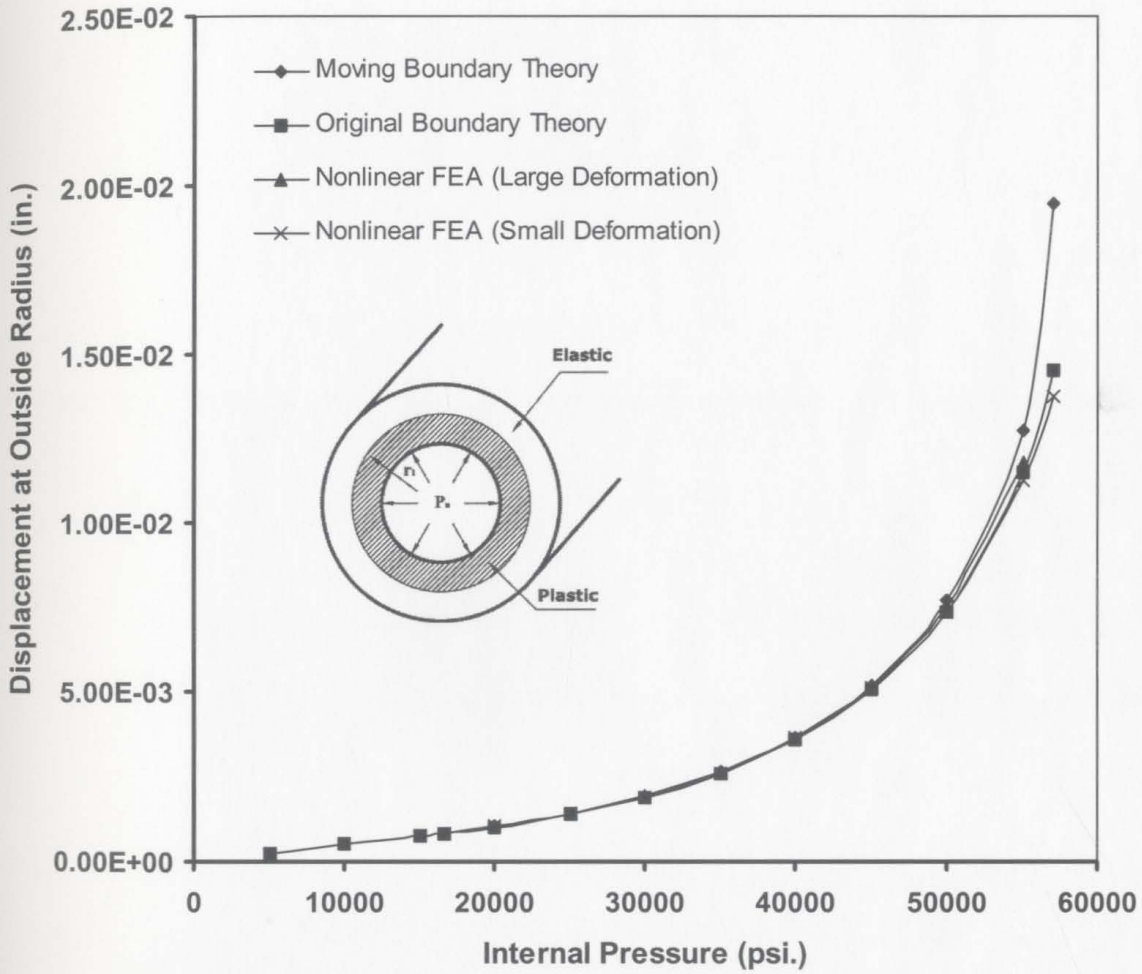

Fig. 4.17 Displacement at outside radius

4.5.5 Energy Calculations

It is important to appropriately represent strain energy in the energy approach in fracture mechanics. An appropriate calculation of energy can be helpful in the evaluation of fracture parameters, such as J integral.

Calculations have been conducted on the cylinder having a 4 *in.* (0.102 *m*) inside radius and a 20 *in.* (0.508 *m*) outside radius. Numerical solutions of the nonlinear FEA have also been performed using the same type of element and related options as those in displacement calculations. For both methods, the end condition is assumed to be plane strain.

Fig. 4.18 demonstrates how the moving boundary may affect the calculation of energy required for elastic plastic deformation. The percentage of energy difference is defined as:

$$Difference\ of\ energy = \frac{U_{moving} - U_{original}}{U_{original}} \times 100\% \tag{4.55}$$

where U_{moving} and $U_{original}$ are the energy calculated on the moving boundary basis and original boundary basis, respectively. Since the percentage is postitive, the energy calculated on the moving boundary basis is greater than original boundary theory. When the internal pressure is below 35,000 *psi* (2.413×10^2 *MPa*), the difference made by moving boundary in term of energy is generally less than 1.0 %. Therefore, in this case,

the geometric change has no significant effect on the calculated energy including strain energy and energy dissipation. When internal pressure increases to 45,000 *psi* (3.103×10^2 *MPa*), the difference of energy calculated by the proposed moving boundary approach and original boundary theory is 2.4%. If the cylinder is loaded with a higher internal pressure, such as 55,000 *psi* (3.792×10^2 *MPa*), the difference of energy obtained by the moving boundary theory and original boundary theory is 12.0%. These results indicate that geometric change of cylinders subject to high internal pressure has a considerable effect on the energy calculation.

In Fig. 4.18, energy obtained by large deformation FEA is 1.8% greater than that of small deformation FEA when the internal pressure is 45,000 *psi* (3.103×10^2 *MPa*). The difference goes up to 6.0% when the internal pressure increases to 55,000 *psi* (3.792×10^2 *MPa*). Therefore, the numerical solution of nonlinear finite element analysis shows the same characteristic as the moving boundary method. Fig. 4.18 shows when the internal pressure is lower than 35,000 *psi* (2.413×10^2 *MPa*), results by the moving boundary approach are in good agreement with those by NLFEA. As the internal pressure increases, the magnitude of difference that large deformation condition can make on energy calculation becomes noticeably less than those calculated by the moving boundary theory. For cylinders subjected to high internal pressure, the stress stiffening effect at inside surface where high internal pressure applies may reduce the effect of geometric change on energy calculation by NLFEA.

Fig. 4.19 shows the energy results calculated by the moving boundary approach and the ANSYS nonlinear finite element analyses. The comparison is favourable in the pressure range up to 50,000 *psi* ($3.447 \times 10^2 MPa$). Therefore, the proposed moving boundary theory is generally consistent with nonlinear finite element analysis.

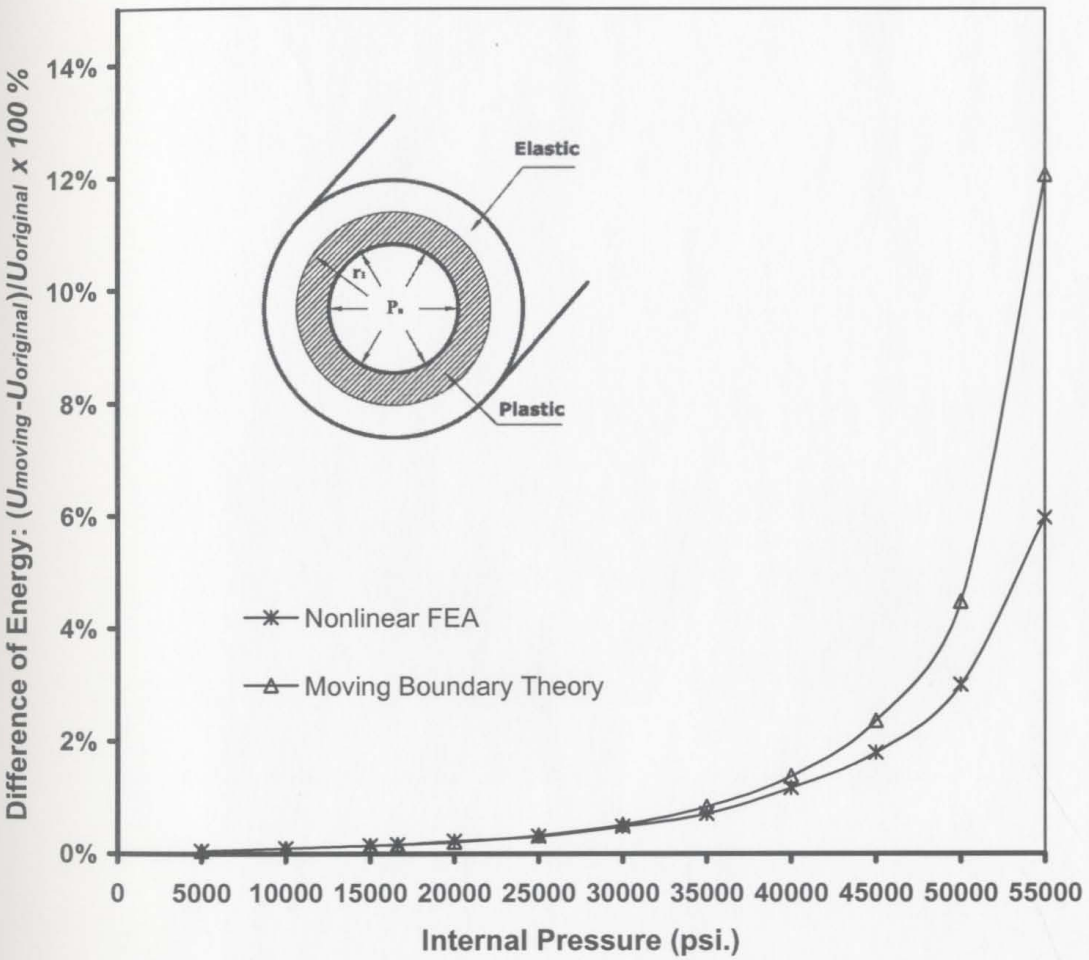

Fig. 4.18 Difference of energy vs. internal pressure

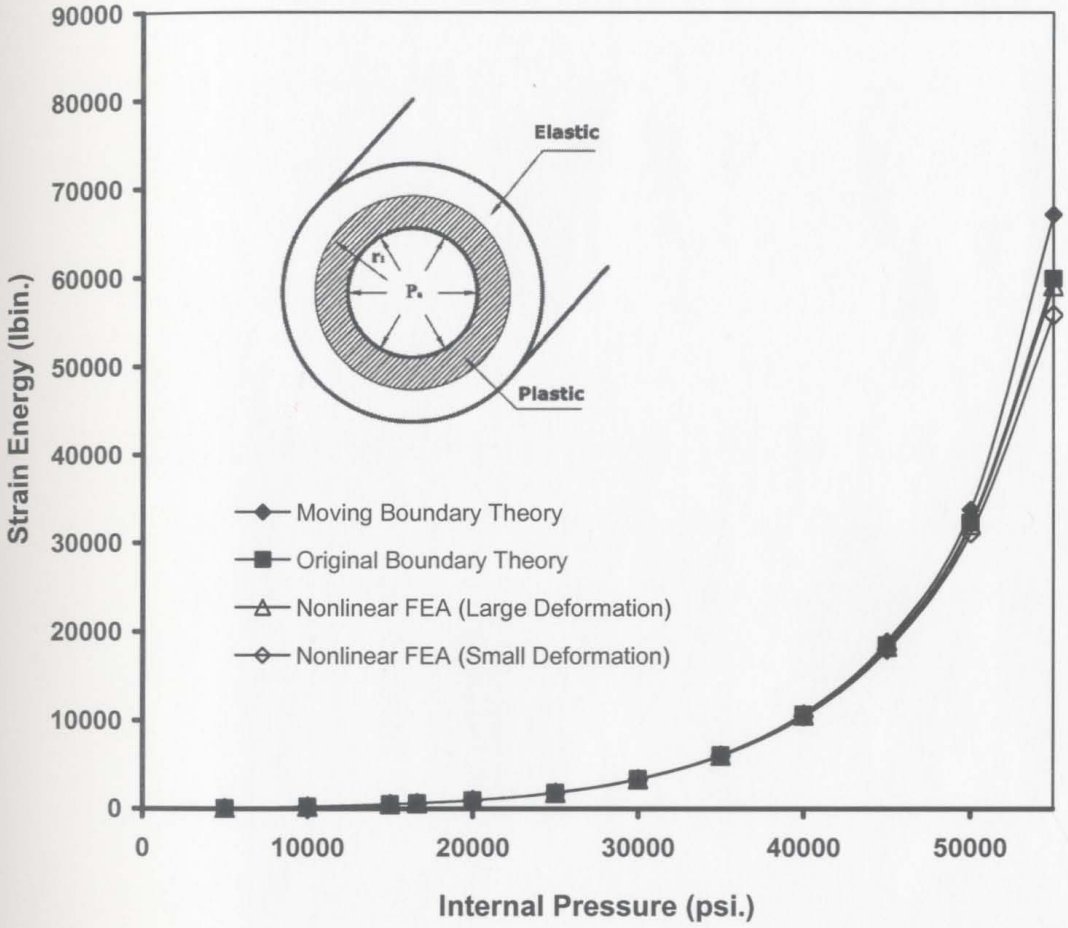

Fig. 4.19 Strain energy vs. internal pressure

4.6 REMARKS

The proposed moving boundary approach represents an analytical method to calculate stress and plastic response on a moving boundary basis for cylinders under high internal pressure. The work involves several features. Firstly, this approach incorporates the geometric change in its formulation. Using an iterative procedure based on the principle of virtual work, it accounts for the effect of deformed geometry due to high internal pressure. Secondly, as a generalized method for thick wall cylinders, solution of the problem is expressed in terms of parametric functions. The formulation yields Lame's solution and the classical elastic perfectly plastic solution as special cases. Thirdly, the general form of piecewise linearized constitutive equation was developed in this study. It provides a necessary condition to solve cylinder problems for inelastic materials exhibiting work hardening behavior.

The Maple 6.0 mathematical program was used for implementing the proposed method. Stress, strain, displacement, and energy were calculated for elastic and plastic material on a moving boundary basis. The effects of geometric change on elastic plastic response for thick wall cylinders under internal pressure have been assessed. Calculations indicated two characteristics. Firstly, radial displacements calculated on a moving boundary basis are larger than those of the original boundary theory. The difference is negligible for elastic material but increases with the internal pressure for plastic material behaviour. Secondly, energy calculated on a moving boundary basis is greater than that by the

original boundary theory. For cylinders subject to high internal pressure up to 55,000 *psi* (3.792×10^2 *MPa*), the energy calculation on moving boundary basis can be 12% greater than that on original boundary basis. Therefore, geometric change has a significant effect on the evaluation of energy required for deformation.

The numerical solutions of nonlinear FEA have demonstrated the same characteristic about the effect that the moving boundary can make on radial displacements and energy calculations. However, magnitudes of energy difference and radial displacement difference estimated by nonlinear FEA are less than those by the moving boundary approach, respectively. For cylinders analyzed by nonlinear FEA, the stress stiffening effect at inside surface where high internal pressure applies may reduce the effect of geometric change.

The comparison of inelastic solutions calculated by the moving boundary approach with nonlinear finite element analyses is favourable. In general, the proposed moving boundary theory is consistent with the nonlinear finite element method in calculations of stress, plastic response, and energy.

5. AUTOFRETTAGE AND SHAKEDOWN

5.1 AUTOFRETTAGE

5.1.1 Introduction

A favorable initial stress pattern, from a standpoint of design enhancement can be obtained by applying a sufficiently high internal pressure to produce plastic deformation in the inner part of the cylinders, and then removing the pressure. Consequently, a residual stress will persist in the wall. Material is strengthened by the existence of compressive hoop stress distribution in the inner portion of the cylindrical vessels.

Materials strengthened by this process are now suitable for the repeated application of internal pressure in that the accompanying hoop or tangential tensile stress must overcome the induced residual compressive stress. In this manner, the internal pressure that a cylinder can withstand is considerably increased. Not only does it increase the strength of a component, but it also has a favorable effect in increasing fatigue life. This method is frequently used in the design of accumulators, hydraulic ram cylinders, gun barrels, and other such applications. This strengthening process is known as autofrettage.

5.1.2 Problem Formulation

When the internal pressure is removed after the cylinder material has been brought to an elastic plastic condition, a residual stress will remain in the wall. This can be calculated by assuming that during unloading the material follows Hooke's law, the stresses obtained by Eq. (4.16) to be subtracted while unloading are those given by Eq. (5.1) and Eq. (5.2):

$$\sigma_{r,ul} = -D_{ul}\left(\frac{r_o^2}{r^2} - 1\right) \tag{5.1}$$

$$\sigma_{\theta,ul} = D_{ul}\left(\frac{r_o^2}{r^2} + 1\right) \tag{5.2}$$

Like A_1 and C_2 in Eq. (4.16), D_{ul} is a constant that depends on the internal pressure P_n. The above two equations are the special cases of Eq. (4.16) for elastic material behavior. The unloading procedure may be simulated by superposing a radial tension, or negative pressure P_n on the inside surface to cancel that pressure causing the initial elastic plastic deformation. Therefore, the residual stresses in that case can be obtained from:

$$\sigma_{r,res} = -A_1\left(\frac{r_o^2}{r^2} - 1\right) + C_2\left(\frac{r_1^2}{r^2} - 1 - 2\ln\frac{r_1}{r}\right) + D_{ul}\left(\frac{r_o^2}{r^2} - 1\right) \tag{5.3}$$

$$\sigma_{\theta,res} = A_1\left(\frac{r_o^2}{r^2}+1\right) - C_2\left(\frac{r_1^2}{r^2}-1+2\ln\frac{r_1}{r}\right) - D_{ul}\left(\frac{r_o^2}{r^2}+1\right) \tag{5.4}$$

This is best illustrated by a particular case for which the stresses and residual stresses are shown in Fig. 5.1. The cylinder calculated in this example is subject to an internal pressure of 30,000 *psi* (2.068 x 10^2 *MPa*). Its inside radius is 4 *in.* (0.102 *m*) and outside radius is 20 *in.* (0.508 *m*). Curve 1 and 2 in Fig. 5.1 (a) are determined by Eq. (4.16). Curve 3 and 4 are determined by Eq. (5.1) and Eq. (5.2). Superposing of loading and unloading leads to the residual stresses illustrated in Fig. 5.1 (b).

In the case of inelastic unloading, the formulation can be expressed as:

$$\sigma_{r,res} = -A_1\left(\frac{r_o^2}{r^2}-1\right) + C_2\left(\frac{r_1^2}{r^2}-1-2\ln\frac{r_1}{r}\right) + D_{ul}\left(\frac{r_o^2}{r^2}-1\right) - H_{ul}\left(\frac{r_{u1}^2}{r^2}-1-2\ln\frac{r_{u1}}{r}\right) \tag{5.5}$$

$$\sigma_{\theta,res} = A_1\left(\frac{r_o^2}{r^2}+1\right) - C_2\left(\frac{r_1^2}{r^2}-1+2\ln\frac{r_1}{r}\right) - D_{ul}\left(\frac{r_o^2}{r^2}+1\right) + H_{ul}\left(\frac{r_{u1}^2}{r^2}-1+2\ln\frac{r_{u1}}{r}\right) \tag{5.6}$$

where D_{ul} and H_{ul} are the constants during inelastic unloading.

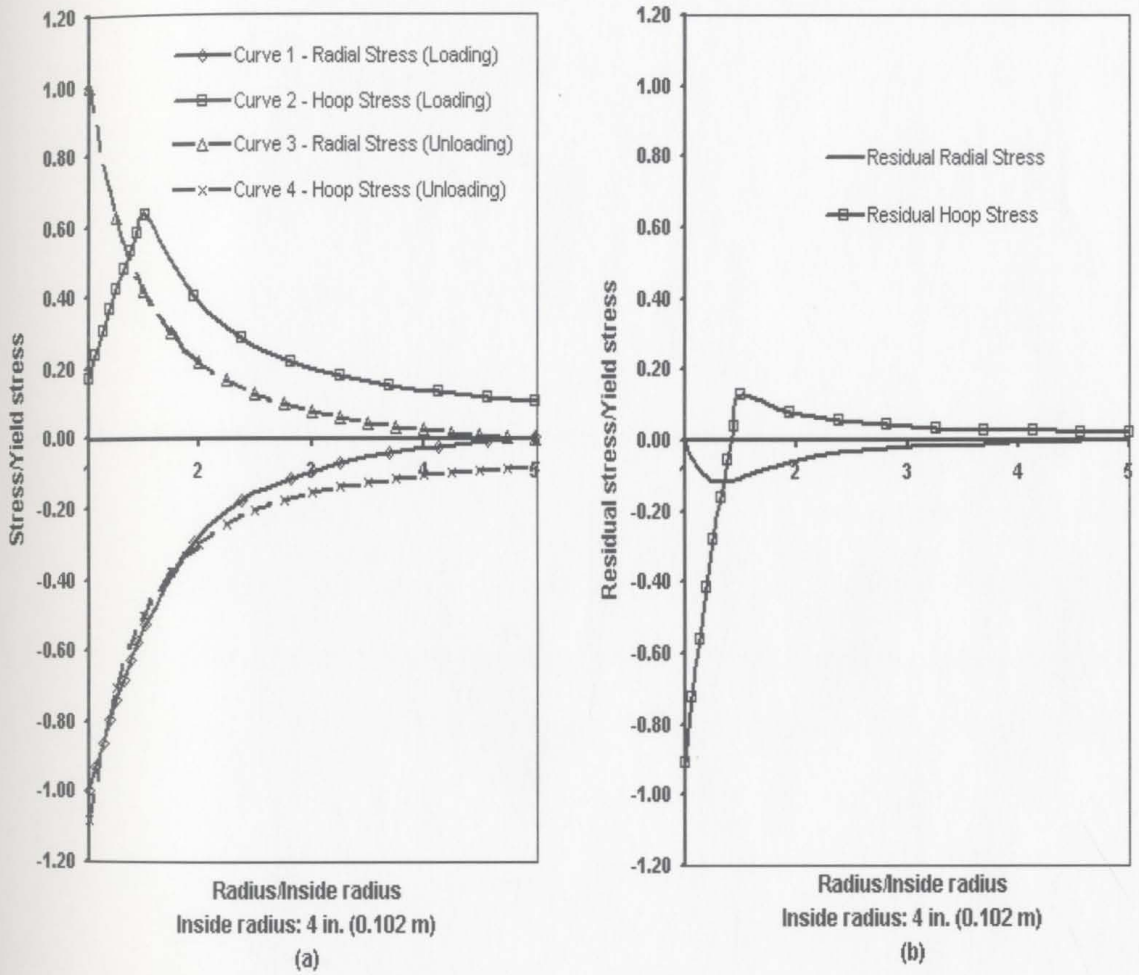

Fig. 5.1 Residual stresses in an autofrettaged thick wall cylinder

5.1.3 Work Hardening Models

Classical theory of autofrettage assumes that the material is perfectly plastic and that it yields under the action of a shearing stress. The proposed method, however, will cover not only the material following perfectly plastic behavior but also the material exhibiting work hardening behavior.

5.1.3.1 Isotropic Hardening

Isotropic hardening rule states that the reverse compressive yield stress is assumed equal to the tensile yield stress. Therefore the isotropic hardening model completely neglects the Bauschinger effect as it assumes that an increased yield point in tension carries over equally in compression. The hardening rule may be expressed mathematically in terms of equivalent stresses in order to utilize the uniaxial stress strain curve. It can be written in the form of Eq. (5.7). The reverse yielding will not occur as long as the difference in equivalent stress before and after unloading is less than twice of the equivalent stress before unloading.

$$\left|\sigma_{eq}^{L} - \sigma_{eq}^{UL}\right| \leq 2\sigma_{eq}^{L} \tag{5.7}$$

5.13.2 Kinematic Hardening

Kinematic hardening rule states that the elastic range is assumed to be unchanged during hardening. Thus, the kinematic hardening rule considers the Bauschinger effect. The reverse yielding will not occur as long as the difference of equivalent stress before and after unloading is less than the twice of initial yield stress. Kinematic hardening rule may be expressed in the form:

$$\left|\sigma_{eq}^{L} - \sigma_{eq}^{UL}\right| \leq 2\sigma_{Y} \tag{5.8}$$

Kinematic hardening rule provides a simple means accounting for the Bauschinger effect. Possible unloading paths of isotropic hardening and kinematic hardening materials on the uniaxial stress strain curve can be illustrated in Fig. 2.6.

5.1.4 Bauschinger Effect

In general, the material properties were considered to be unaffected by strain beyond the yield strength, and yield strength in compression remained equal to the yield strength in tension. However, experimental studies (Chen 1986) show that stress strain curves of material for pressure vessel fabrication have demonstrated work hardening behavior. For an autofrettaged cylinder, the yield strength of the material in compression decreases because of prior deformation in tension. This phenomenon is known as the Bauschinger

effect (BEF), which is defined as the ratio of the yield strength after reverse loading to the initial yield strength:

$$BEF = \frac{\sigma_{comp.Y.P.afteroverstrain\ in\ tension}}{\sigma_{comp.Y.P.\ initially}} \tag{5.9}$$

Making the usual assumption that the initial yield strength in tension and compression are equal, this becomes

$$BEF = \frac{\sigma_{comp.Y.P.}}{\sigma_{ten.Y.P.}} \tag{5.10}$$

Fig. 5.2 illustrates the characteristic of the Bauschinger effect: for the material preloaded to σ_y' in tension, its corresponding compressive yielding occurs at a stress level σ_y'' which is less than the initial yield stress σ_y and the subsequent yield stress σ_y'. The decrease of yield strength in compression shows the phenomenon of the Bauschinger effect.

The proposed method can account for the Bauschinger effect for the kinematic hardening model used in formulation as the Bauschinger effect influences the stress level that needs to be considered for the cracking conditions. It involves piecewise linearization of stress strain curve during unloading to the point where reverse yielding occurs. The actual unloading stress and strain curve may be linearized in the same piecewise manner as employed in loading process.

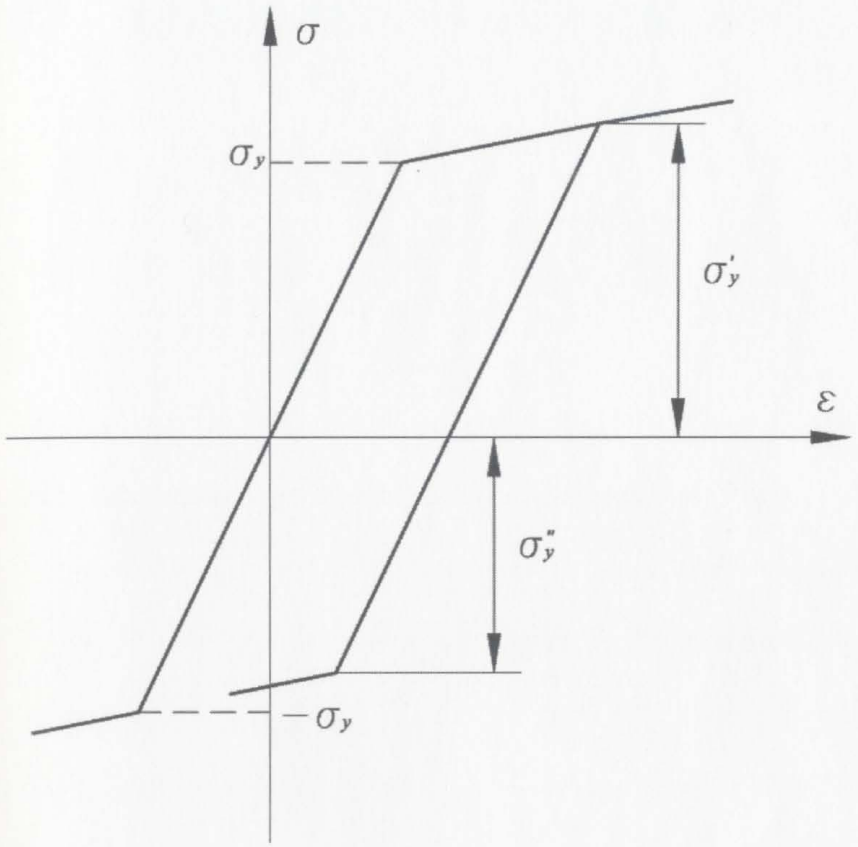

Fig. 5.2 The Bauschinger effect

5.1.5 Examples

In this study, a closed end autofrettaged cylinder is treated as a thick wall cylinder having an inside radius of 4 *in*. (0.102*m*), an outside radius of 20 *in*. (0.508*m*), and a length so great in relation to its mean diameter that the sections sufficiently far from the ends

remain plane in deformation. The first yield pressure of the cylinder is calculated and found to be $1.663\text{x}10^4$ *psi* ($1.146\text{x}10^2$ *MPa*). The autofrettage pressures applied are 20,000 *psi* ($1.379\text{x}10^2$ *MPa*), 25,000 *psi* ($1.724\text{x}10^2$ *MPa*), and 30,000 *psi* ($2.068\text{x}10^2$ *MPa*), respectively. The material behavior is assumed to be bilinear with work hardening. The material parameters used in the examples are:

$\sigma_Y = 30{,}000\,psi.\left(2.068\times10^2\ MPa\right)$,

$E = 30\times10^6\ psi.\left(2.068\times10^5\,MPa\right)$

$E_2 = 30\times10^4\ psi.\left(2.068\times10^3\,MPa\right)$

Maple 6.0 programming language has been used to perform autofrettage calculation on the moving boundary basis. As well, finite element models have been developed. The ANSYS finite element computer program has been used to generate the FEA models and perform autofrettage calculation. 2-D solid element, Plane 42, is used with axisymmetric option to calculate residual stress and strain. Results of nonlinear finite element analysis (NLFEA) have been obtained to compare with those of the proposed method.

Residual stress and strain distributions obtained by the proposed method and the NLFEA with various meshing intensity are plotted in Fig. 5.3 and Fig. 5.4. The applied internal pressure is 30,000 *psi* ($2.068\text{x}10^2$ *MPa*). Fig. 5.3 indicates that there is a minor discrepancy between the results of residual stress using proposed method and finite element analysis attributable to the relatively coarse meshing. However, the difference is significantly reduced as finer meshing is employed in finite element analysis, and eventually the results coincide. Therefore, the proposed method and finite element

analysis are consistent in autofrettage calculations. Fig. 5.4 shows the results of residual strain calculated by the proposed method are in good agreement with those by nonlinear finite element analysis.

Fig. 5.5 demonstrates the successive residual stress distributions as the internal pressure varies in magnitude of 20,000 *psi* (1.379×10^2 *MPa*), 25,000 *psi* (1.724×10^2 *MPa*), and 30,000 *psi* (2.068×10^2 *MPa*), respectively. Results in Fig. 5.5, as well, indicate the consistency of the proposed method and nonlinear finite element analysis.

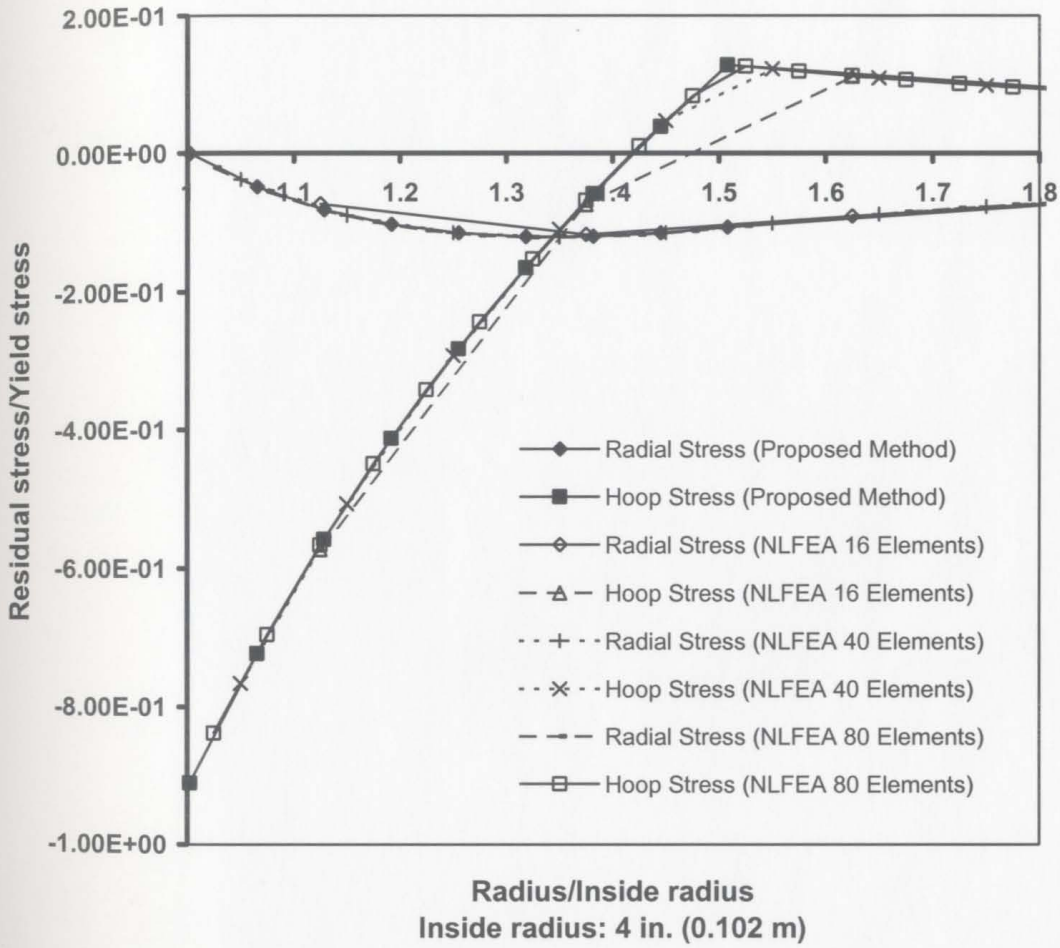

Fig. 5.3 Residual stress distribution

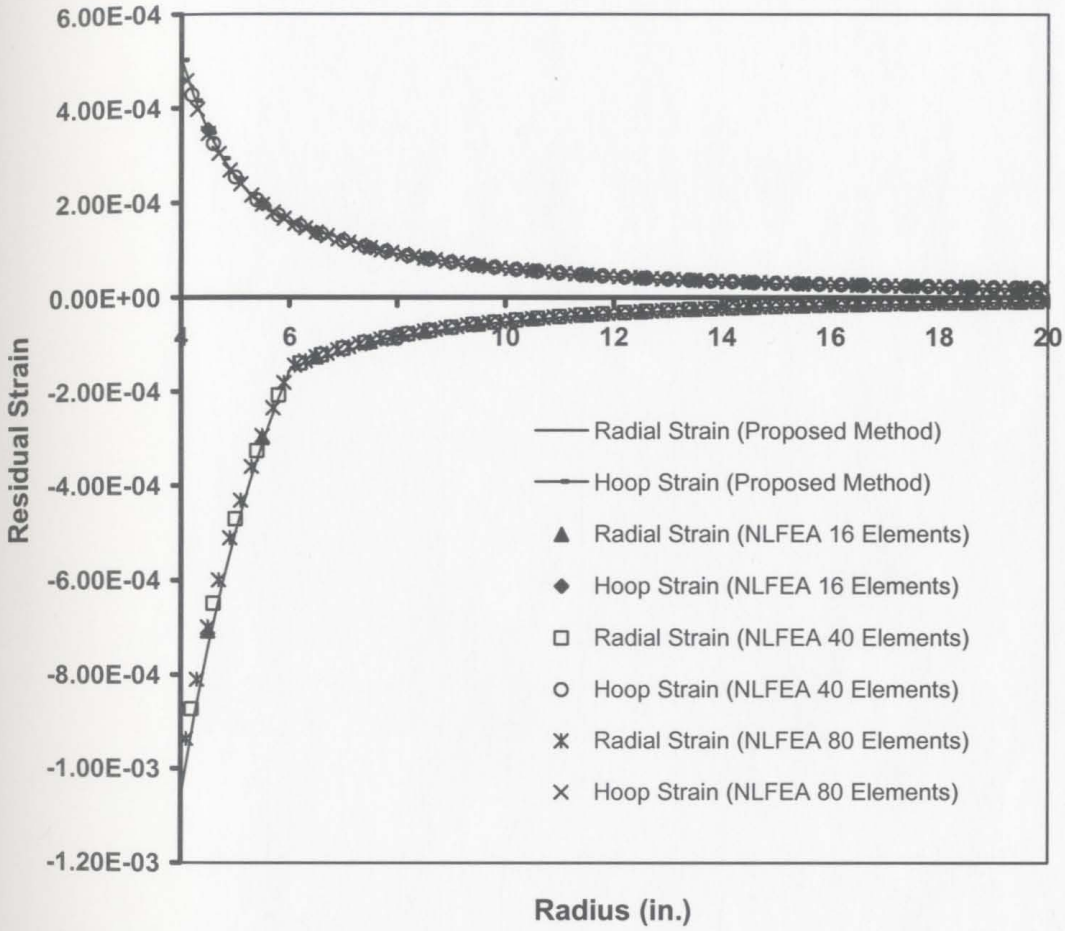

Fig. 5.4 Residual strain distribution

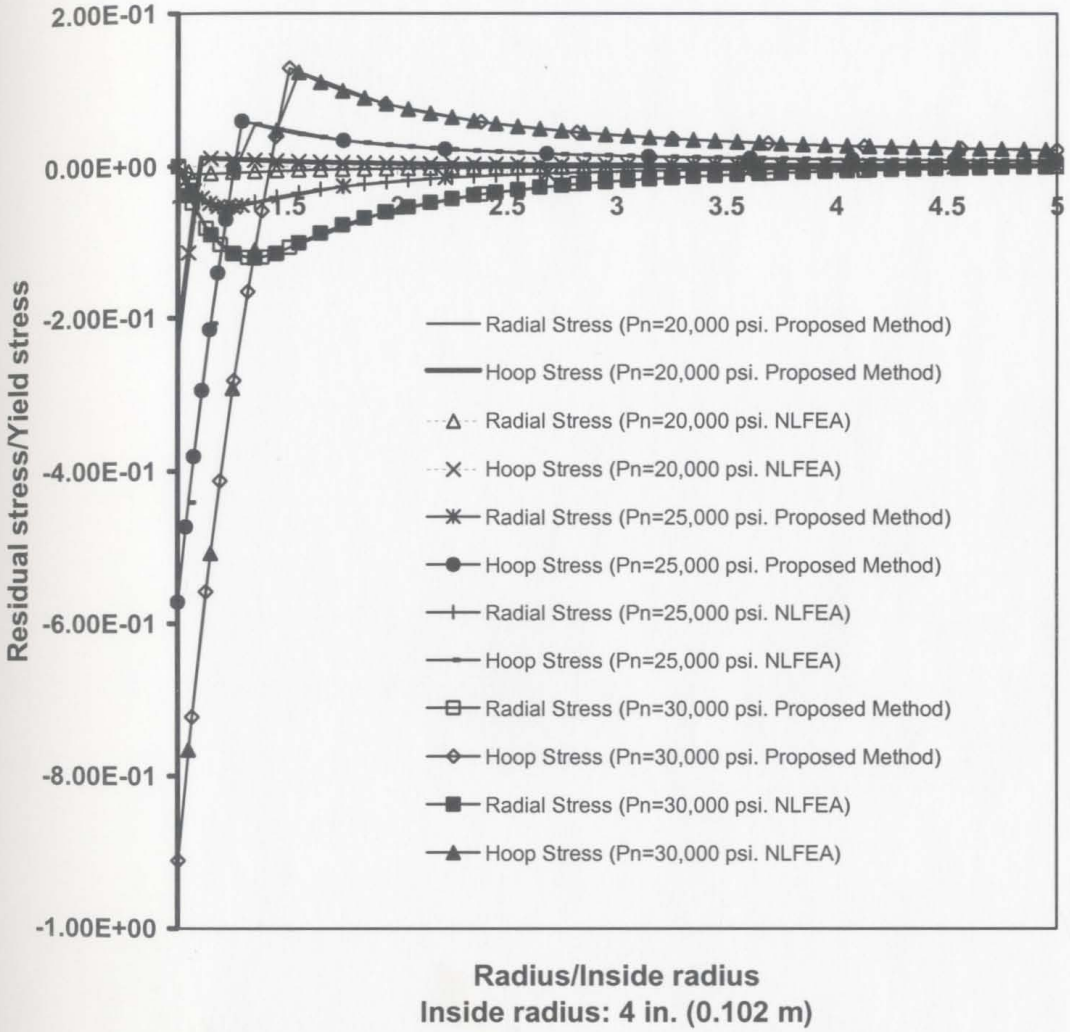

Fig. 5.5 Residual stress distributions for various internal pressures

5.2 SHAKEDOWN

5.2.1 Introduction

The concept of shakedown provides an avenue to deal with the design of thick wall cylinders under cyclic loadings. Essentially, a structure develops residual state of stress and strain under certain loading and unloading conditions. The structure is said to shakedown if its behavior is elastic during subsequent cycle of same loading and unloading.

5.2.2 Formulation

For a cylinder that has experienced shakedown, stresses during the subsequent loading of internal pressure can be obtained using the superposition illustrated in Fig. 5.1 and Eqs. (5.1), (5.2), (5.3), and (5.4) since the subsequent reloading cycles are elastic. Therefore, the stresses of such cylinders can be written in a form similar to Eqs (5.3) and (5.4):

$$\sigma_r = \sigma_{r,res} - A_s\left(\frac{r_o^2}{r^2} - 1\right) \tag{5.11}$$

$$\sigma_\theta = \sigma_{\theta,res} + A_s\left(\frac{r_o^2}{r^2} + 1\right) \tag{5.12}$$

where $\sigma_{r,res}$ and $\sigma_{\theta,res}$ are the residual radial and hoop stresses at radius r. The constant A_s depends on the applied internal pressure. The radial stress would vanish at the external boundary $r = r_o$. At this point, therefore, the only non-zero stress in plane stress condition is

$$\sigma_\theta = \sigma_{\theta,res} + 2A_s \tag{5.13}$$

After a loading and unloading cycle, residual radial stresses at the external and internal boundaries are zero since there is no load applied on the boundaries. Therefore, from Eq. (5.11), stresses at $r = r_n$ during subsequent loading to internal pressure P_S are

$$\sigma_r\big|_{r=r_n} = -P_S = -A_s\left(\frac{r_o^2}{r_n^2} - 1\right) \tag{5.14}$$

$$\sigma_\theta\big|_{r=r_n} = \sigma_{\theta,res}\big|_{r=r_n} + P_S\frac{r_o^2 + r_n^2}{r_o^2 - r_n^2} \tag{5.15}$$

At the external boundary $r = r_o$,

$$\sigma_r\big|_{r=r_o} = 0 \tag{5.16}$$

$$\sigma_\theta\big|_{r=r_o} = \sigma_{\theta,res}\big|_{r=r_o} + 2P_S\frac{r_n^2}{r_o^2 - r_n^2} \tag{5.17}$$

5.2.3 Implementation

The proposed method calculates the shakedown pressure on a moving boundary basis. To obtain shakedown pressures of moving boundary basis, the principle of virtual energy can be used to create an iterative updating scheme to account for the deformed geometry because it is applicable for both elastic and plastic materials.

Firstly, stresses and residual stresses are calculated on the original boundary basis for an inelastic loading and elastic unloading cylinder. Shakedown pressure for the undeformed geometry is implemented by applying the kinematic work hardening rule. Geometry or boundary of the cylinder is updated using the deformation calculated by the principle of virtual work. Then a successive calculation is carried out, and energy for deformation and work done by external pressure are evaluated on a moving boundary basis. The current solutions are used to update the geometry of the cylinder and the parametric functions in an iterative manner. The final solution of shakedown pressure is obtained until the convergence at required accuracy is achieved.

This iterative calculation procedure for shakedown pressures is illustrated by the flow chart in Fig. 5.6

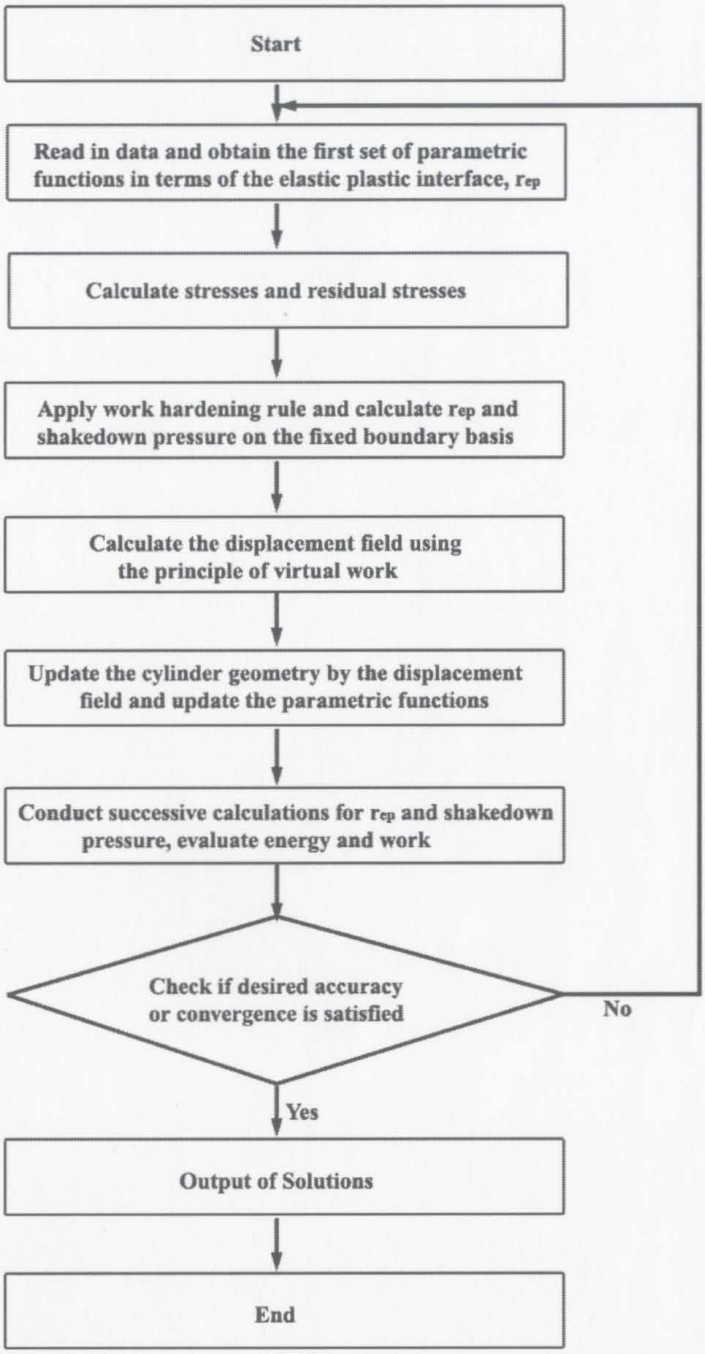

Fig. 5.6 Shakedown pressure calculation on a moving boundary basis

5.2.4 Examples

Shakedown pressures are calculated by the proposed moving boundary approach. Results are compared with those obtained by classical small deformation theory. The analyzed models are thick wall cylinders having an inside radius 4 *in* (0.102 *m*) with plane strain, open end and closed end conditions. Diameter ratio ranges from 1.8 to 6. The material behavior is assumed to follow kinematic work hardening rule because the Bauschinger effect generally occurs in the materials for pressure vessel fabrication. The material parameters used in these examples are:

$\sigma_Y = 30{,}000\,psi.\left(2.068\times10^2\ MPa\right)$,

$E = 30\times10^6\ psi.\left(2.068\times10^5 MPa\right)$

$E_2 = 30\times10^4\ psi.\left(2.068\times10^3 MPa\right)$

5.2.4.1 Effect of Moving Boundary

The difference of shakedown pressure estimation for original boundary and moving boundary is defined by the following equation:

$$Difference\ of\ Shakedown\ Pressure\ Estimation = \frac{P_{S\_original} - P_{S\_moving}}{P_{S\_original}} \times 100\% \qquad (5.18)$$

where $P_{S\_original}$ and P_{S_moving} are the shakedown pressure on original boundary basis and moving boundary basis, respectively.

Calculation has been performed to investigate the effect of deformed geometry on shakedown pressure estimation and the results are shown in Fig. 5.7. For the plane strain condition, the differece of shakedown pressure estimation drops down as the cylinder diameter ratio decreases. The reason for this phenomenon could be the geometric change has less effect on shakedown pressure for cylinders with wall thinner than 2.2. In general, results indicate the difference on shakedown pressure estimation due to geometric change is generally less than one percent. Therefore, the effect of deformed geometry on shakedown pressure calculations is negligible.

5.2.4.2 Effect of End Conditions

Calculation in this study indicates that shakedown pressure estimations are different for various end condition. The results in Fig. 5.8 indicate that the shakedown pressure estimation may be significantly affected by end conditions as the difference between open end and closed end or plane strain can be approximately 16 percent.

5.2.4.3 Effect of Diameter Ratio

Fig. 5.8 shows that the curves of shakedown pressures vs. diameter ratios undergo relatively abrupt slope changes when diameter ratios are in a range of 2.2 to 2.3 for

various end conditions. This indicates that estimation of shakedown pressure is subjected to the influence of the diameter ratio of cylinders. For the diameter ratios smaller than 2.2, the gradient of the curve is greater than that of diameter ratios greater than 2.2. Therefore, for diameter ratios smaller than 2.2, the shakedown pressure increases more than that of diameter ratios greater than 2.2 as the cylinder wall thickness increases.

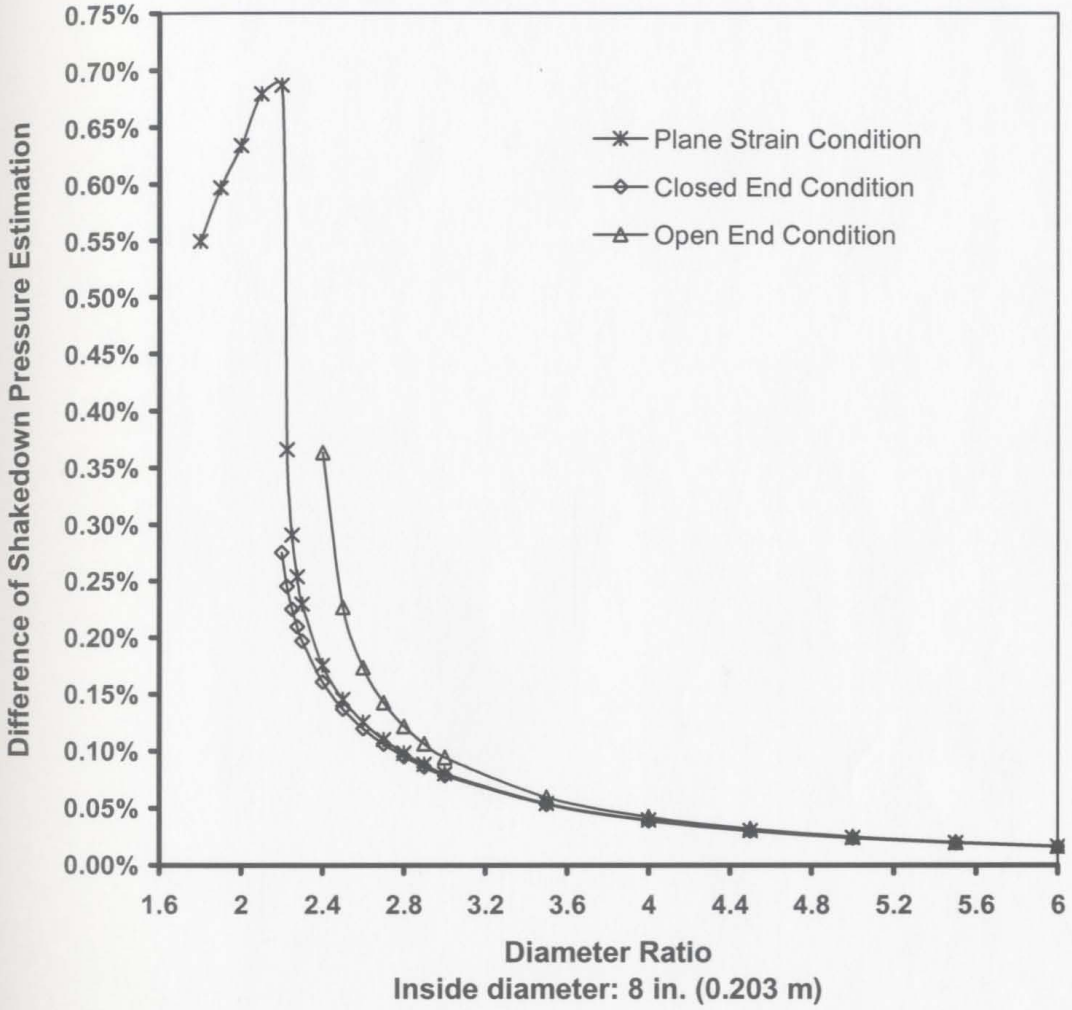

Fig. 5.7 Effect of deformed geometry on shakedown pressure

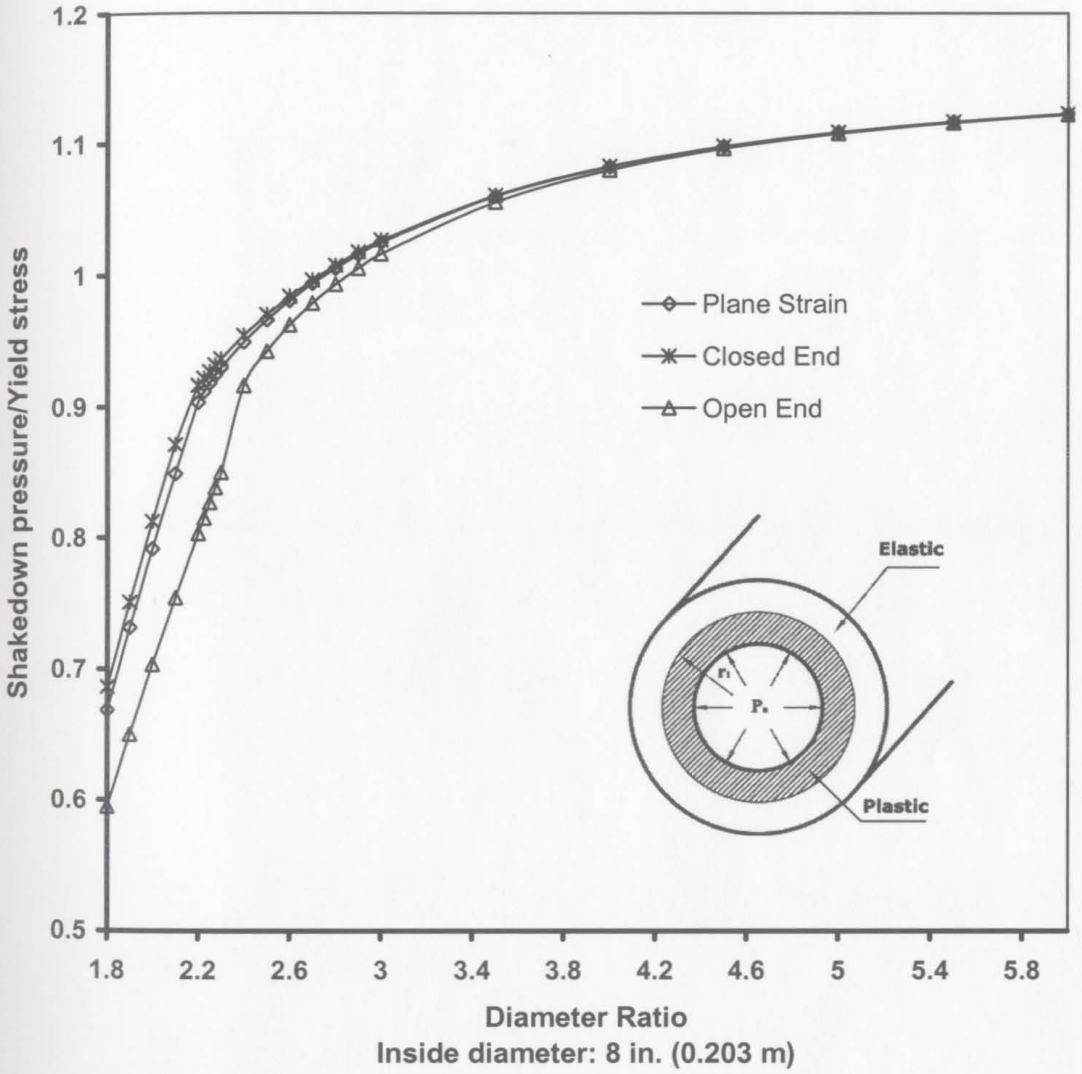

Fig. 5.8 Shakedown pressures of various end conditions

5.3 Remarks

An analytical method for autofrettaged cylinders obeying work hardening stress strain law has been described in this chapter. Analytical solutions based on deformed geometry have been obtained and then compared with finite element analysis. The moving boundary formulation has been verified by comparing results of the analytical method and inelastic FEA. While results are obtained for linear elastic unloading, it is possible to apply this formulation to inelastic unloading using the piecewise linearization technique. As well, the Bauschinger effect has been included in the presented analysis for a kinematic work hardening material.

An iterative procedure for shakedown pressure estimation has been developed using the principle of virtual work. Shakedown pressures have been calculated for both the undeformed geometry and the deformed geometry for cylinders of closed end, open end, and plane strain conditions. It has been found that difference in shakedown pressure estimation due to geometric change is not particularly pronounced, as the difference is generally less than one percent. Calculations have indicated that the shakedown pressure estimation may be significantly affected by end conditions as the difference between open end and closed end or plane strain can be as much as 16 percent.

6. ESTIMATION OF PLASTIC COLLAPSE LOADS

6.1 INTRODUCTION

As an analytical approach for elastic plastic analysis, the proposed method is able to describe the spreading process of the contained plastic flow for thick wall cylinder under internal pressure on a moving boundary basis. Yet it also provides an alternative method for estimating limit loads of cylindrical geometries. In general, the classical limit analysis applies strictly to the idealized structures or components, in which the material is assumed perfectly plastic, and deformation is small. Therefore, geometric description of structure remains invariant. The proposed method can, however, calculate the plastic collapse loads of thick wall cylinders exhibiting work hardening behavior and involving geometric changes.

Plastic collapse load for thick wall cylinder is the load under which the uncontained or unrestricted plastic flow occurs. This approach can be used to obtain plastic collapse loads for situations involving the geometric change of boundary, by invoking the principle of virtual work. The piecewise linearization of material curve enables the estimation of plastic collapse load for work hardening material. In this chapter, the proposed method has been applied to cylinders with an inside diameter 8 *in.* (0.203 *m*) and an outside diameter ranging from 12.8 *in.* (0.325*m*) to 40 *in.* (1.016 *m*). The dimensions of cylinders are expressed by diameter ratios. The calculated plastic collapse pressures are normalized by making use of the yield stress. The material behavior is

assumed to be an elastic plastic model with linear work hardening. The material parameters are:

$\sigma_Y = 30{,}000 psi.\left(2.068\times10^2\ MPa\right)$,

$E = 30\times10^6\ psi.\left(2.068\times10^5 MPa\right)$

$E_2 = 30\times10^4\ psi.\left(2.068\times10^3 MPa\right)$

In this study, plastic collapse loads under different end conditions including closed end, plane stress and plane strain are calculated to understand the effect of end conditions. Plastic collapse loads estimated on the original boundary basis are compared with those on a moving boundary basis to assess the effect of geometric changes.

The proposed method is implemented using the Maple 6 software. For the purpose of comparison, inelastic finite element analyses for small deformation theory and large deformation theory are conducted using the ANSYS software. The finite element models are generated using Plane 42, the 2-D solid element, in finite element routines.

6.2 EFFECT OF END CONDITIONS

For cylinders with various stipulated diameter ratios, Fig 6.1 shows that the choice of end conditions for cylindrical vessels makes a difference in plastic collapse load estimation. For a given set of dimensions, the closed end condition cylinders have the highest load bearing capability, while the open end cylinders demonstrate the least load bearing capability. The case of plane strain is intermediate to the other two cases, yet it has plastic

collapse load values nearer to those of closed end cylinders, as stress equations for plane strain are intermediate to the other two cases.

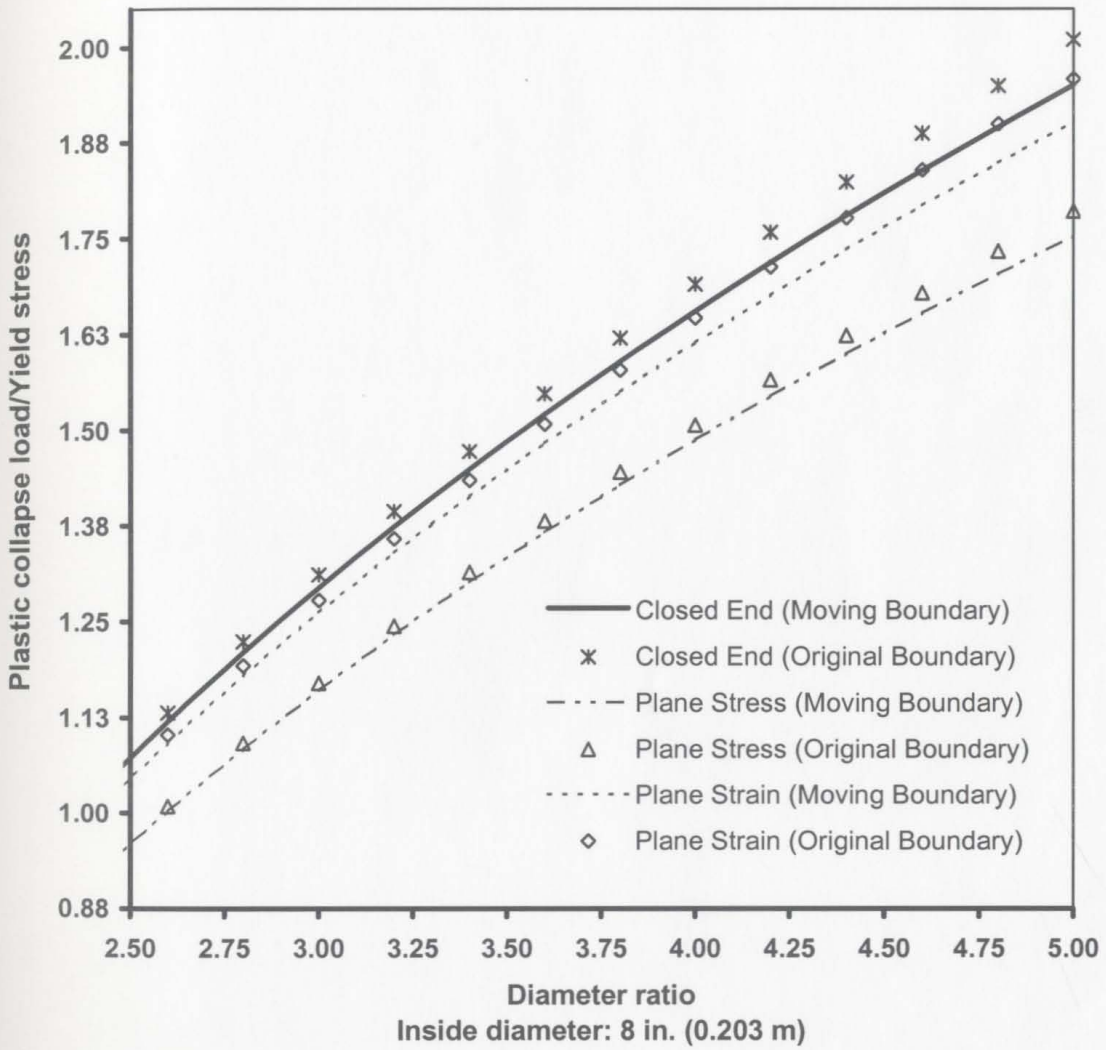

Fig. 6.1 Plastic collapse load estimations for various end conditions

6.3 EFFECT OF DEFORMED GEOMETRY

Besides the effect of end conditions, Fig. 6.1 also reveals the effect of deformed geometry on plastic collapse load estimations. Results indicate that plastic collapse loads calculated on a moving boundary basis are less than those on the original boundary basis. The effect of deformed geometry due to high internal pressure is further assessed in Fig. 6.2. It shows the difference of plastic collapse load estimated on deformed geometry and undeformed geometry.

In Fig. 6.2, the percentage of difference is calculated using the following formula:

$$Percentage\ of\ Difference = \frac{P_C^D - P_C^U}{P_C^U} \times 100\%, \tag{6.1}$$

where P_C^D is the plastic collapse load calculated on the deformed geometry basis and P_C^U is the plastic collapse load calculated on the undeformed geometry basis.

Several characteristics are shown in Fig. 6.2. Firstly, the difference is dependent on the end conditions for von Mises material. For cylinders with closed end condition, the difference is larger than the other two end conditions. For cylinders having an inside diameter of 8 *in.* (0.203 *m*) and an outside diameter of 40 *in.* (1.016 *m*), the difference is about 3.0%. For cylinders with open end condition, the difference is the least. For

cylinders with plane strain conditions, the difference is intermediate to the other two conditions.

Secondly, the difference in plastic collapse load estimation is affected by the diameter ratio of thick wall cylinder having the same inside diameter. Consider cylinders with closed end conditions for examples. When diameter ratio is 1.6 (the inside diameter is 8 *in.* (0.203 *m*) and outside diameter is 12.8 *in.* (0.325 *m*)), the difference the deformed geometry can make on the value of plastic collapse load is about 0.5%. The difference increases with the diameter ratio. For a thick wall cylinder having an outside diameter of 40 *in.* (1.016 *m*) and an inside diameter 8 *in.* (0.203 *m*), the difference of plastic collapse loads estimation is about 3.0%.

The negative values of the difference in Fig. 6.2 reveal that plastic collapse loads estimated on a moving boundary basis are less than those on the original boundary basis. Therefore, the proposed moving boundary approach provides conservative solutions in plastic collapse load estimation.

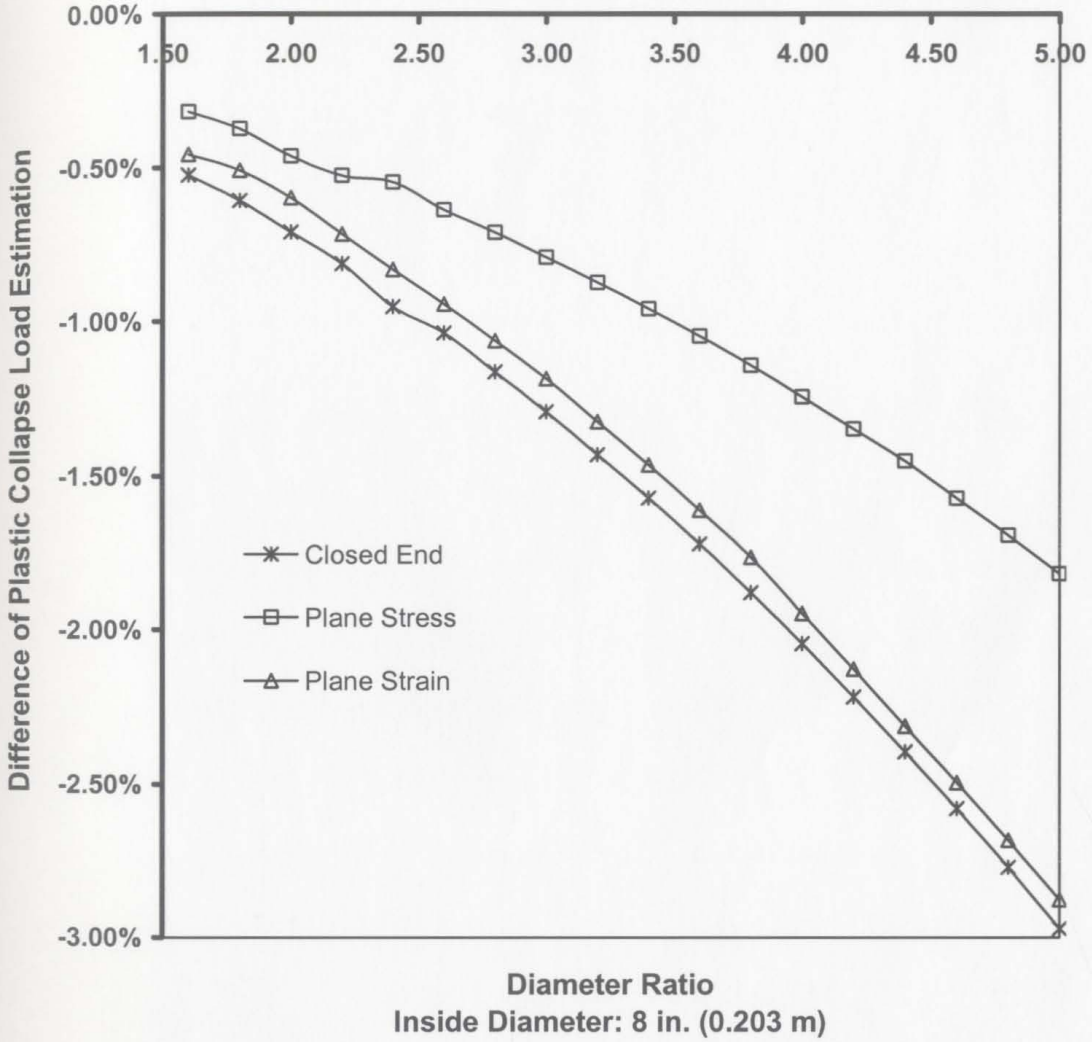

Fig. 6.2 Collapse load estimations on moving boundary and original boundary

6.4 EFFECT OF WORK HARDENING

The plastic collapse loads have been calculated for cylinders exhibiting linear work hardening materials. The effect of work hardening has been assessed using the moving boundary theory and small deformation theory. Results have been plotted in Fig. 6.3 and Fig. 6.4, respectively. Young's modulus of the material is $30x10^6$ *psi* ($2.068x10^5$ *MPa*). The analyzed plane strain cylinders have an inside diameter of 8 *in.* (0.203 *m*) and an outside diameter ranging from 12.8 *in.* (0.325 *m*) to 40 *in.* (1.016 *m*).

Fig.6.3 indicates that the plastic collapse load depends on the work hardening behavior. For a particular material whose tangent modulus of plastic region is $30x10^5$ *psi* ($2.068x10^4$ *MPa*), the plastic collapse load of the cylinder is $9.333x10^4$ *psi* ($6.435x10^2$ *MPa*). For a material exhibiting less work hardening behavior, whose tangent modulus of plastic region is $12x10^5$ *psi* ($0.827x10^4$ *MPa*), the calculated plastic collapse load is $6.928x10^4$ *psi* ($4.777x10^2$ *MPa*). The plastic collapse loads calculated by small deformation theory are shown in Fig. 6.4, where the same characteristic found in moving boundary solutions can be observed.

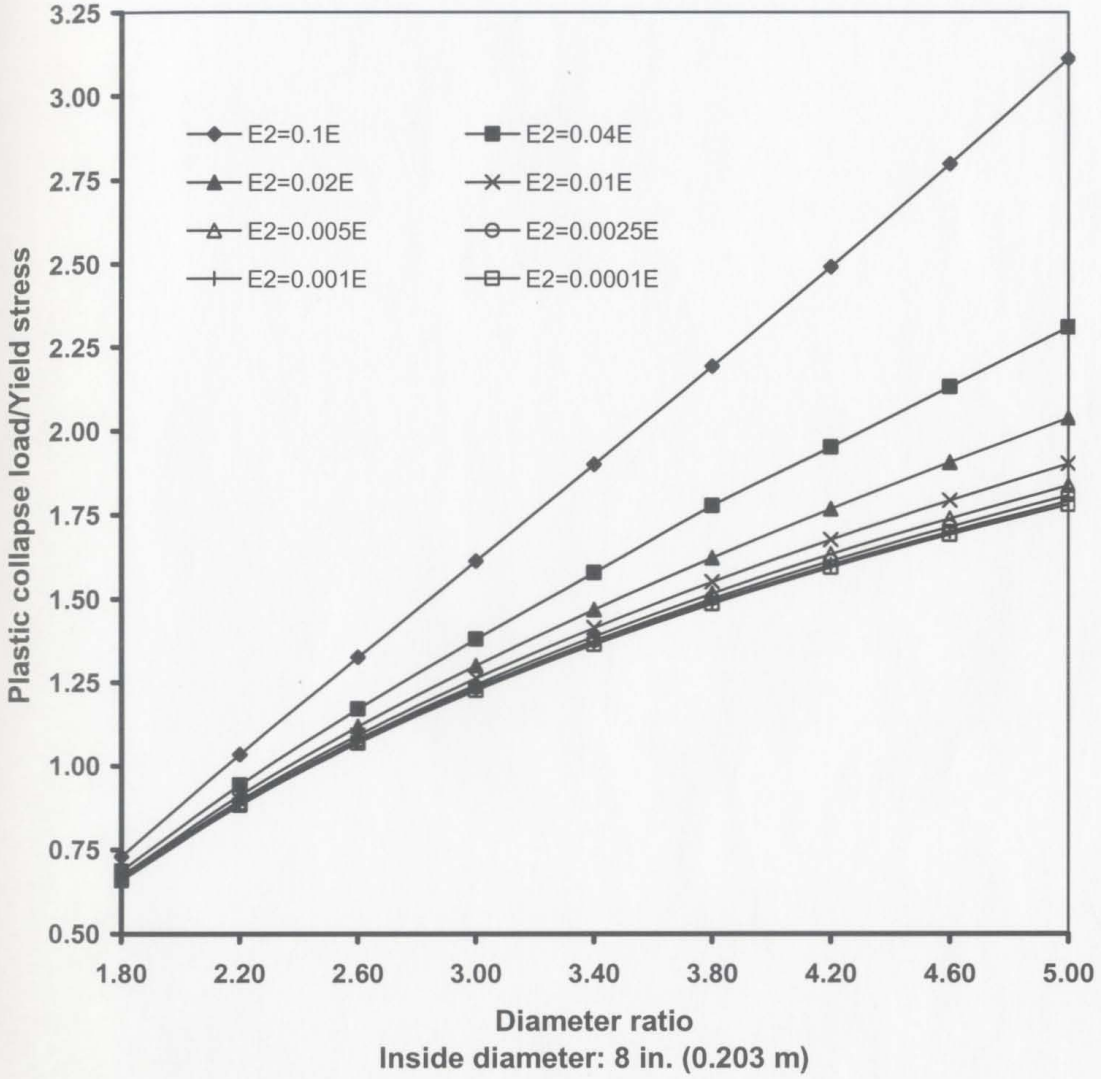

Fig. 6.3 Plastic collapse load vs. diameter ratio – moving boundary theory

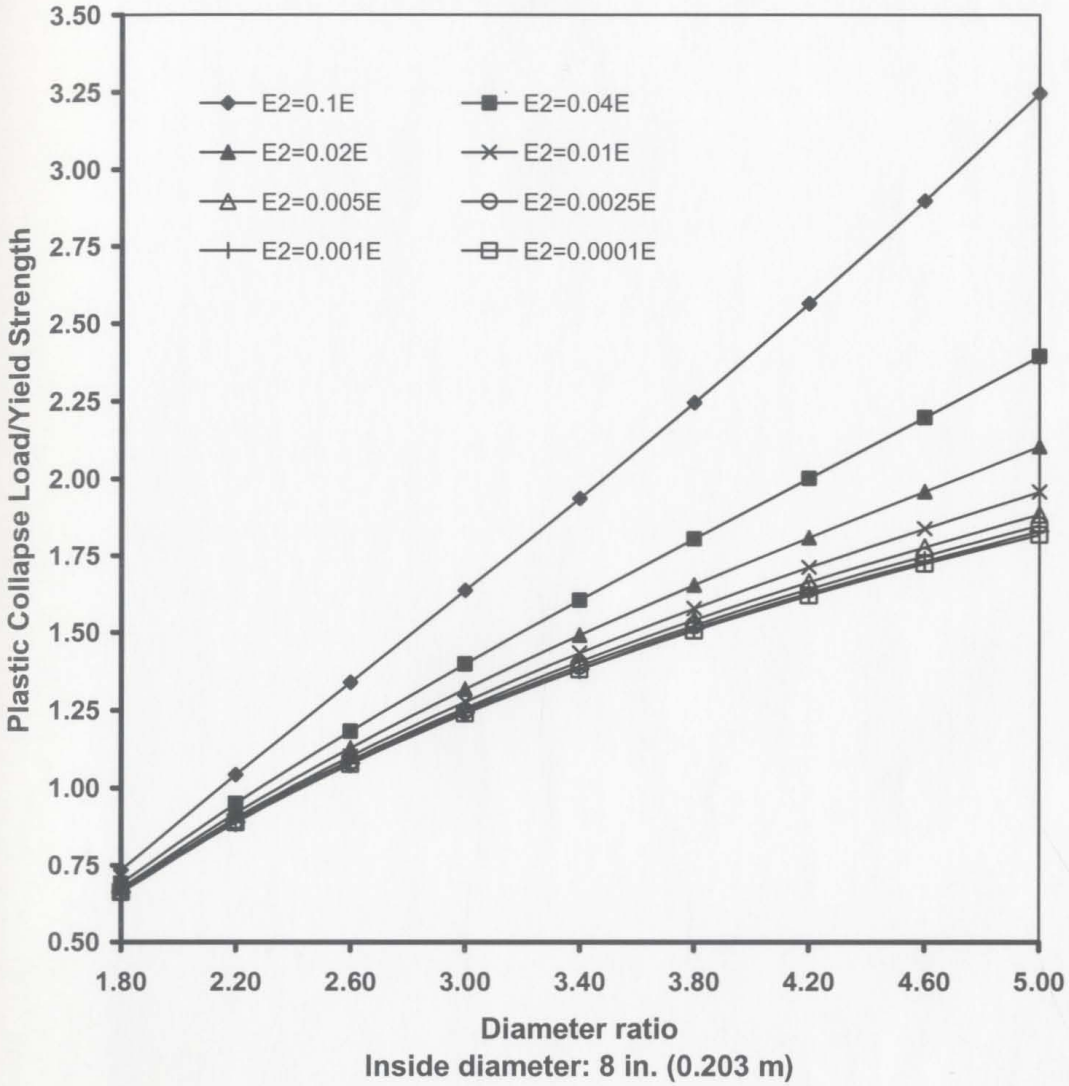

Fig. 6.4 Plastic collapse load vs. diameter ratio – original boundary theory

6.5 RESULTS COMPARISON WITH INELASTIC FEA

Inelastic finite element analyses have been performed using the ANSYS software. The two dimensional solid element with axisymmetric option is used for generating the FEA models for cylinders having an inside diameter of 8 *in.* (0.203 *m*) and an outside diameter ranging from 12.8 *in.* (0.325 *m*) to 40 *in.* (1.016 *m*). The work hardening behavior is postulated as $E_2/E = 1/100$, where E_2 is the tangent modulus of the plastic region on stress and strain curve. The numerical solutions of inelastic FEA have been calculated for large deformation theory and small deformation theory. Plastic collapse loads estimated by inelastic FEA are compared with those obtained by the moving boundary approach. The comparison in Fig. 6.5 indicates that the results obtained by the moving boundary approach are in good agreement with those by the large deformation inelastic FEA.

Inelastic FEA results in Fig. 6.6 indicate that the plastic collapse loads estimated by large deformation finite element analyses are less in value than those by small deformation finite element analyses. It demonstrates the same characteristic observed in the plastic collapse load calculation using the moving boundary approach. Therefore, the proposed formulation is appropriate in plastic collapse load estimation for work hardening material. Conservative solutions can be obtained by the moving boundary approach as it has incorporated the effect of deformed geometry.

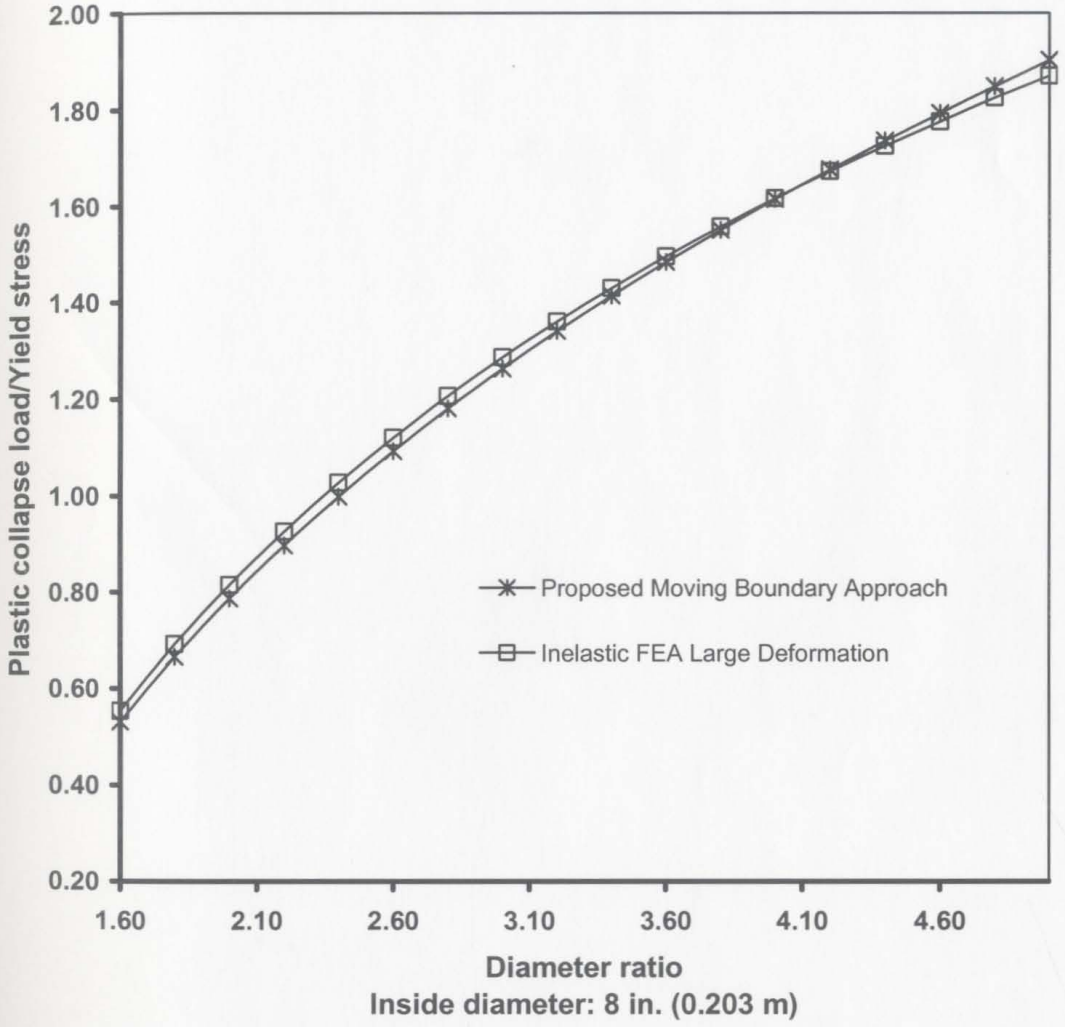

Fig. 6.5 Plastic collapse load estimation by proposed method and inelastic FEA

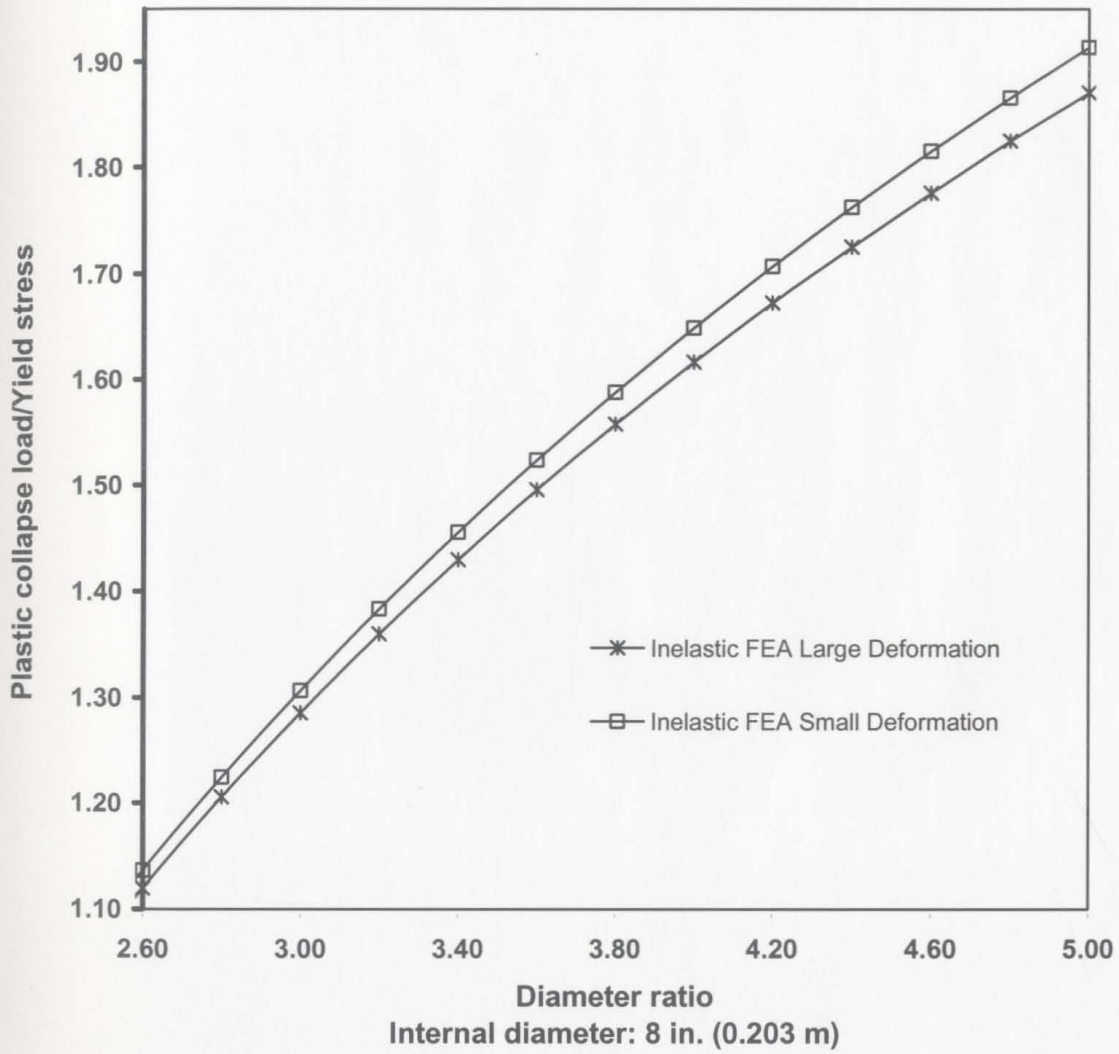

Fig. 6.6 Plastic collapse load estimation by inelastic finite element analysis

6.6 REMARKS

The calculations in this chapter indicate that the proposed formulation is appropriate to carry out plastic collapse load estimation for thick wall cylinders of work hardening material. For von Mises material with same dimensions, cylinders of closed end condition have the highest plastic collapse load while open end cylinders demonstrate the least load bearing capability. Thick wall cylinders of plane strain condition are intermediate to the other two cases yet its load bearing capability is nearer to closed end cylinders. It has been observed in calculations that plastic collapse load for a thick wall cylinder depends on the work hardening behavior of material.

Plastic collapse loads calculated by the moving boundary approach are less than those calculated by small deformation theory. This difference in plastic collapse loads estimation is affected as dimensions of cylinders changes. For cylinders having a same inside diameter, the difference increases with the diameter ratio. Therefore, the moving boundary approach provides conservative solutions in plastic collapse load estimation.

Results by the moving boundary approach have been compared with those by the inelastic finite element analyses. In general, the solutions are comparable and consistent. As an analytical method implemented by the mathematical software MAPLE 6, this method provides an economical and powerful complement to nonlinear finite element analysis since it requires much less calculating cost and implementing efforts.

7. FRACTURE CONSIDERATIONS

7.1 INTRODUCTION

The J integral, which was developed by Rice in 1968, is an important inelastic fracture parameter that characterizes nonlinear material behavior ahead of a crack. Rice found that the nonlinear energy release rate for nonlinear materials could be expressed as a path-independent integral evaluated along an arbitrary contour around a crack, as illustrated in Fig. 7.1.

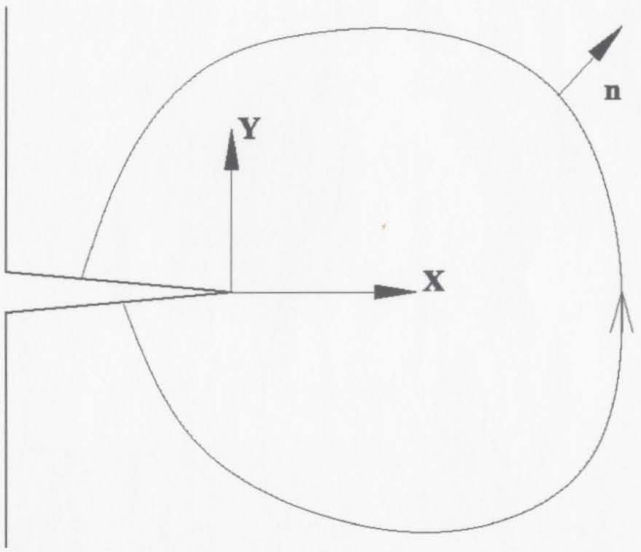

Fig. 7.1 J integral contour around the tip of a crack

The current J integral estimations of crack tip are based primarily on small deformation formulation in which the changes of geometry are assumed to be infinitesimal. The appropriateness of the small deformation theory is based on the condition that the results with this assumption are assumed to be the same or without significant difference with those from deformed geometry formulation. However, it has been observed in this study that energy calculated on the basis of the deformed geometry differs with those obtained on traditional small deformation theory, and the difference can be quite significant. Therefore, it may be inappropriate to neglect the difference for thick wall cylinders under high internal pressure.

In this chapter, energy calculations are carried out for sample cylinders of material with various levels of work hardening behavior. The difference of energy estimations for the undeformed and deformed geometry is further addressed and its effect on the Griffith-type energy balance in elastic plastic fracture mechanics is discussed. Subsequently, the effect of moving boundary on J integral estimations is examined for an inelastic material. The numerical examples involve various cylindrical pressure vessels with a postulated circumferential flaw. The inelastic energy release rates are calculated and compared for both small deformations as well as large deformations based formulations.

7.2 ENERGY CALCULATION ON DEFORMED GEOMETRY

The proposed formulation has been applied to sample thick wall cylindrical vessels in order to calculate the energy stored on the basis of theories that use deformed geometry as well as undeformed geometry for boundaries where the internal pressure is applied. The results of two sample cylinders are listed and compared in Table 7.1 and Table 7.2.

The material properties are:

$\sigma_Y = 30{,}000\,psi.\left(2.068\times10^2\ MPa\right),\ E = 30\times10^6\ psi.\left(2.068\times10^5\ MPa\right)$

Elastic plastic material exhibiting linear work hardening behavior is assumed for both cylinders. Table 1 is listed for a cylinder having an inside radius of 4 *in.* (0.102 *m*) and an outside radius of 20 *in.* (0.508 *m*), while Table 2 is for a cylinder with an inside radius of 6 *in.* (0.152 *m*) and an outside radius of 36 *in.* (0.914 *m*). The cylinder in Table 1 is subjected to an internal pressure of 50,000 *psi* (3.447x10^2 *MPa*), while the one in Table 2 is under an internal pressure of 55,000 *psi* (3.792x10^2 *MPa*).

The comparison of results indicates that the difference of strain energy obtained by formulations based on deformed and undeformed pressure boundaries is not negligible especially when E_2, the tangent modulus of the plastic domain, is small. Thus, the effect of geometric change of the pressure boundary can be significant, and it is therefore appropriate to take the effect into account using the proposed formulation in the energy approach of fracture mechanics.

Table 7.1: Energy required for elastic and inelastic deformation

$r_n = 4\ in.\ (0.102m)\ \ r_o = 20 in.\ (0.508m)$

$P_n = 50{,}000\ psi.\ (3.447 \times 10^2\ MPa)$

Modulus ratio	Energy *In.lb (N.m)*	
	Undeformed geometry	Deformed geometry
E/E_2 =1	0.606×10^4 (0.685×10^3)	0.609×10^4 (0.688×10^3)
E/E_2 =10	1.770×10^4 (2.000×10^3)	1.801×10^4 (2.035×10^3)
E/E_2 =100	3.230×10^4 (3.650×10^3)	3.375×10^4 (3.813×10^3)
E/E_2 =1000	3.708×10^4 (4.189×10^3)	3.930×10^4 (4.440×10^3)

Table 7.2: Energy required for elastic and inelastic deformation

$r_n = 6\ in.\ (0.152m)\ \ r_o = 36\ in.\ (0.914m)$

$P_n = 55{,}000\ psi.\ (3.792 \times 10^2\ MPa)$

Modulus ratio	Energy *In.lb (N.m)*	
	Undeformed geometry	Deformed geometry
E/E_2 =1	0.163×10^5 (0.184×10^4)	0.164×10^5 (0.185×10^4)
E/E_2 =10	0.516×10^5 (0.583×10^4)	0.526×10^5 (0.594×10^4)
E/E_2=100	1.015×10^5 (1.147×10^4)	1.067×10^5 (1.206×10^4)
E/E_2 =1000	1.196×10^5 (1.351×10^4)	1.282×10^5 (1.448×10^4)

7.3 ENERGY APPROACH IN FRACTURE MECHANICS

Many strength failures are caused by dominant plastic deformation where they lead to uncontained large plastic flow, or dominant fracture in that fracture precedes net-section yielding. For thick wall cylinders, failures that are fracture related could occur due to flaws in the material or imperfection generated during fabrication. Research in fracture mechanics, especially the works of Griffith (1920), Wells (1955), Rice (1968), and Hutchinson (1968), provide a basis for modern fracture mechanics. The energy approach is one of the most popular methods that have been applied in engineering design. It was proposed by Griffith (1920) and then further developed by Irwin (1956). Griffith formulated his fracture mechanics theory on the basis of the energy balance principle. According to his theory, a crack can form or an existing crack can grow only if such a process causes the total energy where crack growth occurs to decrease or remain constant. In order for this crack to increase in size, sufficient potential energy must be available from the internal energy and external work to overcome the surface energy of the material.

7.3.1 Griffith Energy Balance

The Griffith model is based on a global energy balance: for fracture to occur or crack to increase in size, the energy stored in the structure must be sufficient to overcome the surface energy of the material. The Griffith energy balance for an incremental increase in the crack area, dA, under equilibrium conditions can be expressed in the following way:

$$\frac{d\Pi}{dA} + \frac{dW_S}{dA} = 0 \tag{7.1}$$

where W_S is the work required to create new surfaces and Π is the potential energy supplied by the internal strain energy and external forces, as defined in the following equation:

$$\Pi = U - W \tag{7.2}$$

7.3.2 Energy Release Rate, *G*

In 1956, Irwin proposed an energy approach equivalent to the Griffith model using the concept of energy release rate, G:

$$G = -\frac{d\Pi}{dA} \tag{7.3}$$

where Π is potential energy and A is crack area. G is a measure of the energy available for an increment of crack extension and it is also called the crack extension force or the crack driving force.

There are two parameters that describe the behavior of cracks: the energy release rate G and the stress intensity factor K. The energy release rate describes global behavior by

quantifying the net change in potential energy that accompanies an increment of crack extension; the stress intensity factor K is a local parameter as it characterizes the stresses, strains, and displacements near the crack tip. For linear elastic materials, the relationship between K and G for both plane stress and plane strain can be expressed by the following equation:

$$G = \frac{K_I^2}{E'} \tag{7.4}$$

$E' = E$ for plane stress and (7.5a)

$$E' = \frac{E}{1-\nu^2} \text{ for plane strain} \tag{7.5b}$$

7.3.3 J Integral

J integral is a path-independent contour integral for analysis of cracks, which is equal to the energy release rate in a nonlinear elastic body that contains a crack. Thus, J for Mode 1 opening is defined by the following equation:

$$J = -\frac{d\Pi}{dA} = \frac{K_I^2}{E'} \tag{7.6}$$

For a cracked body that exhibits a nonlinear load displacement behavior, we can express J in terms of load and displacement:

$$J = \int_0^P \left(\frac{\partial \Delta}{\partial a} \right)_P dP \text{ for load control,} \tag{7.7}$$

$$J = -\int_0^\Delta \left(\frac{\partial P}{\partial a} \right)_\Delta d\Delta \text{ for displacement control.} \tag{7.8}$$

where a is length of crack, Δ and P are displacement and load respectively.

The work of Rice (1968) proved that the J integral could be successfully applied to nonlinear materials including nonlinear elastic material and elastic plastic material, provided no unloading occurs. Therefore, an analysis that assumes nonlinear elastic behavior may be valid for an elastic plastic material as long as the stresses in both materials increase monotonically.

As a path-independent line integral, the J integral measures the amplitude of the singularity in terms of the stresses and strains near a crack tip. For a crack in its two dimensional form as shown in Fig. 7.1, the J is given by:

$$J = \int_\Gamma U_0 dy - \int_\Gamma \left(T_x \frac{\partial u_x}{\partial x} + T_y \frac{\partial u_y}{\partial x} \right) ds \tag{7.9}$$

where: Γ = any path surrounding the crack tip

U_0 = strain energy density (that is, strain energy per unit volume)

T_x = traction vector along x axis

T_y = traction vector along y axis

n = unit outer normal vector to path Γ

u = displacement vector

s = distance along the path Γ

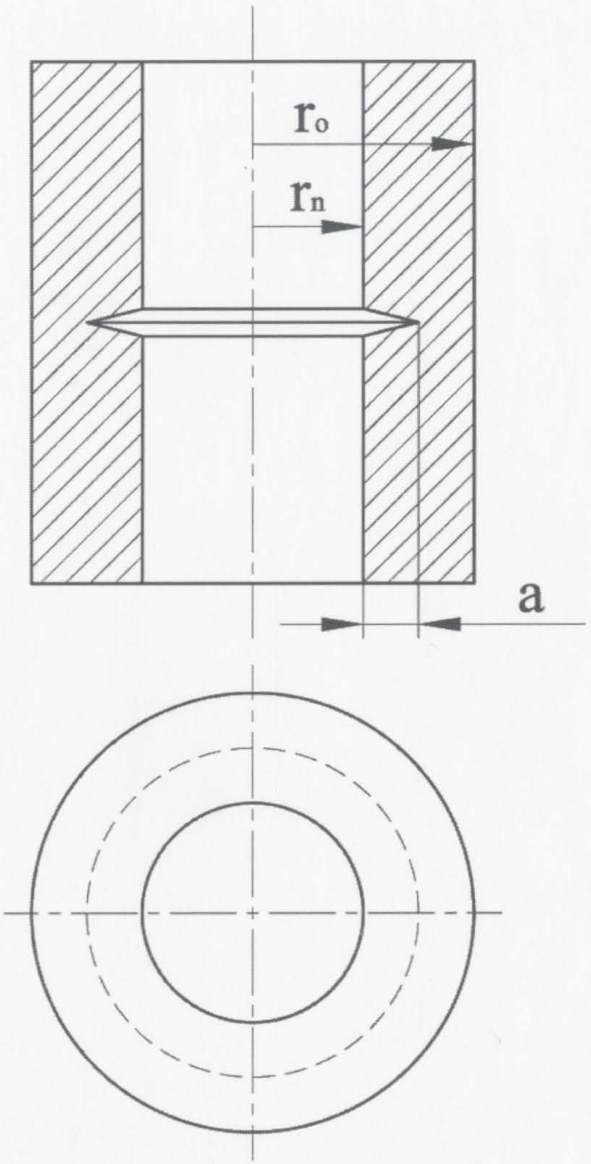

Fig. 7.2 A cylindrical vessel with a circumferential crack

7.4 NUMERICAL CALCULATION OF J INTEGRAL

The analysis of defects, such as circumferential flaws in pressure vessels, is of importance in the evaluation of the fracture integrity of welds in nuclear reactor pressure vessels. In this research, pressure vessels with a circumferential flaw are treated as thick wall cylinders having a flaw with a crack length of a in the radial direction. The flaw is assumed to be circumferentially continuous, as illustrated in Fig. 7.2.

Two sizes of sample cylinders are used to calculate the J integral in this study. They are cylinders with an inside radius of 4 *in.* (0.102 *m*) and an outside radius of 8 *in.* (0.203 *m*) and 20 *in.* (0.508 *m*). The material behavior is assumed to be elastic plastic characterized with linear work hardening. The following values of material properties are used in the analysis:

$E = 30 \times 10^6 \ psi \left(2.068 \times 10^5 \ MPa\right);$
$\sigma_Y = 30{,}000 \ psi \left(2.068 \times 10^2 \ MPa\right); \ \nu = 0.3$

The inelastic J integral is calculated using the ANSYS finite element software with large deformation option to examine the effect of geometric change. The procedure of J integral calculation consists of the following operations:

1. Calculate the strain energy density
2. Define a path for line integral
3. Map the strain energy density onto the path defined
4. Map the component stresses onto the path defined
5. Define the path unit normal vector

6. Calculate T_x and T_y

7. Shift the path a small distance in the positive and negative x directions to calculate the derivatives of the displacement vectors $\frac{\partial u_x}{\partial x}$ and $\frac{\partial u_y}{\partial x}$, as shown in Fig. 7.3. Displacements $u_i^{(1)}$ are mapped onto the path $\Gamma - \frac{\Delta x}{2}$; while displacements $u_i^{(2)}$ are mapped onto the path $\Gamma + \frac{\Delta x}{2}$, then $\frac{du_i}{dx} \cong \frac{u_i^{(2)} - u_i^{(1)}}{\Delta x}$.

8. Integrate the strain energy density with respect to global y, and integrate $\left(T_x \frac{\partial u_x}{\partial x} + T_y \frac{\partial u_y}{\partial x} \right)$ with respect to the path distance s

9. Calculate J integral using Eq. (7.9).

7.4.1 FEA Modeling

The finite element model of the cylinder with circumferential crack is generated using the ANSYS software. The 2-D eight-node PLANE82 element is used, which is a higher order version of the 2-D, four-node element PLANE42. It provides more accurate results for mixed (quadrilateral elements and triangular elements) automatic meshes and can tolerate irregular shapes without as much loss of accuracy. Six crack tip elements (singular elements) are used. The radius of the first array of elements at the tip of crack is $0.2a$ and the ratio of size of the second row of elements to the first row is 0.5. Only the upper half of the cylinder is modeled because of symmetry considerations.

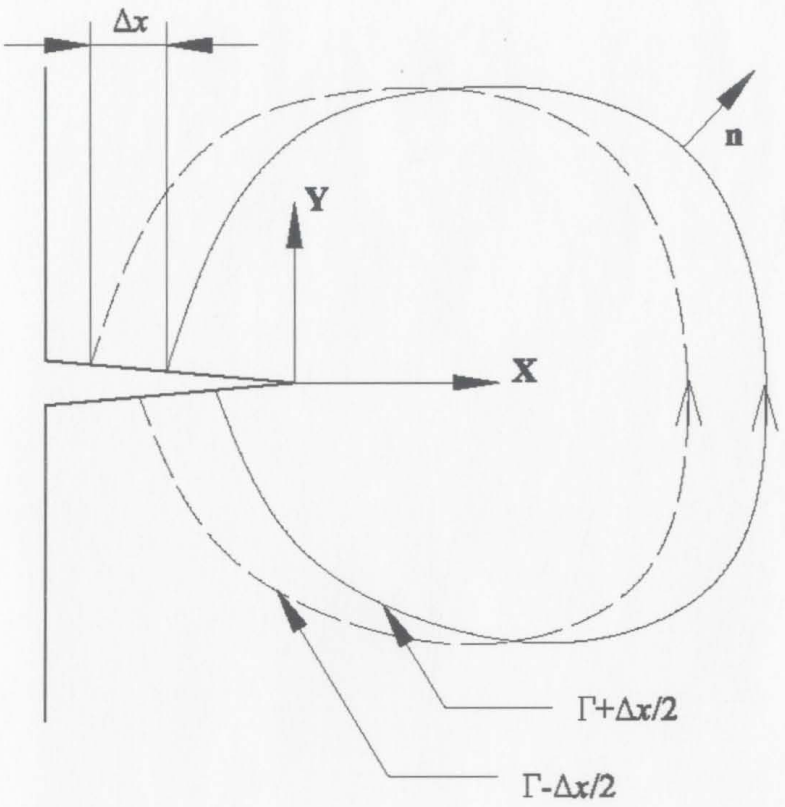

Fig. 7.3 Calculation of derivatives of the displacement vector

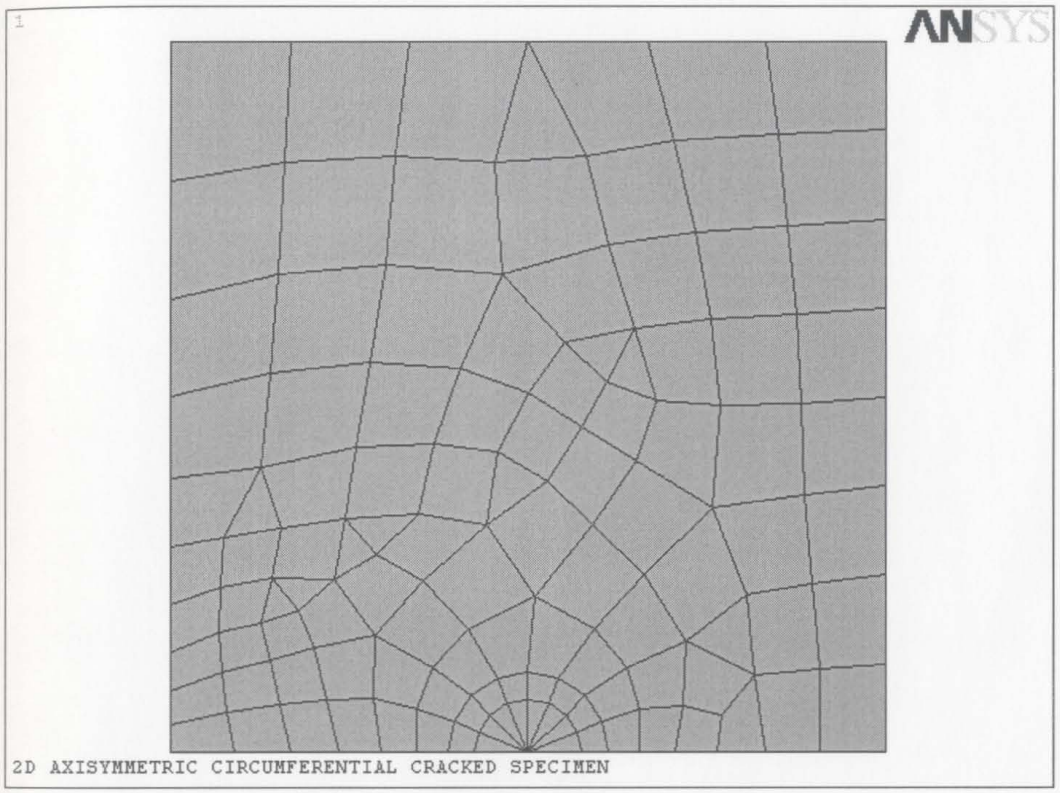

Fig. 7.4. 2D FEA model for a cylinder with circumferential crack

7.4.2 J Integral Calculations for Small Deformation and Large deformation

Results of J integral estimation are shown in Fig. 7.5, Fig. 7.6, and Fig. 7.7 for cylindrical vessels having a circumferential crack. The crack length is assumed to be half of the wall thickness, $a = 0.5T$. The computed J integral values are normalized by making use of $(a\sigma_Y)$, i.e., $\bar{J} = J/(a\sigma_Y)$ and normalized axial load is designated as P_a/σ_Y, where P_a is the remote axial stress applied on the top the crack model.

For a cylindrical vessel having an inside radius of 4 *in* (0.102 *m*) and an outside radius of 8 *in* (0.203 *m*), inelastic energy release rates have been calculated using inelastic finite element analysis on both small deformation assumption and large deformation assumption. The work hardening behavior is characterized by a postulated tangent modulus of $30\text{x}10^4$ *psi* ($2.068\text{x}10^3$ *MPa*). Results for cylinders under various internal pressures are illustrated in Fig. 7.5.

Fig. 7.5 shows the results of large deformation and small deformation analyses are coincident as the axial load increases up to about 0.255 (Internal pressure: 22,900 *psi* or $1.579\text{x}10^2$ *MPa*). This would be the pressure range where the small deformation theory is valid. For higher loads, discrepancy of J integral calculations occurs between large deformation assumption and small deformation assumption. It is found that J integrals calculated on large deformation basis has greater values than those calculated on small deformation basis. Therefore, conservative estimations of energy release rates can be achieved by the large deformation assumption.

Calculation has been conducted to assess the effect of hardening material behavior on a cylindrical vessel having an inside radius of 4 *in* (0.102 *m*) and an outside radius of 8 *in* (0.203 *m*). For elastic plastic materials characterized with three postulated work hardening levels, Fig. 7.6 shows the inelastic results of J integral estimation based on small deformation assumption and large deformation assumption. In the case of same material used, the comparison indicates that the values of J integral estimation using large deformation analysis are larger than those obtained using small deformation analysis for higher pressures. Besides, the difference increases as internal pressure or axial load increases.

Fig. 7.6 also demonstrates that for the same axial load, materials exhibiting less work hardening characteristic have higher energy release rate. Another characteristic in Fig. 7.6 is that the difference in term of J integral between the large deformation analysis and the small deformation analysis depends on the hardening material behavior. For example, when the internal pressure is 22,800 *psi* (1.572×10^2 *MPa*), the difference of J integral calculations due to pressure boundary change is about 2.0% for material I, 10.2% for material II, and up to around 17.7% for material III, the one exhibiting the least hardening behavior among the three materials. Therefore, the less work hardening behavior the material characterizes, the more significant effect the geometric change can generate in the context of energy release rate estimation.

For all three materials, a special point on each curve can be found. For example, this point is at $P_a/\sigma_Y = 0.245$ (Internal pressure: 22,100 *psi* or $1.524\text{x}10^2$ *MPa*) for material II; while at $P_a/\sigma_Y = 0.255$ (Internal pressure: 22,900 *psi* or $1.579\text{x}10^2$ *MPa*) for material I. If the applied axial loads are greater than the axial load at this point, J integral estimates based on small deformation assumption are less than those on large deformation theory. The difference becomes noteworthy as the load increases from this point. Therefore, the conventional small deformation theory provides reasonable J integral estimates for cylindrical vessels subjected to internal pressures up to this point. For higher internal pressures, however, analyses based on large deformation assumption may be appropriate as it can obtain conservative estimates of energy release rate.

For a cylindrical vessel having an inside radius of 4 *in* (0.102 *m*) and an outside radius of 20 *in* (0.508 *m*), inelastic energy release rates have been calculated based on both small deformation assumption and large deformation assumption. Results are plotted in Fig.7.7, where the similar characteristics can be observed as in Fig. 7.5.

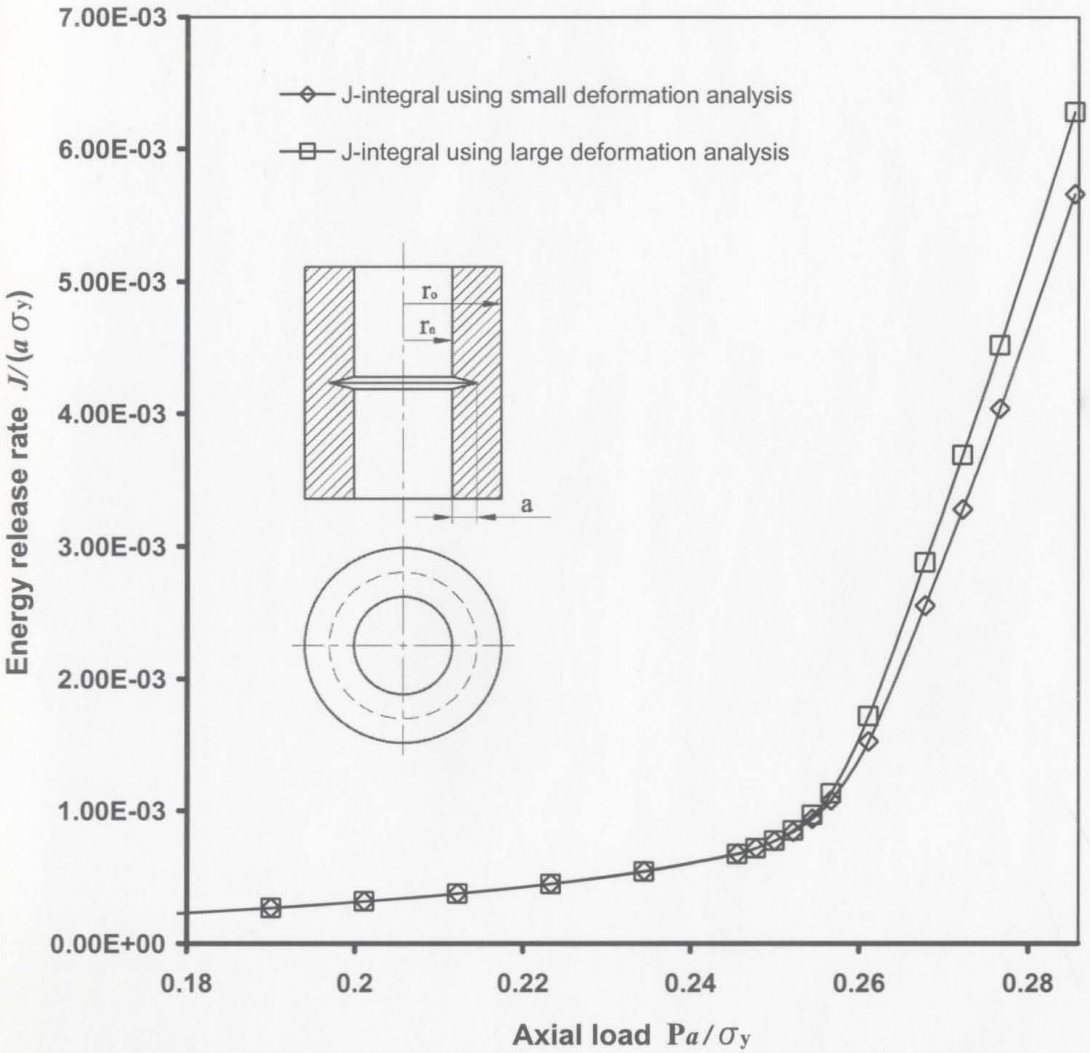

Fig. 7.5 J integral estimations for a cylinder with a circumferential crack

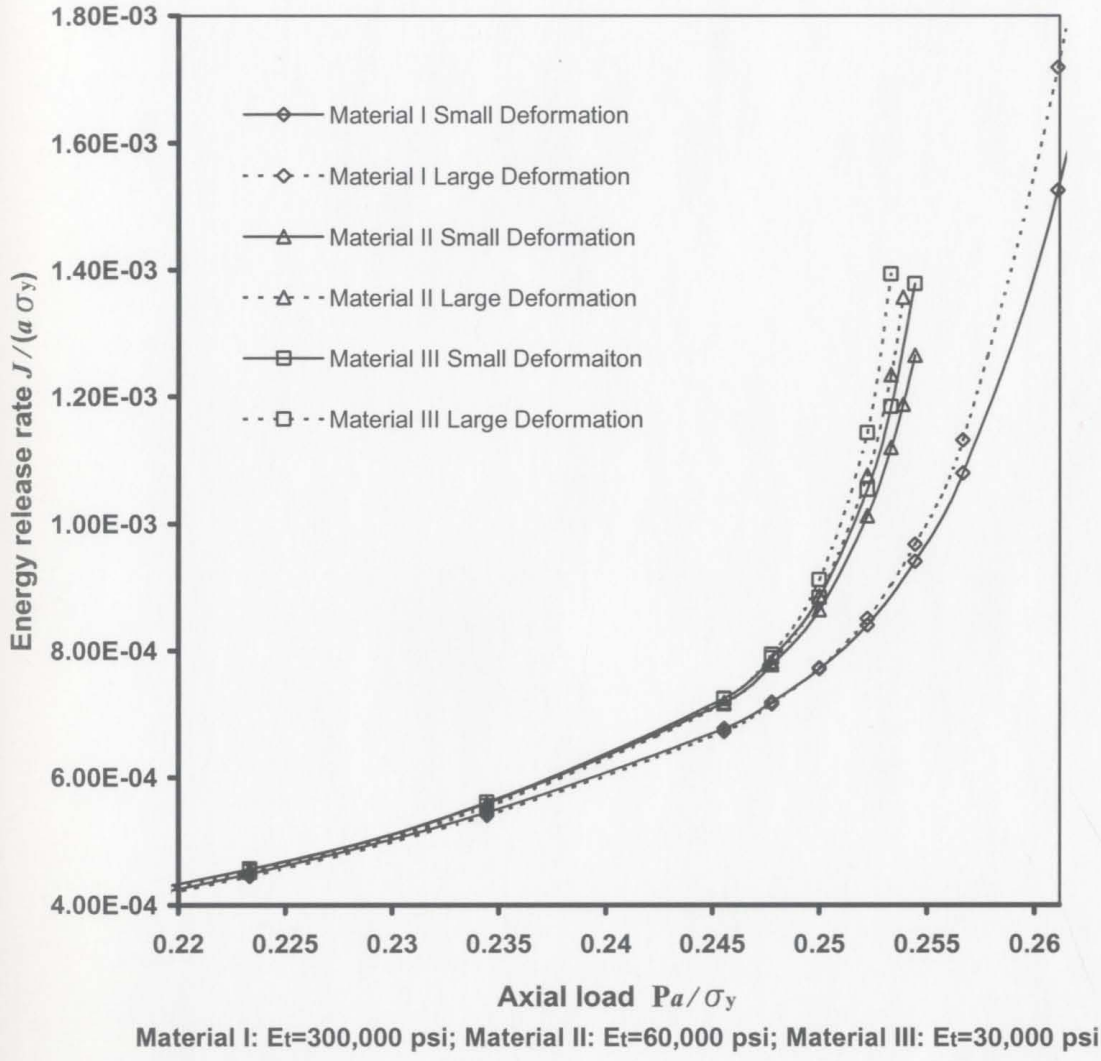

Fig. 7.6 J integral estimations for cylinders with a circumferential crack

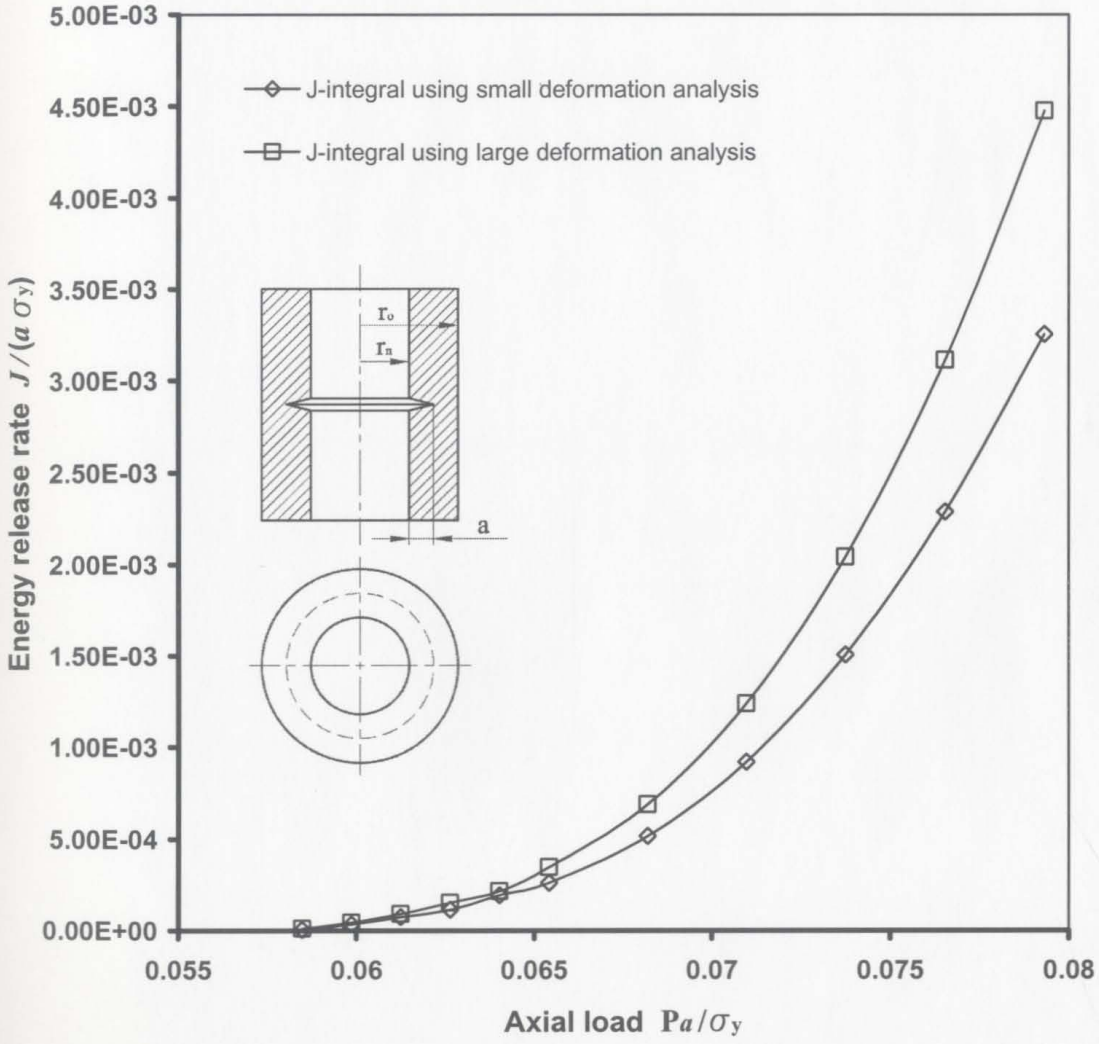

Fig. 7.7 J integral estimations for a cylinder with a circumferential crack

7.5 REMARKS

The computational evaluation of J integral on thick wall cylinders with a circumferential flaw has shown that there can be significant difference between analyses using large deformation and small deformation theory. This difference increases as internal pressure or axial load increases. It is found that the difference is also influenced by material behavior. If a lower work hardening material is used in analysis, then the effect of geometric change is more significant.

The proposed formulation is appropriate in evaluating strain energy for fracture considerations, since it incorporates the effect of geometric changes due to high internal pressures. Therefore, the new formulation is appropriate for elastic plastic fracture calculation in the context of the determination of energy release rate based on fixed and deformed geometry makes a considerable difference. It can be seen that neglecting this difference in designs would likely lead to unconservative situations.

8. CONCLUSIONS AND FUTURE RESEARCH

8.1 CONCLUSIONS

In this dissertation, a moving boundary approach for thick wall cylinders under high internal pressure is developed. The proposed analytical approach is capable of predicting stress, strain, displacement, and energy for deformation on a moving boundary basis. The moving boundary formulation is applicable to analyses for inelastic thick wall cylinders, autofrettage, shakedown and limit analysis.

The moving boundary approach differs from the conventional analytical method for thick wall cylinders with an important feature, which is the incorporation of deformed geometry into the analytical formulation for inelastic analyses on thick wall cylinders. Known prior research can hardly be found on this topic as inelastic formulations are usually based on the basic idealization of original geometry in place of deformed geometry. Such idealization, though may appear to be seemingly simple, yet might not replicate in situ conditions with the reasonable accuracy when the deformation is caused by high pressure. In this study, the principle of virtual work has been employed in the development of an iterative calculation program for inelastic solutions on a moving boundary basis. Using this iterative procedure, the proposed approach accounts for the effect of deformed geometry due to high internal pressure.

The proposed work also involves features in the following aspects. Firstly, a generalized method for axisymmetric analysis on thick wall cylinder has been formulated using parametric functions. Secondly, it provides a generalized elastic plastic solution for thick wall cylinders, which yields Lame's solution and the classical elastic perfectly plastic solution as special cases. Thirdly, it is shown that the actual uniaxial stress and strain curves of materials for high pressure vessels can be linearized in a piecewise manner to simulate the nonlinear material behaviors. The general form of piecewise linearized constitutive equation has been developed in this study. It provides a necessary condition to solve cylinder problems for inelastic materials exhibiting work hardening behavior.

The Maple 6.0 mathematical program has been used for implementing the moving boundary approach. Stress, strain, displacement, and energy have been calculated for elastic and plastic material on a moving boundary basis. The effects of geometric change on elastic plastic analyses for thick wall cylinders under internal pressure have been assessed. Calculations indicate two characteristics. Firstly, radial displacements calculated on a moving boundary basis are larger than those of the original boundary theory. The difference is negligible for elastic material but increases with the internal pressure for plastic material behavior. Secondly, energy calculated on a moving boundary basis is greater than that by the original boundary theory. For cylinders subject to high internal pressure, geometric change has a significant effect on the evaluation of energy required for deformation.

For the purpose of comparison, nonlinear finite element analyses (NLFEA) have been conducted using the ANSYS program. The comparison of inelastic solutions calculated by the moving boundary approach with those of nonlinear finite element analyses is favorable. The numerical solutions of NLFEA have demonstrated the same characteristic as the moving boundary approach about the effect that the moving boundary makes on radial displacements and energy calculations. In general, the proposed moving boundary theory is consistent with NLFEA.

The moving boundary formulation for autofrettaged cylinders obeying work hardening stress strain law has also been developed. Analytical solutions based on deformed geometry have been obtained. The moving boundary formulation has been verified by comparing results of the analytical method and inelastic FEA. As well, the Bauschinger effect has been included in the presented analysis for kinematic work hardening materials.

An iterative implementation procedure for shakedown calculation has been developed using the principle of virtual work to account for the effect of geometric change. Shakedown pressures have been calculated on both the undeformed geometry and the deformed geometry for cylinders of closed end, open end, and plane strain conditions. It has been found that difference in shakedown pressure estimation due to geometric change is not particularly pronounced. However, it has been shown that the shakedown pressure calculation can be significantly affected by various end conditions as the difference between open end and closed end or plane strain is not negligible.

The moving boundary approach has been applied to plastic collapse load estimations wherein it has been compared with inelastic finite element analyses. In general, the solutions are comparable and consistent. Plastic collapse loads calculated by the moving boundary approach are less than those calculated by small deformation theory. This difference in plastic collapse loads estimation is affected as dimensions of cylinders changes. For cylinders having a same inside diameter, the difference increases with the diameter ratio. The moving boundary approach provides more conservative plastic collapse loads than the traditional small deformation theory. Therefore, the proposed formulation is appropriate for plastic collapse load estimations of large deformation thick wall cylinders exhibiting work hardening.

The computation of the J integral for thick wall cylinders with circumferential flaw using the ANSYS program indicates that there is a significant difference between analyses using large deformation and small deformation. This difference depends on the magnitudes of the internal pressure or axial load, and also the influence of material behavior. As a lower work hardening material is used in the analysis, the effect of geometric change is more significant. This confirms that the proposed formulation is appropriate for representing energy in fracture mechanics evaluation as it incorporates the effect of geometric change due to high internal pressures. Because the determination of energy release rate based on undeformed and deformed geometry exhibits a considerable difference, it can be concluded that neglecting this difference can be unconservative in the evaluation of the inelastic fracture mechanics parameter.

In summary, the moving boundary approach presented in this dissertation is appropriate for inelastic analysis, including autofrettage, shakedown, and limit analysis of thick wall cylinders because the effect of deformed geometry is incorporated in the formulation. This approach is also appropriate for the inelastic fracture calculation because the incorporation of deformed geometry can avoid an unconservative situation as it pertains to the design integrity of high pressure cylindrical vessels. Furthermore, since the proposed formulation of stress strain law is mathematically simpler to use than the incremental theory of plasticity, it represents an alternative assessment tool that can be used for inelastic analysis, which is usually performed by expensive and elaborate nonlinear finite element analyses.

8.2 FUTURE RESEARCH

The moving boundary approach has been found to be useful and appropriate for determining inelastic response for thick wall cylinders subjected to high internal pressure. Continuing efforts should be directed to further explore its usefulness in other applications of inelastic analyses incorporating the effect of geometric change.

Future research should focus on extending the moving boundary formulation and solving three-dimensional pressure components, such as cylinders with T-junction openings. Another area for further work is the determination of inelastic fracture mechanics parameters using the moving boundary theory. Preliminary efforts have been made in this dissertation and should be continued and extended to the applications of three-dimensional pressure components with defects. The nature of high pressure vessels is such that analyses of components with flaws require safe and conservative calculations in inelastic fracture mechanics. The moving boundary approach would serve as an appropriate means in evaluation of inelastic fracture parameters. It would be therefore highly rewarding to conduct research in this area.

REFERENCES

Anderson, T. L., 1991, *Fracture Mechanics Fundamentals and Applications*, CRC Press, Boca Raton.

ASME Boiler & Pressure Vessel Code, 1998, Section VIII, Division 3-Alternative Rules for High Pressure Vessels, The American Society of Mechanical Engineers, New York.

Baumel, Jr. A., and Seeger, T., *Materials Data for Cyclic Loading*, Elsevier Science Publishing Company, Inc., New York.

Budiansky, B., 1959, "A Reassessment of Deformation Theories of Plasticity," *ASME Journal of Applied Mechanics*, Vol. 26, pp. 259-264.

Chakraborty, J., 1987, *Theory of Plasticity*, McGraw Hill, New York.

Char, B. W., 1991, *Maple V Language Reference Manual*, Springer-Verlag.

Chen, P. C. T., 1973, "A Comparison of Flow and Deformation Theories in a Radially Stressed Annular Plate," *ASME Journal of Applied Mechanics*, Vol. 40, pp. 283-287.

Chen, P. C. T., 1986, "The Bauschinger and Hardening Effect on Residual Stresses in an Autofrettaged Thick-Walled Cylinder," *Journal of Pressure Vessel Technology, ASME Trans.*, Vol. 108, pp. 108-112.

Chen, P. C. T., 1992, "Nonlinear Stress Analysis of Composite-Jacketed Steel Cylinders Subjected to High Internal Pressure," *ASME PVP* Vol. 40, pp. 283-287.

Chen, R., 1996, "Constraint Based Fracture Assessment of Pipeline Surface Cracks," *M. A. Sc. Thesis*, Department of Mechanical Engineering, University of Waterloo, Canada.

Chen, W. F., and Han, D. J., 1988, *Plasticity for Structural Engineers*, Springer-Verlag, New York.

Dhalla, A. K., Jones, G. L., 1986, "ASME Code Classification of Pipe Stresses: A Simplified Elastic Procedure," *International Journal of PVP*, Vol. 26, pp. 145-166.

Dowling, N. E., 1993, *Mechanical Behavior of Materials*, Prentice Hall, New Jersey.

Dubey, R. N., and Seshadri, R., 2000, "Analysis of Thick Elastic-Plastic Cylinders," *Proceedings of the 8th International Symposium on Plasticity and Its Current Applications,* Whistler, B. C., Canada.

Durban, D., 1979, "Large Strain Solution for Pressurized Elasto/Plastic Tubes," *ASME Journal of Applied Mechanics*, Vol. 64, pp. 228-230.

Durban, D., and Kubi, M., 1992, "A General Solution for the Pressurized Elastoplastic Tubes," *ASME Journal of Applied Mechanics*, Vol. 59, pp. 20-26.

Franklin, G., Morrison, J.L.M., 1960, "Autofrettage of Cylinders: Prediction of Pressure/External Expansion Curve and Calculation of Residual Stresses," *Proceedings of International Mechanical Engineers*, Vol. 174, No. 35, pp. 947-965.

Fryer, D.M., and Harvey, J.F., 1998, *High Pressure Vessels*, Chapman & Hall, New York.

Gould, P.L., 1983, *Introduction to Linear Elasticity*, Springer-Verlag, New York.

Griffith, A. A., 1920, "The Phenomena of Rupture and Flow in Solids," *Philosophical Transactions*, Series A, Vol. 221, pp. 163-198.

Hill, R., 1950, *The Mathematical Theory of Plasticity*, Clarendon Press. Oxford.

Hill, R., Lee, E. H., and Tupper, S. J., 1951, "Plastic Flow in Closed-End Tube with Internal Pressure," *Proceeding of the First US National Congress on Applied Mechanics*, Chicago, Illinois.

Hodge, P. G., and White, Jr., G. N., and Providence, R. I., 1952, "A Quantitative Comparison of Flow and Deformation Theories of Plasticity," *ASME Journal of Applied Mechanics*, Vol. 17, No. 2, pp. 180-184.

Hutchinson, J.W., 1968, "Singular Behavior at the End of a Tensile Crack Tip in a Hardening Material," Journal of the Mechanics and Physics of Solids, Vol. 16, pp. 13-31.

Ilyushin, A.A., 1946, "Some Problems in the Theory of Plastic Deformation," RMB-12, Translation from *Prikl. Math. Mech.*, Vol. 7, 1943, pp. 245-272, by Division of Applied Mathematics, Brown University.

Irwin, G.R., 1956, "Onset of Fast Crack Propagation in High Strength Steel and Aluminum Alloys," Sagamore Research Conference Proceedings, Vol.2, pp. 289-305.

Jahed, H., 1997, "A Variable Material Property Approach for Elastic-plastic Analysis of Proportional and Nonproportional Loading," *Ph. D. Thesis*, University of Waterloo, Waterloo, Canada.

Jahed, H., and Dubey, R.N., 1996, "A Consistent Inelastic Formulation Analogous to Elastic Problems with Variable Coefficients," *ASME PVP*, Vol. 343, Development Validation, and Application of Inelastic Methods for Structural Analysis and Design, pp. 215-223.

Jahed, H., and Dubey, R.N., 1996, "Residual Stresses Calculation in Autofrettage Using Variable Material Properties Method," *ASME PVP*, Vol. 327, Residual Stress in Design, Fabrication, Assessment and Repair, pp. 181-188.

Jahed, H., and Dubey, R. N., 1997, "An Axisymmetric Method of Elastic-Plastic Analysis Capable of Predicting Residual Stress Field," *Journal of Pressure Vessel Technology, Transactions of ASME,* Vol. 119, pp. 264-273.

Jones, G. L., and Dhalla, A. K., 1981, "Classification of Clamp Induced Stresses in Thin Walled Pipe," *Proc. ASME PVP Conference*, Denver, CO. Vol. 81, pp. 17-23.

Kendall, D.P., 2000, "A Short History of High Pressure Technology from Bridgman to Division 3," *Journal of Pressure Vessel Technology*, Vol. 122, pp. 229-233.

Lubliner, J., 1990, *Plasticity Theory*, Macmillan Publishing Company, New York.

Mackenzie, D., and Boyle, J.T., 1993, " A Method of Estimating Limit Loads by Iterative Elastic Analysis I – Simple Examples," *International Journal of PVP*, Vol. 53, pp. 77-95.

Marriott, D.L., 1988, "Evaluation of Deformation or Load Control of Stress under Inelastic Conditions using Elastic Finite Element Stress Analysis," *ASME PVP*, Vol. 136, Pittsburgh.

Mendelson, A., 1968, *Plasticity: Theory and Application*, The Macmillan Company, New York.

Mendelson, A., and Manson, S.S., 1959, "Practical Solution of Plastic Deformation in the Elastic-Plastic Range," *NACA Technical Report* R-28.

Milligan, R. V., Koo, W. H., and Davidson, T. E., 1966, "The Bauschinger Effect in a High-Strength Steel," *ASME Journal of Basic Engineering*, pp. 480-488.

Moftakhar, A., Buczynski, A., and Glinka, G., 1995, "Calculation of Elasto-Plastic Stress and Strain in Notches under Multiaxial Loading," *International Journal of Fracture*, Vol. 70, pp. 357-373.

Mroz, E., and Olszak, A. H., 1963, *Recent Advancement in the Mathematical Theory of Plasticity,* Pergamon Press.

Nadai, A., 1950, *Theory of Flow and Fracture of Solids*, McGrow-Hill, London.

Parker, A. P., 2001, "Autofrettage of Open End Tubes – Pressures, Stresses, Strains and Code Comparisons", *Journal of Pressure Vessel Technology*, 123, pp. 271-281.

Perl, M., and Arone, R., 1988, "Stress Intensity Factors for a Radially Muticracked Partially Autofrettaged Pressurized Thick-Walled Cylinder," *Journal of Pressure Vessel Technology, ASME Trans.*, Vol. 110, pp. 147-154.

Perl, M., and Arone, R., 1994, "An Axisymmetric Stress Release Method for Measuring the Autofrettage Level in Thick-Walled Cylinders – Part I: Basic Concept and Numerical Simulation," *Journal of Pressure Vessel Technology,* Vol. 116, pp. 384-388.

Perl, M., 2000, "The Change in Overstrain Level Resulting From Machining of an Autofrettaged Thick-Walled Cylinder," *Journal of Pressure Vessel Technology, ASME Trans.*, Vol. 122, pp. 9-14.

Prager, W., 1957, "A New Method of Analyzing Stress and Strains in Work-Hardening Plastic Solids," *ASME Journal of Applied Mechanics*, Vol. 23, pp. 493-496.

Reinhardt, W.D., and Seshadri, R., 2003, "Limit Load Bounds for the $\mathbf{m}_\alpha$ Multiplier," *Journal of Pressure Vessel Technology, ASME Trans.,* Vol.125, pp. 11-18.

Rice, J.R. "A Path Independent Integral and the Approximate Analysis of Strain Concentration by Notches and Cracks." *Journal of Applied Mechanics*, Vol. 35, 1968, pp.379-386

Rice, J.R., and Rosengren, G.F., 1968, "Plane Strain Deformation near a Crack Tip in a Power-Law Hardening Material," *Journal of the Mechanics and Physics of Solids*, Vol. 16, pp. 1-12.

Seeger, T., 1985, " A Generalized Method for Estimating Multiaxial Elastic-Plastic Notch Stresses and Strains Part 1: Theory," *ASME Journal of Engineering Materials and Technology*, Vol. 107, pp. 250-254.

Seshadri, R., 1990, "The Effect of Multiaxiality and Follow-Up on Creep Damage," *Journal of Pressure Vessel Technology, ASME Trans.,* Vol.112, pp. 378-385.

Seshadri, R., 1991, "Simplified Methods for Determining Multiaxial Relaxation and Creep Damage," *Proceedings of ASME Pressure Vessels and Piping Conference, San Diego, ASME PVP* 210-2, pp. 173-180.

Seshadri, R., 1991, "The Generalized Local Stress Strain (GLOSS) Analysis – Theory and Applications," *Journal of Pressure Vessel Technology, ASME Trans.*, Vol.113, pp. 219-227.

Seshadri, R., 1994, "Residual Stress Estimation and Shakedown Evaluation Using GLOSS Analysis," *Journal of Pressure Vessel Technology, ASME Trans.*, Vol. 116, pp. 290-294.

Seshadri, R., 2000, "Limit Loads Using Extended Variational Concepts in Plasticity," *Journal of Pressure Vessel Technology, ASME Trans.*, Vol.122, pp. 379-385.

Seshadri, R., and Fernando, C.P.D., 1992, "Limit Loads of Mechanical Components and Structures Using the GLOSS R-Node Method," *Journal of Pressure Vessel Technology, ASME Trans.*, Vol. 114, pp. 201-208.

Seshadri, R., and Mangalaramanan, S. P., 1997, "Lower Bound Limit Loads Using Variational Concepts: The $\mathbf{m}_\alpha$-method," *International Journal of PVP*, Vol. 71, pp. 93-106.

Seshadri, R., and Marriott, D. L., 1992, "On Relating the Reference Stress, Limit Load, and the ASME Stress Classification Concepts," *ASME PVP*, Vol. 113, pp. 350-353.

Seshadri, R. and Mikulcik, E. C.,1989, "On Relating Multiaxial and Uniaxial Stress Relaxation in Pressure Components," *Trans. of the CSME*, Vol. 13, pp. 11-16.

Wells, A.A., 1955, "The Condition of Fast Fracture in Aluminum Alloys with Particular Reference to Comet Failures," *British Welding Research Association Report*.

Zhao, W., Dubey, R. N., and Seshadri, R., 2001, "A Simplified Method for Estimating Residual Stresses Fields in Elastic-plastic Thick-walled Cylinder Subjected to High Internal Pressure," *Proceedings of 18th Canadian Congress of Applied Mechanics*, St. John's, NF, Canada, vol. 2, pp. 325-326.

Zhao, W., Seshadri, R., and Dubey, R.N., 2002, "On Thick-walled Cylinder under Internal Pressure", *Proceedings of GUN TUBES 2002 Conference*, Oxford, United Kingdom, Session S1P2, pp. 1-9.

Zhao, W., Seshadri, R., and Dubey, R.N., 2003, "On Thick-Walled Cylinder Under Internal Pressure," *Journal of Pressure Vessel Technology, ASME Trans.*, Vol. 125, pp. 267-273.

Ziegler, H., 1959, "A Modification of Prager's Hardening Rule," Quarterly of Mathematics, Vol.17, No. 1, pp. 55-65

APPENDIX A: Maple 6 Programs For Inelastic Analyses

This appendix lists the MAPLE 6 procedure for implementing the inelastic analysis on thick walled cylinders subject to high internal pressure based on deformed geometry and undeformed geometry.

A.1 Maple 6 Program for Inelastic Stress Calculations

Elastic Plastic Analysis of Thick Walled Cylinder
General Procedure for Closed Ends, Plane Strain, and Plane Stress Conditions
Formulation Based on Virtual Work Principle
In Plane Stress, q=0; in Plane Strain, q = 2*nu; q = 1 for Closed Ends
Plane Strain

```
> restart: Digits:=10:with(linalg): with(plots):
```

Properties and Conditions

```
> S_Y:=30000;
> E_1:=30*10^6;
> E_2:=E_1/100;
> E_p:=1/((1/E_2)-(1/E_1)):
> nu_1:=0.3: nu_p:=0.5: nu_2:=E_2*((nu_1/E_1)+(0.5/E_p )):
> p_0:=0: p_n:=30000:
> R_0:=20.0: R_n:=4.0:  r_0:=R_0: r_n:=R_n: t:=r_0/r_n: T:=R_0/R_n:
> 'E_1'=E_1,'E_2'=E_2,'E_p'=E_p,'p_n'=p_n;
> q:=2*nu_1;
```

Original Geometry

```
> g_1:=x^2*S_Y/sqrt(3*r_0^4+(1-q)^2*x^4):
> g_2:=g_1*(1+nu_p)*E_2*r_0^2/(2*(1-nu_2^2)*E_p*x^2):
> f:=g_1*(r_0^2-r_n^2)-g_2*((x^2-r_n^2)-2*r_n^2*ln(x/r_n))-p_n*r_n^2:
> r_1:=fsolve(f,x): x:=r_1: g_1c:=g_1:g_2c:=g_2: x:='x':
> '[g_1c,g_2c,r_1]'=[g_1c,g_2c,r_1];
> Eenel:=3.14159*g_1c^2*(1+nu_1)*(r_0^2-r_1^2)/E_1*(r_0^2/r_1^2+(1-2*nu_1));
> sigma_rP:=-g_1c*(r_0^2/r^2-1)+g_2c*(r_1^2/r^2-1-2*ln(r_1/r)):
> sigma_tP:=g_1c*(r_0^2/r^2+1)-g_2c*(r_1^2/r^2-1+2*ln(r_1/r)):
> sigma_zP:=4*nu_2*g_2c*ln(r/r_1)+q*g_1c:
> sigma_rE:=-g_1c*(r_0^2/r^2-1):
> sigma_tE:=g_1c*(r_0^2/r^2+1):
> sigma_zE:=q*g_1c:
> etE:=(sigma_tE-nu_1*sigma_rE-nu_1*sigma_zE)/E_1:
> r:=r_0:etE0:=etE: r:='r':
> u_0:=r_0*etE0;
> sijsij_P:=sigma_rP^2+sigma_tP^2+sigma_zP^2:
> skk_P:=sigma_rP+sigma_tP+sigma_zP:
> sijsij_E:=sigma_rE^2+sigma_tE^2+sigma_zE^2:
> skk_E:=sigma_rE+sigma_tE+sigma_zE:
> r:=r_1:sijsij_P1:=sijsij_P:skk_P1:=skk_P:sijsij_E1:=sijsij_E:skk_E1:=skk_E:r:='r':
> eta:=((1+nu_2)*sijsij_P-nu_2*skk_P^2)/(2*E_2)-((1+nu_2)*sijsij_P1-
nu_2*skk_P1^2)/(2*E_2)+((1+nu_1)*sijsij_E1-nu_1*skk_E1^2)/(2*E_1):
> Eenpl:=2*3.14159*int(eta*r,r=r_n..r_1);
> Energy:= Eenel + Eenpl;
> Work:=3.14159*p_n*u_n*(R_n+r_n)/2;
> FF:=evalf(Energy - Work):
> y_c:=solve(FF,u_n); u_n:=y_c; W:=Work;
> r_n:=R_n+u_n;r_0:=R_0+u_0;  u_n:='u_n':
> print('[r_0,r_1,r_n,g_1,g_2,Energy,Work]'=[r_0,r_1,r_n,g_1c,g_2c,Energy,W]);
> sigma_rP:=-g_1c*(r_0^2/r^2-1)+g_2c*(r_1^2/r^2-1-2*ln(r_1/r)):
> sigma_tP:=g_1c*(r_0^2/r^2+1)-g_2c*(r_1^2/r^2-1+2*ln(r_1/r)):
```

```
> sigma_zP:=4*nu_2*g_2c*ln(r/r_1)+q*g_1c:
> sigma_rE:=-g_1c*(r_0^2/r^2-1):
> sigma_tE:=g_1c*(r_0^2/r^2+1):
> sigma_zE:=q*g_1c:
> p_e:=plot([sigma_rE,sigma_tE,sigma_zE],r=r_1..R_0):
> p_p:=plot([sigma_rP,sigma_tP,sigma_zP],r=R_n..r_1):display({p_e,p_p});
```

Deformed Geometry

```
> for i from 1 to 5 do
> g_1:=x^2*S_Y/sqrt(3*r_0^4+(1-q)^2*x^4):
g_2:=g_1*(1+nu_p)*E_2*r_0^2/(2*(1-nu_2^2)*E_p*x^2):
f:=g_1*(r_0^2-r_n^2)-g_2*((x^2-r_n^2)-2*r_n^2*ln(x/r_n))-p_n*r_n^2:
> r_1:=fsolve(f,x): x:=r_1: g_1c:=g_1:g_2c:=g_2: x:='x':
'[g_1c,g_2c,r_1]'=[g_1c,g_2c,r_1];
> Eenel:=3.14159*g_1c^2*(1+nu_1)*(r_0^2-r_1^2)/E_1*(r_0^2/r_1^2+(1-2*nu_1));
> sigma_rP:=-g_1c*(r_0^2/r^2-1)+g_2c*(r_1^2/r^2-1-2*ln(r_1/r)):
> sigma_tP:=g_1c*(r_0^2/r^2+1)-g_2c*(r_1^2/r^2-1+2*ln(r_1/r)):
> sigma_zP:=4*nu_2*g_2c*ln(r/r_1)+q*g_1c:
> sigma_rE:=-g_1c*(r_0^2/r^2-1):
> sigma_tE:=g_1c*(r_0^2/r^2+1):
> sigma_zE:=q*g_1c:
> etE:=(sigma_tE-nu_1*sigma_rE-nu_1*sigma_zE)/E_1:
> r:=r_0:etE0:=etE: r:='r':
> u_0:=r_0*etE0;
> sijsij_P:=sigma_rP^2+sigma_tP^2+sigma_zP^2:
> skk_P:=sigma_rP+sigma_tP+sigma_zP:
> sijsij_E:=sigma_rE^2+sigma_tE^2+sigma_zE^2:
> skk_E:=sigma_rE+sigma_tE+sigma_zE:
> r:=r_1:sijsij_P1:=sijsij_P:skk_P1:=skk_P:sijsij_E1:=sijsij_E:skk_E1:=skk_E:r:='r':
```

```
> eta:=((1+nu_2)*sijsij_P-nu_2*skk_P^2)/(2*E_2)-((1+nu_2)*sijsij_P1-
nu_2*skk_P1^2)/(2*E_2)+((1+nu_1)*sijsij_E1-nu_1*skk_E1^2)/(2*E_1):
> Eenpl:=2*3.14159*int(eta*r,r=r_n..r_1);
> Energy:= Eenel + Eenpl;
> Work:=3.14159*p_n*u_n*(R_n+r_n)/2;
> FF:=evalf(Energy - Work):
> y_c:=solve(FF,u_n); u_n:=y_c; W:=Work;
> r_n:=R_n+u_n;r_0:=R_0+u_0;  u_n:='u_n':
> print('[r_0,r_1,r_n,g_1,g_2,Energy,Work]'=[r_0,r_1,r_n,g_1c,g_2c,Energy,W]);
> od:
> sigma_rP:=-g_1c*(r_0^2/r^2-1)+g_2c*(r_1^2/r^2-1-2*ln(r_1/r)):
> sigma_tP:=g_1c*(r_0^2/r^2+1)-g_2c*(r_1^2/r^2-1+2*ln(r_1/r)):
> sigma_zP:=4*nu_2*g_2c*ln(r/r_1)+q*g_1c:
> sigma_rE:=-g_1c*(r_0^2/r^2-1):
> sigma_tE:=g_1c*(r_0^2/r^2+1):
> sigma_zE:=q*g_1c:
> p_em:=plot([sigma_rE,sigma_tE,sigma_zE],r=r_1..r_0):
> p_pm:=plot([sigma_rP,sigma_tP,sigma_zP],r=r_n..r_1):
> display({p_e,p_p,p_em,p_pm});

> c:=0:step_p:=(r_1-r_n)/8:step_e:=(r_0-r_1)/8:
> for r from r_n by step_p to r_1 do
> c:=c+1:r:=r:
> rad[c]:=r:
> lprint(rad[c]);
> od:
> r_11:=r_1+step_e:
> for r from r_11 by step_e to r_0 do
> c:=c+1:r:=r:
> rad[c]:=r:
> lprint(rad[c]);
```

```
> od:

> c:=0:step_p:=(r_1-r_n)/8:step_e:=(r_0-r_1)/8:
> for r from r_n by step_p to r_1 do
> c:=c+1:r:=r:sigma_rP:=-g_1c*(r_0^2/r^2-1)+g_2c*(r_1^2/r^2-1-2*ln(r_1/r)):
> rad[c]:=r:sigma_rP[c]:=sigma_rP:
> lprint(sigma_rP[c]);
> od:
> r_11:=r_1+step_e:
> for r from r_11 by step_e to r_0 do
> c:=c+1:r:=r:sigma_rE:=-g_1c*(r_0^2/r^2-1):
> rad[c]:=r:sigma_rE[c]:=sigma_rE:
> lprint(sigma_rE[c]);
> od:

> c:=0:step_p:=(r_1-r_n)/8:step_e:=(r_0-r_1)/8:
> for r from r_n by step_p to r_1 do
> c:=c+1:r:=r:sigma_tP:=g_1c*(r_0^2/r^2+1)-g_2c*(r_1^2/r^2-1+2*ln(r_1/r)):
> rad[c]:=r:sigma_tP[c]:=sigma_tP:
> lprint(sigma_tP[c]);
> od:
> r_11:=r_1+step_e:
> for r from r_11 by step_e to r_0 do
> c:=c+1:r:=r:sigma_tE:=g_1c*(r_0^2/r^2+1):
> rad[c]:=r:sigma_tE[c]:=sigma_tE:
> lprint(sigma_tE[c]);
> od:

> c:=0:step_p:=(r_1-r_n)/8:step_e:=(r_0-r_1)/8:
> for r from r_n by step_p to r_1 do
> c:=c+1:r:=r:sigma_zP:=4*nu_2*g_2c*ln(r/r_1)+q*g_1c:
```

```
> rad[c]:=r:sigma_zP[c]:=sigma_zP:
> lprint(sigma_zP[c]);
> od:
> r_11:=r_1+step_e:
> for r from r_11 by step_e to r_0 do
> c:=c+1:r:=r:sigma_zE:=q*g_1c:
> rad[c]:=r:sigma_zE[c]:=sigma_zE:
> lprint(sigma_zE[c]);
> od:
```

A.2 Maple 6 Program for Determining Displacements

General procedure for inelastic analysis

Displacement calculation at inside and outside boundaries

Calculations of elastic plastic interface

Plane strain

In plane stress, q=0; in plane strain, q = 2*nu; and in closed end, q = 1.

```
> restart: Digits:=10:with(linalg): with(plots):
```

Properties and Conditions

```
> S_Y:=30000;
> E_1:=30*10^6;
> E_2:=E_1/100;
> E_p:=1/((1/E_2)-(1/E_1)):
> nu_1:=0.3: nu_p:=0.5: nu_2:=E_2*((nu_1/E_1)+(0.5/E_p )):
> p_0:=0: p_n:=30000:
> R_0:=20.0: R_n:=4.0:  r_0:=R_0: r_n:=R_n: t:=r_0/r_n: T:=R_0/R_n:
> 'E_1'=E_1,'E_2'=E_2,'E_p'=E_p,'p_n'=p_n;
```

```
> q:=2*nu_1;
```

Elastic Plastic Solutions:

Original Geometry

```
> g_1:=x^2*S_Y/sqrt(3*r_0^4+(1-2*nu_1)^2*x^4):
> g_2:=g_1*(1+nu_p)*E_2*r_0^2/(2*(1-nu_2^2)*E_p*x^2):
> f:=g_1*(r_0^2-r_n^2)-g_2*((x^2-r_n^2)-2*r_n^2*ln(x/r_n))-p_n*r_n^2:
> r_1:=fsolve(f,x): x:=r_1: g_1c:=g_1:g_2c:=g_2: x:='x':
> '[g_1c,g_2c,r_1]'=[g_1c,g_2c,r_1];
> Eenel:=3.14159*g_1c^2*(1+nu_1)*(r_0^2-r_1^2)/E_1*(r_0^2/r_1^2+(1-2*nu_1));
> sigma_rP:=-g_1c*(r_0^2/r^2-1)+g_2c*(r_1^2/r^2-1-2*ln(r_1/r)):
> sigma_tP:=g_1c*(r_0^2/r^2+1)-g_2c*(r_1^2/r^2-1+2*ln(r_1/r)):
> sigma_zP:=4*nu_2*g_2c*ln(r/r_1)+q*g_1c:
> sigma_rE:=-g_1c*(r_0^2/r^2-1):
> sigma_tE:=g_1c*(r_0^2/r^2+1):
> sigma_zE:=q*g_1c:
> etE:=(sigma_tE-nu_1*sigma_rE-nu_1*sigma_zE)/E_1:
> r:=r_0:etE0:=etE: r:='r':
> u_0:=r_0*etE0;
> sijsij_P:=sigma_rP^2+sigma_tP^2+sigma_zP^2:
> skk_P:=sigma_rP+sigma_tP+sigma_zP:
> sijsij_E:=sigma_rE^2+sigma_tE^2+sigma_zE^2:
> skk_E:=sigma_rE+sigma_tE+sigma_zE:
> r:=r_1:sijsij_P1:=sijsij_P:skk_P1:=skk_P:sijsij_E1:=sijsij_E:skk_E1:=skk_E:r:='r':
> eta:=((1+nu_2)*sijsij_P-nu_2*skk_P^2)/(2*E_2)-((1+nu_2)*sijsij_P1-
nu_2*skk_P1^2)/(2*E_2)+((1+nu_1)*sijsij_E1-nu_1*skk_E1^2)/(2*E_1);
> Eenpl:=2*3.14159*int(eta*r,r=r_n..r_1);
> Energy:= Eenel + Eenpl;
> Work:=3.14159*p_n*u_n*(R_n+r_n)/2;
> FF:=evalf(Energy - Work):
```

```
> y_c:=solve(FF,u_n); u_n:=y_c; W:=Work;
> r_n:=R_n+u_n;r_0:=R_0+u_0;  u_n:='u_n':
> print('[u_0,r_1,u_n,g_1,g_2,Energy,Work]'=[u_0,r_1,r_n-R_n,g_1c,g_2c,Energy,W]);
```

Deformed Geometry

```
> for i from 1 to 10 do
> g_1:=x^2*S_Y/sqrt(3*r_0^4+(1-2*nu_1)^2*x^4):
> g_2:=g_1*(1+nu_p)*E_2*r_0^2/(2*(1-nu_2^2)*E_p*x^2):
> f:=g_1*(r_0^2-r_n^2)-g_2*((x^2-r_n^2)-2*r_n^2*ln(x/r_n))-p_n*r_n^2:
> r_1:=fsolve(f,x): x:=r_1: g_1c:=g_1:g_2c:=g_2: x:='x':
> '[g_1c,g_2c,r_1]'=[g_1c,g_2c,r_1];
> Eenel:=3.14159*g_1c^2*(1+nu_1)*(r_0^2-r_1^2)/E_1*(r_0^2/r_1^2+(1-2*nu_1));
> sigma_rP:=-g_1c*(r_0^2/r^2-1)+g_2c*(r_1^2/r^2-1-2*ln(r_1/r)):
> sigma_tP:=g_1c*(r_0^2/r^2+1)-g_2c*(r_1^2/r^2-1+2*ln(r_1/r)):
> sigma_zP:=4*nu_2*g_2c*ln(r/r_1)+q*g_1c:
> sigma_rE:=-g_1c*(r_0^2/r^2-1):
> sigma_tE:=g_1c*(r_0^2/r^2+1):
> sigma_zE:=q*g_1c:
> etE:=(sigma_tE-nu_1*sigma_rE-nu_1*sigma_zE)/E_1:
> r:=r_0:etE0:=etE: r:='r':
> u_0:=r_0*etE0;
> sijsij_P:=sigma_rP^2+sigma_tP^2+sigma_zP^2:
> skk_P:=sigma_rP+sigma_tP+sigma_zP:
> sijsij_E:=sigma_rE^2+sigma_tE^2+sigma_zE^2:
> skk_E:=sigma_rE+sigma_tE+sigma_zE:
> r:=r_1:sijsij_P1:=sijsij_P:skk_P1:=skk_P:sijsij_E1:=sijsij_E:skk_E1:=skk_E:r:='r':
> eta:=((1+nu_2)*sijsij_P-nu_2*skk_P^2)/(2*E_2)-((1+nu_2)*sijsij_P1-
nu_2*skk_P1^2)/(2*E_2)+((1+nu_1)*sijsij_E1-nu_1*skk_E1^2)/(2*E_1);
> Eenpl:=2*3.14159*int(eta*r,r=r_n..r_1);
> Energy:= Eenel + Eenpl;
```

```
> Work:=3.14159*p_n*u_n*(R_n+r_n)/2;
> FF:=evalf(Energy - Work):
> y_c:=solve(FF,u_n); u_n:=y_c; W:=Work;
> r_n:=R_n+u_n;r_0:=R_0+u_0;  u_n:='u_n':
> print('[u_0,u_n,r_1,g_1,g_2]'=[ u_0,r_n-R_n,r_1,g_1c,g_2c]);
> od:
```

A.3 Maple 6 Program for Inelastic Strain Calculations

Elastic Plastic Analysis of Thick Walled Cylinder
Formulation Based on Virtual Work Principle
Closed End
In Plane Stress, q=0; in Plane Strain, q = 2*nu; q = 1 for Closed Ends

```
> restart: Digits:=10:with(linalg): with(plots):
```

Properties and Conditions

```
> S_Y:=30000;
> E_1:=30*10^6;
> E_2:=E_1/100;
> E_p:=1/((1/E_2)-(1/E_1)):
> nu_1:=0.3: nu_p:=0.5: nu_2:=E_2*((nu_1/E_1)+(0.5/E_p )):
> p_0:=0: p_n:=30000:
> R_0:=20.0: R_n:=4.0:  r_0:=R_0: r_n:=R_n: t:=r_0/r_n: T:=R_0/R_n:
> 'E_1'=E_1,'E_2'=E_2,'E_p'=E_p,'p_n'=p_n;
> q:=1;
```

Elastic Plastic Solutions:
Original Geometry

```
> g_1:=x^2*S_Y/sqrt(3*r_0^4+(1-q)^2*x^4):
> g_2:=g_1*(1+nu_p)*E_2*r_0^2/(2*(1-nu_2^2)*E_p*x^2):
> f:=g_1*(r_0^2-r_n^2)-g_2*((x^2-r_n^2)-2*r_n^2*ln(x/r_n))-p_n*r_n^2:
> r_1:=fsolve(f,x): x:=r_1: g_1c:=g_1:g_2c:=g_2: x:='x':
> '[g_1c,g_2c,r_1]'=[g_1c,g_2c,r_1];
> Eenel:=3.14159*g_1c^2*(1+nu_1)*(r_0^2-r_1^2)/E_1*(r_0^2/r_1^2+(1-2*nu_1));
> sigma_rP:=-g_1c*(r_0^2/r^2-1)+g_2c*(r_1^2/r^2-1-2*ln(r_1/r)):
> sigma_tP:=g_1c*(r_0^2/r^2+1)-g_2c*(r_1^2/r^2-1+2*ln(r_1/r)):
> sigma_zP:=4*nu_2*g_2c*ln(r/r_1)+q*g_1c:
> sigma_rE:=-g_1c*(r_0^2/r^2-1):
> sigma_tE:=g_1c*(r_0^2/r^2+1):
> sigma_zE:=q*g_1c:
> etE:=(sigma_tE-nu_1*sigma_rE-nu_1*sigma_zE)/E_1:
> r:=r_0:etE0:=etE: r:='r':
> u_0:=r_0*etE0;
> sijsij_P:=sigma_rP^2+sigma_tP^2+sigma_zP^2:
> skk_P:=sigma_rP+sigma_tP+sigma_zP:
> sijsij_E:=sigma_rE^2+sigma_tE^2+sigma_zE^2:
> skk_E:=sigma_rE+sigma_tE+sigma_zE:
> r:=r_1:sijsij_P1:=sijsij_P:skk_P1:=skk_P:sijsij_E1:=sijsij_E:skk_E1:=skk_E:r:='r':
> eta:=((1+nu_2)*sijsij_P-nu_2*skk_P^2)/(2*E_2)-((1+nu_2)*sijsij_P1-
nu_2*skk_P1^2)/(2*E_2)+((1+nu_1)*sijsij_E1-nu_1*skk_E1^2)/(2*E_1);
> Eenpl:=2*3.14159*int(eta*r,r=r_n..r_1);
> Energy:= Eenel + Eenpl;
> Work:=3.14159*p_n*u_n*(R_n+r_n)/2;
> FF:=evalf(Energy - Work):
> y_c:=solve(FF,u_n); u_n:=y_c; W:=Work;
> r_n:=R_n+u_n;r_0:=R_0+u_0;  u_n:='u_n':
> print('[r_0,r_1,r_n,g_1,g_2,Energy,Work]'=[r_0,r_1,r_n,g_1c,g_2c,Energy,W]);
> sigma_rP:=-g_1c*(r_0^2/r^2-1)+g_2c*(r_1^2/r^2-1-2*ln(r_1/r)):
> sigma_tP:=g_1c*(r_0^2/r^2+1)-g_2c*(r_1^2/r^2-1+2*ln(r_1/r)):
```

```
> sigma_zP:=4*nu_2*g_2c*ln(r/r_1)+q*g_1c:
> sigma_rE:=-g_1c*(r_0^2/r^2-1):
> sigma_tE:=g_1c*(r_0^2/r^2+1):
> sigma_zE:=q*g_1c:
> rP:=(sigma_rP-nu_2*sigma_tP-nu_2*sigma_zP)/E_2;
> tP:=(sigma_tP-nu_2*sigma_rP-nu_2*sigma_zP)/E_2;
> zP:=(sigma_zP-nu_2*sigma_rP-nu_2*sigma_tP)/E_2;
> rE:=(sigma_rE-nu_1*sigma_tE-nu_1*sigma_zE)/E_1;
> tE:=(sigma_tE-nu_1*sigma_rE-nu_1*sigma_zE)/E_1;
> zE:=(sigma_zE-nu_1*sigma_tE-nu_1*sigma_rE)/E_1;
> r:=r_1:
> rP_1:=rP;tP_1:=tP;zP_1:=zP;rE_1:=rE;tE_1:=tE;zE_1:=zE;
> r:='r':
> e_rP:=rP-rP_1+rE_1;e_tP:=tP-tP_1+tE_1;e_zP:=zP-zP_1+zE_1;
> e_rE:=rE;e_tE:=tE;e_zE:=zE;
> p_e:=plot([e_rE,e_tE,e_zE],r=r_1..R_0):p_p:=plot([e_rP,e_tP,e_zP],r=R_n..r_1):
> display({p_e,p_p});
```

Deformed Geometry

```
> for i from 1 to 5 do
> g_1:=x^2*S_Y/sqrt(3*r_0^4+(1-q)^2*x^4):
> g_2:=g_1*(1+nu_p)*E_2*r_0^2/(2*(1-nu_2^2)*E_p*x^2):
> f:=g_1*(r_0^2-r_n^2)-g_2*((x^2-r_n^2)-2*r_n^2*ln(x/r_n))-p_n*r_n^2:
> r_1:=fsolve(f,x): x:=r_1: g_1c:=g_1:g_2c:=g_2: x:='x':
> '[g_1c,g_2c,r_1]'=[g_1c,g_2c,r_1];
> Eenel:=3.14159*g_1c^2*(1+nu_1)*(r_0^2-r_1^2)/E_1*(r_0^2/r_1^2+(1-2*nu_1));
> sigma_rP:=-g_1c*(r_0^2/r^2-1)+g_2c*(r_1^2/r^2-1-2*ln(r_1/r)):
> sigma_tP:=g_1c*(r_0^2/r^2+1)-g_2c*(r_1^2/r^2-1+2*ln(r_1/r)):
> sigma_zP:=4*nu_2*g_2c*ln(r/r_1)+q*g_1c:
> sigma_rE:=-g_1c*(r_0^2/r^2-1):
```

```
> sigma_tE:=g_1c*(r_0^2/r^2+1):
> sigma_zE:=q*g_1c:
> etE:=(sigma_tE-nu_1*sigma_rE-nu_1*sigma_zE)/E_1:
> r:=r_0:etE0:=etE: r:='r':
> u_0:=r_0*etE0;
> sijsij_P:=sigma_rP^2+sigma_tP^2+sigma_zP^2:
> skk_P:=sigma_rP+sigma_tP+sigma_zP:
> sijsij_E:=sigma_rE^2+sigma_tE^2+sigma_zE^2:
> skk_E:=sigma_rE+sigma_tE+sigma_zE:
> r:=r_1:sijsij_P1:=sijsij_P:skk_P1:=skk_P:sijsij_E1:=sijsij_E:skk_E1:=skk_E:r:='r':
> eta:=((1+nu_2)*sijsij_P-nu_2*skk_P^2)/(2*E_2)-((1+nu_2)*sijsij_P1-
nu_2*skk_P1^2)/(2*E_2)+((1+nu_1)*sijsij_E1-nu_1*skk_E1^2)/(2*E_1);
> Eenpl:=2*3.14159*int(eta*r,r=r_n..r_1);
> Energy:= Eenel + Eenpl;
> Work:=3.14159*p_n*u_n*(R_n+r_n)/2;
> FF:=evalf(Energy - Work):
> y_c:=solve(FF,u_n); u_n:=y_c; W:=Work;
> r_n:=R_n+u_n;r_0:=R_0+u_0;  u_n:='u_n':
> print('[r_0,r_1,r_n,g_1,g_2,Energy,Work]'=[r_0,r_1,r_n,g_1c,g_2c,Energy,W]);
> od:
> sigma_rP:=-g_1c*(r_0^2/r^2-1)+g_2c*(r_1^2/r^2-1-2*ln(r_1/r)):
> sigma_tP:=g_1c*(r_0^2/r^2+1)-g_2c*(r_1^2/r^2-1+2*ln(r_1/r)):
> sigma_zP:=4*nu_2*g_2c*ln(r/r_1)+q*g_1c:
> sigma_rE:=-g_1c*(r_0^2/r^2-1):
> sigma_tE:=g_1c*(r_0^2/r^2+1):
> sigma_zE:=q*g_1c:
> rP:=(sigma_rP-nu_2*sigma_tP-nu_2*sigma_zP)/E_2;
> tP:=(sigma_tP-nu_2*sigma_rP-nu_2*sigma_zP)/E_2;
> zP:=(sigma_zP-nu_2*sigma_rP-nu_2*sigma_tP)/E_2;
> rE:=(sigma_rE-nu_1*sigma_tE-nu_1*sigma_zE)/E_1;
> tE:=(sigma_tE-nu_1*sigma_rE-nu_1*sigma_zE)/E_1;
```

```
> zE:=(sigma_zE-nu_1*sigma_tE-nu_1*sigma_rE)/E_1;
> r:=r_1:
> rP_1:=rP;tP_1:=tP;zP_1:=zP;rE_1:=rE;tE_1:=tE;zE_1:=zE;
> r:='r':
> e_rP:=rP-rP_1+rE_1;e_tP:=tP-tP_1+tE_1;e_zP:=zP-zP_1+zE_1;
> e_rE:=rE;e_tE:=tE;e_zE:=zE;
> p_em:=plot([e_rE,e_tE,e_zE],r=r_1..r_0):p_pm:=plot([e_rP,e_tP,e_zP],r=r_n..r_1):
> display({p_e,p_p,p_em,p_pm});

> err:=0.001:
> c:=0:step_p:=(r_1-r_n)/8:step_e:=(r_0-r_1)/8:
> for r from r_n by step_p to r_1+err do
> c:=c+1:r:=r:
> rad[c]:=r:
> lprint(rad[c]);
> od:
> r_11:=r_1+step_e:
> for r from r_11 by step_e to r_0+err do
> c:=c+1:r:=r:
> rad[c]:=r:
> lprint(rad[c]);
> od:

> c:=0:step_p:=(r_1-r_n)/8:step_e:=(r_0-r_1)/8:
> for r from r_n by step_p to r_1+err do
> c:=c+1:r:=r:e_rP := rP-rP_1+rE_1:
> rad[c]:=r:e_rP[c]:=e_rP:
> lprint(e_rP[c]);
> od:
> r_11:=r_1+step_e:
> for r from r_11 by step_e to r_0+err do
```

```
> c:=c+1:r:=r:e_rE := rE:
> rad[c]:=r:e_rE[c]:=e_rE:
> lprint(e_rE[c]);
> od:

> c:=0:step_p:=(r_1-r_n)/8:step_e:=(r_0-r_1)/8:
> for r from r_n by step_p to r_1+err do
> c:=c+1:r:=r:e_tP := tP-tP_1+tE_1:
> rad[c]:=r:e_tP[c]:=e_tP:
> lprint(e_tP[c]);
> od:
> r_11:=r_1+step_e:
> for r from r_11 by step_e to r_0+err do
> c:=c+1:r:=r:e_tE := tE:
> rad[c]:=r:e_tE[c]:=e_tE:
> lprint(e_tE[c]);
> od:

> c:=0:step_p:=(r_1-r_n)/8:step_e:=(r_0-r_1)/8:
> for r from r_n by step_p to r_1+err do
> c:=c+1:r:=r:e_zP := zP-zP_1+zE_1:
> rad[c]:=r:e_zP[c]:=e_zP:
> lprint(e_zP[c]);
> od:
> r_11:=r_1+step_e:
> for r from r_11 by step_e to r_0+err do
> c:=c+1:r:=r:e_zE:=zE:
> rad[c]:=r:e_zE[c]:=e_zE:
> lprint(e_zE[c]);
> od:
```

A.4 Maple 6 Program for Calculations of Strain Energy and External Work

Formulation Based on Virtual Work Principle

General Procedure for Closed Ends, Plane Strain, and Plane Stress Conditions

In Plane Stress, q=0; in Plane Strain, q = 2*nu; in Closed Ends, q = 1.

```
> restart: Digits:=10:with(linalg): with(plots):
```

Properties and Conditions

```
> S_Y:=30000;
> E_1:=30*10^6;
> E_2:=E_1/100;
> E_p:=1/((1/E_2)-(1/E_1)):
> nu_1:=0.3: nu_p:=0.5: nu_2:=E_2*((nu_1/E_1)+(0.5/E_p )):
> p_0:=0: p_n:=30000:
> R_0:=18.0: R_n:=4.0:  r_0:=R_0: r_n:=R_n: t:=r_0/r_n: T:=R_0/R_n:
> 'E_1'=E_1,'E_2'=E_2,'E_p'=E_p,'p_n'=p_n;
> q:=2*nu_1;
```

Original Geometry

```
> g_1:=x^2*S_Y/sqrt(3*r_0^4+(1-2*nu_1)^2*x^4):
> g_2:=g_1*(1+nu_p)*E_2*r_0^2/(2*(1-nu_2^2)*E_p*x^2):
> f:=g_1*(r_0^2-r_n^2)-g_2*((x^2-r_n^2)-2*r_n^2*ln(x/r_n))-p_n*r_n^2:
> r_1:=fsolve(f,x): x:=r_1: g_1c:=g_1:g_2c:=g_2: x:='x':
> '[g_1c,g_2c,r_1]'=[g_1c,g_2c,r_1];
> Eenel:=3.14159*g_1c^2*(1+nu_1)*(r_0^2-r_1^2)/E_1*(r_0^2/r_1^2+(1-2*nu_1));
> sigma_rP:=-g_1c*(r_0^2/r^2-1)+g_2c*(r_1^2/r^2-1-2*ln(r_1/r)):
> sigma_tP:=g_1c*(r_0^2/r^2+1)-g_2c*(r_1^2/r^2-1+2*ln(r_1/r)):
> sigma_zP:=4*nu_2*g_2c*ln(r/r_1)+q*g_1c:
```

```
> sigma_rE:=-g_1c*(r_0^2/r^2-1):
> sigma_tE:=g_1c*(r_0^2/r^2+1):
> sigma_zE:=q*g_1c:
> etE:=(sigma_tE-nu_1*sigma_rE-nu_1*sigma_zE)/E_1:
> r:=r_0:etE0:=etE: r:='r':
> u_0:=r_0*etE0;
> sijsij_P:=sigma_rP^2+sigma_tP^2+sigma_zP^2:
> skk_P:=sigma_rP+sigma_tP+sigma_zP:
> sijsij_E:=sigma_rE^2+sigma_tE^2+sigma_zE^2:
> skk_E:=sigma_rE+sigma_tE+sigma_zE:
> r:=r_1:sijsij_P1:=sijsij_P:skk_P1:=skk_P:sijsij_E1:=sijsij_E:skk_E1:=skk_E:r:='r':
> eta:=((1+nu_2)*sijsij_P-nu_2*skk_P^2)/(2*E_2)-((1+nu_2)*sijsij_P1-
nu_2*skk_P1^2)/(2*E_2)+((1+nu_1)*sijsij_E1-nu_1*skk_E1^2)/(2*E_1);
> Eenpl:=2*3.14159*int(eta*r,r=r_n..r_1);
> Energy:= Eenel + Eenpl;
> Work:=3.14159*p_n*u_n*(R_n+r_n)/2;
> FF:=evalf(Energy - Work):
> y_c:=solve(FF,u_n); u_n:=y_c; W:=Work;
> r_n:=R_n+u_n;r_0:=R_0+u_0;  u_n:='u_n':
> print('[u_0,r_1,u_n,g_1,g_2,Energy,Work]'=[u_0,r_1,r_n-R_n,g_1c,g_2c,Energy,W]);
```

Deformed Geometry

```
> for i from 1 to 10 do
> g_1:=x^2*S_Y/sqrt(3*r_0^4+(1-2*nu_1)^2*x^4):
> g_2:=g_1*(1+nu_p)*E_2*r_0^2/(2*(1-nu_2^2)*E_p*x^2):
> f:=g_1*(r_0^2-r_n^2)-g_2*((x^2-r_n^2)-2*r_n^2*ln(x/r_n))-p_n*r_n^2:
> r_1:=fsolve(f,x): x:=r_1: g_1c:=g_1:g_2c:=g_2: x:='x':
> '[g_1c,g_2c,r_1]'=[g_1c,g_2c,r_1];
> Eenel:=3.14159*g_1c^2*(1+nu_1)*(r_0^2-r_1^2)/E_1*(r_0^2/r_1^2+(1-2*nu_1));
> sigma_rP:=-g_1c*(r_0^2/r^2-1)+g_2c*(r_1^2/r^2-1-2*ln(r_1/r)):
```

```
> sigma_tP:=g_1c*(r_0^2/r^2+1)-g_2c*(r_1^2/r^2-1+2*ln(r_1/r)):
> sigma_zP:=4*nu_2*g_2c*ln(r/r_1)+q*g_1c:
> sigma_rE:=-g_1c*(r_0^2/r^2-1):
> sigma_tE:=g_1c*(r_0^2/r^2+1):
> sigma_zE:=q*g_1c:
> etE:=(sigma_tE-nu_1*sigma_rE-nu_1*sigma_zE)/E_1:
> r:=r_0:etE0:=etE: r:='r':
> u_0:=r_0*etE0;
> sijsij_P:=sigma_rP^2+sigma_tP^2+sigma_zP^2:
> skk_P:=sigma_rP+sigma_tP+sigma_zP:
> sijsij_E:=sigma_rE^2+sigma_tE^2+sigma_zE^2:
> skk_E:=sigma_rE+sigma_tE+sigma_zE:
> r:=r_1:sijsij_P1:=sijsij_P:skk_P1:=skk_P:sijsij_E1:=sijsij_E:skk_E1:=skk_E:r:='r':
> eta:=((1+nu_2)*sijsij_P-nu_2*skk_P^2)/(2*E_2)-((1+nu_2)*sijsij_P1-
nu_2*skk_P1^2)/(2*E_2)+((1+nu_1)*sijsij_E1-nu_1*skk_E1^2)/(2*E_1);
> Eenpl:=2*3.14159*int(eta*r,r=r_n..r_1);
> Energy:= Eenel + Eenpl;
> Work:=3.14159*p_n*u_n*(R_n+r_n)/2;
> FF:=evalf(Energy - Work):
> y_c:=solve(FF,u_n); u_n:=y_c; W:=Work;
> r_n:=R_n+u_n;r_0:=R_0+u_0;  u_n:='u_n':
> print('[g_1,g_2,Energy,Work]'=[g_1c,g_2c,Energy,W]);
> od:
```

A.5 Maple 6 Program for Autofrettage – Residual Stress

Autofrettage of Thick Walled Cylinder

Formulation Based on Virtual Work Principle

General Procedure for Closed Ends, Plane Strain, and Plane Stress Conditions

In Plane Stress, q=0; in Plane Strain, q = 2*nu; in Closed Ends, q = 1.

Closed End in This Example

```
> restart: Digits:=10:with(linalg): with(plots):
```

Properties and Conditions

```
> S_Y:=30000;
> E_1:=30*10^6;
> E_2:=E_1/100;
> E_p:=1/((1/E_2)-(1/E_1)):
> nu_1:=0.3: nu_p:=0.5: nu_2:=E_2*((nu_1/E_1)+(0.5/E_p )):
> p_0:=0: p_n:=30000:
> R_0:=16.0: R_n:=4.0:  r_0:=R_0: r_n:=R_n: t:=r_0/r_n: T:=R_0/R_n:
> 'E_1'=E_1,'E_2'=E_2,'E_p'=E_p,'p_n'=p_n;
> q:=1;
```

Original Geometry

```
> g_1:=x^2*S_Y/sqrt(3*r_0^4+(1-q)^2*x^4):
> g_2:=g_1*(1+nu_p)*E_2*r_0^2/(2*(1-nu_2^2)*E_p*x^2):
> f:=g_1*(r_0^2-r_n^2)-g_2*((x^2-r_n^2)-2*r_n^2*ln(x/r_n))-p_n*r_n^2:
> r_1:=fsolve(f,x): x:=r_1: g_1c:=g_1:g_2c:=g_2: x:='x':
> '[g_1c,g_2c,r_1]'=[g_1c,g_2c,r_1];
> Eenel:=3.14159*g_1c^2*(1+nu_1)*(r_0^2-r_1^2)/E_1*(r_0^2/r_1^2+(1-2*nu_1));
> sigma_rP:=-g_1c*(r_0^2/r^2-1)+g_2c*(r_1^2/r^2-1-2*ln(r_1/r)):
```

```
> sigma_tP:=g_1c*(r_0^2/r^2+1)-g_2c*(r_1^2/r^2-1+2*ln(r_1/r)):
> sigma_zP:=4*nu_2*g_2c*ln(r/r_1)+q*g_1c:
> sigma_rE:=-g_1c*(r_0^2/r^2-1):
> sigma_tE:=g_1c*(r_0^2/r^2+1):
> sigma_zE:=q*g_1c:
> etE:=(sigma_tE-nu_1*sigma_rE-nu_1*sigma_zE)/E_1:
> r:=r_0:etE0:=etE: r:='r':
> u_0:=r_0*etE0;
> sijsij_P:=sigma_rP^2+sigma_tP^2+sigma_zP^2:
> skk_P:=sigma_rP+sigma_tP+sigma_zP:
> sijsij_E:=sigma_rE^2+sigma_tE^2+sigma_zE^2:
> skk_E:=sigma_rE+sigma_tE+sigma_zE:
> r:=r_1:sijsij_P1:=sijsij_P:skk_P1:=skk_P:sijsij_E1:=sijsij_E:skk_E1:=skk_E:r:='r':
> eta:=((1+nu_2)*sijsij_P-nu_2*skk_P^2)/(2*E_2)-((1+nu_2)*sijsij_P1-
nu_2*skk_P1^2)/(2*E_2)+((1+nu_1)*sijsij_E1-nu_1*skk_E1^2)/(2*E_1):
> Eenpl:=2*3.14159*int(eta*r,r=r_n..r_1);
> Energy:= Eenel + Eenpl;
> Work:=3.14159*p_n*u_n*(R_n+r_n)/2;
> FF:=evalf(Energy - Work):
> y_c:=solve(FF,u_n); u_n:=y_c; W:=Work;
> r_n:=R_n+u_n;r_0:=R_0+u_0;  u_n:='u_n':
> print('[r_0,r_1,r_n,g_1,g_2,Energy,Work]'=[r_0,r_1,r_n,g_1c,g_2c,Energy,W]);
> sigma_rP:=-g_1c*(r_0^2/r^2-1)+g_2c*(r_1^2/r^2-1-2*ln(r_1/r)):
> sigma_tP:=g_1c*(r_0^2/r^2+1)-g_2c*(r_1^2/r^2-1+2*ln(r_1/r)):
> sigma_zP:=4*nu_2*g_2c*ln(r/r_1)+q*g_1c:
> sigma_rE:=-g_1c*(r_0^2/r^2-1):
> sigma_tE:=g_1c*(r_0^2/r^2+1):
> sigma_zE:=q*g_1c:
> g_3:=r_n^2*p_n/(r_0^2-r_n^2):
> usigma_rP:=g_3*(r_0^2/r^2-1):usigma_tP:=-g_3*(r_0^2/r^2+1):usigma_zP:=-q*g_3:
> usigma_rE:=g_3*(r_0^2/r^2-1):usigma_tE:=-g_3*(r_0^2/r^2+1):usigma_zE:=-q*g_3:
```

```
> rsigma_rP:=sigma_rP+usigma_rP:rsigma_tP:=sigma_tP+usigma_tP:
> rsigma_zP:=sigma_zP+usigma_zP:
> rsigma_rE:=sigma_rE+usigma_rE:rsigma_tE:=sigma_tE+usigma_tE:
> rsigma_zE:=sigma_zE+usigma_zE:
> p_e:=plot([rsigma_rE,rsigma_tE,rsigma_zE],r=r_1..R_0):
> p_p:=plot([rsigma_rP,rsigma_tP,rsigma_zP],r=R_n..r_1):display({p_e,p_p});
```

Deformed Geometry

```
> for i from 1 to 5 do
> g_1:=x^2*S_Y/sqrt(3*r_0^4+(1-q)^2*x^4):
> g_2:=g_1*(1+nu_p)*E_2*r_0^2/(2*(1-nu_2^2)*E_p*x^2):
> f:=g_1*(r_0^2-r_n^2)-g_2*((x^2-r_n^2)-2*r_n^2*ln(x/r_n))-p_n*r_n^2:
> r_1:=fsolve(f,x): x:=r_1: g_1c:=g_1:g_2c:=g_2: x:='x':
> '[g_1c,g_2c,r_1]'=[g_1c,g_2c,r_1];
> Eenel:=3.14159*g_1c^2*(1+nu_1)*(r_0^2-r_1^2)/E_1*(r_0^2/r_1^2+(1-2*nu_1));
> sigma_rP:=-g_1c*(r_0^2/r^2-1)+g_2c*(r_1^2/r^2-1-2*ln(r_1/r)):
> sigma_tP:=g_1c*(r_0^2/r^2+1)-g_2c*(r_1^2/r^2-1+2*ln(r_1/r)):
> sigma_zP:=4*nu_2*g_2c*ln(r/r_1)+q*g_1c:
> sigma_rE:=-g_1c*(r_0^2/r^2-1):
> sigma_tE:=g_1c*(r_0^2/r^2+1):
> sigma_zE:=q*g_1c:
> etE:=(sigma_tE-nu_1*sigma_rE-nu_1*sigma_zE)/E_1:
> r:=r_0:etE0:=etE: r:='r':
> u_0:=r_0*etE0;
> sijsij_P:=sigma_rP^2+sigma_tP^2+sigma_zP^2:
> skk_P:=sigma_rP+sigma_tP+sigma_zP:
> sijsij_E:=sigma_rE^2+sigma_tE^2+sigma_zE^2:
> skk_E:=sigma_rE+sigma_tE+sigma_zE:
> r:=r_1:sijsij_P1:=sijsij_P:skk_P1:=skk_P:sijsij_E1:=sijsij_E:skk_E1:=skk_E:r:='r':
```

```
> eta:=((1+nu_2)*sijsij_P-nu_2*skk_P^2)/(2*E_2)-((1+nu_2)*sijsij_P1-
nu_2*skk_P1^2)/(2*E_2)+((1+nu_1)*sijsij_E1-nu_1*skk_E1^2)/(2*E_1):
> Eenpl:=2*3.14159*int(eta*r,r=r_n..r_1);
> Energy:= Eenel + Eenpl;
> Work:=3.14159*p_n*u_n*(R_n+r_n)/2;
> FF:=evalf(Energy - Work):
> y_c:=solve(FF,u_n); u_n:=y_c; W:=Work;
> r_n:=R_n+u_n;r_0:=R_0+u_0;  u_n:='u_n':
> print('[r_0,r_1,r_n,g_1,g_2,Energy,Work]'=[r_0,r_1,r_n,g_1c,g_2c,Energy,W]);
> od:
> sigma_rP:=-g_1c*(r_0^2/r^2-1)+g_2c*(r_1^2/r^2-1-2*ln(r_1/r)):
> sigma_tP:=g_1c*(r_0^2/r^2+1)-g_2c*(r_1^2/r^2-1+2*ln(r_1/r)):
> sigma_zP:=4*nu_2*g_2c*ln(r/r_1)+q*g_1c:
> sigma_rE:=-g_1c*(r_0^2/r^2-1):
> sigma_tE:=g_1c*(r_0^2/r^2+1):
> sigma_zE:=q*g_1c:
> g_3:=r_n^2*p_n/(r_0^2-r_n^2):
> usigma_rP:=g_3*(r_0^2/r^2-1):usigma_tP:=-g_3*(r_0^2/r^2+1):usigma_zP:=-q*g_3:
> usigma_rE:=g_3*(r_0^2/r^2-1):usigma_tE:=-g_3*(r_0^2/r^2+1):usigma_zE:=-q*g_3:
> rsigma_rP:=sigma_rP+usigma_rP:rsigma_tP:=sigma_tP+usigma_tP:
> rsigma_zP:=sigma_zP+usigma_zP:
> rsigma_rE:=sigma_rE+usigma_rE:rsigma_tE:=sigma_tE+usigma_tE:
> rsigma_zE:=sigma_zE+usigma_zE:
> p_em:=plot([rsigma_rE,rsigma_tE,rsigma_zE],r=r_1..r_0):
> p_pm:=plot([rsigma_rP,rsigma_tP,rsigma_zP],r=r_n..r_1):
> display({p_e,p_p,p_em,p_pm});


> err:=0.001:
> c:=0:step_p:=(r_1-r_n)/8:step_e:=(r_0-r_1)/8:
> for r from r_n by step_p to r_1+err do
> c:=c+1:r:=r:
```

```
> rad[c]:=r:
> lprint(rad[c]);
> od:
> r_11:=r_1+step_e:
> for r from r_11 by step_e to r_0+err do
> c:=c+1:r:=r:
> rad[c]:=r:
> lprint(rad[c]);
> od:

> c:=0:step_p:=(r_1-r_n)/8:step_e:=(r_0-r_1)/8:
> for r from r_n by step_p to r_1+err do
> c:=c+1:r:=r:rsigma_rP:=sigma_rP+usigma_rP:
> rad[c]:=r:rsigma_rP[c]:=rsigma_rP:
> lprint(rsigma_rP[c]);
> od:
> r_11:=r_1+step_e:
> for r from r_11 by step_e to r_0+err do
> c:=c+1:r:=r:rsigma_rE:=sigma_rE+usigma_rE:
> rad[c]:=r:rsigma_rE[c]:=rsigma_rE:
> lprint(rsigma_rE[c]);
> od:

> c:=0:step_p:=(r_1-r_n)/8:step_e:=(r_0-r_1)/8:
> for r from r_n by step_p to r_1+err do
> c:=c+1:r:=r:rsigma_tP:=sigma_tP+usigma_tP:
> rad[c]:=r:rsigma_tP[c]:=rsigma_tP:
> lprint(rsigma_tP[c]);
> od:
> r_11:=r_1+step_e:
> for r from r_11 by step_e to r_0+err do
```

```
> c:=c+1:r:=r:rsigma_tE:=sigma_tE+usigma_tE:
> rad[c]:=r:rsigma_tE[c]:=rsigma_tE:
> lprint(rsigma_tE[c]);
> od:

> c:=0:step_p:=(r_1-r_n)/8:step_e:=(r_0-r_1)/8:
> for r from r_n by step_p to r_1+err do
> c:=c+1:r:=r:rsigma_zP:=sigma_zP+usigma_zP:
> rad[c]:=r:rsigma_zP[c]:=rsigma_zP:
> lprint(rsigma_zP[c]);
> od:
> r_11:=r_1+step_e:
> for r from r_11 by step_e to r_0+err do
> c:=c+1:r:=r:rsigma_zE:=sigma_zE+usigma_zE:
> rad[c]:=r:rsigma_zE[c]:=rsigma_zE:
> lprint(rsigma_zE[c]);
> od:
```

A.6 Maple 6 Program for Autofrettage – Residual Strain

```
Autofrettage of Thick Walled Cylinder
Formulation Based on Virtual Work Principle
General Procedure for Closed Ends, Plane Strain, and Plane Stress Conditions
In Plane Stress, q=0; in Plane Strain, q = 2*nu; in Closed Ends, q = 1.
Closed End in This Example

> restart: Digits:=10:with(linalg): with(plots):

Properties and Conditions

> S_Y:=30000;
```

```
> E_1:=30*10^6;
> E_2:=E_1/100;
> E_p:=1/((1/E_2)-(1/E_1)):
> nu_1:=0.3: nu_p:=0.5: nu_2:=E_2*((nu_1/E_1)+(0.5/E_p )):
> p_0:=0: p_n:=20000:
> R_0:=20.0: R_n:=4.0:  r_0:=R_0: r_n:=R_n: t:=r_0/r_n: T:=R_0/R_n:
> 'E_1'=E_1,'E_2'=E_2,'E_p'=E_p,'p_n'=p_n;
> q:=1;
```

Original Geometry

```
> g_1:=x^2*S_Y/sqrt(3*r_0^4+(1-q)^2*x^4):
> g_2:=g_1*(1+nu_p)*E_2*r_0^2/(2*(1-nu_2^2)*E_p*x^2):
> f:=g_1*(r_0^2-r_n^2)-g_2*((x^2-r_n^2)-2*r_n^2*ln(x/r_n))-p_n*r_n^2:
> r_1:=fsolve(f,x): x:=r_1: g_1c:=g_1:g_2c:=g_2: x:='x':
> '[g_1c,g_2c,r_1]'=[g_1c,g_2c,r_1];
> Eenel:=3.14159*g_1c^2*(1+nu_1)*(r_0^2-r_1^2)/E_1*(r_0^2/r_1^2+(1-2*nu_1));
> sigma_rP:=-g_1c*(r_0^2/r^2-1)+g_2c*(r_1^2/r^2-1-2*ln(r_1/r)):
> sigma_tP:=g_1c*(r_0^2/r^2+1)-g_2c*(r_1^2/r^2-1+2*ln(r_1/r)):
> sigma_zP:=4*nu_2*g_2c*ln(r/r_1)+q*g_1c:
> sigma_rE:=-g_1c*(r_0^2/r^2-1):
> sigma_tE:=g_1c*(r_0^2/r^2+1):
> sigma_zE:=q*g_1c:
> etE:=(sigma_tE-nu_1*sigma_rE-nu_1*sigma_zE)/E_1:
> r:=r_0:etE0:=etE: r:='r':
> u_0:=r_0*etE0;
> sijsij_P:=sigma_rP^2+sigma_tP^2+sigma_zP^2:
> skk_P:=sigma_rP+sigma_tP+sigma_zP:
> sijsij_E:=sigma_rE^2+sigma_tE^2+sigma_zE^2:
> skk_E:=sigma_rE+sigma_tE+sigma_zE:
> r:=r_1:sijsij_P1:=sijsij_P:skk_P1:=skk_P:sijsij_E1:=sijsij_E:skk_E1:=skk_E:r:='r':
```

```
> eta:=((1+nu_2)*sijsij_P-nu_2*skk_P^2)/(2*E_2)-((1+nu_2)*sijsij_P1-
nu_2*skk_P1^2)/(2*E_2)+((1+nu_1)*sijsij_E1-nu_1*skk_E1^2)/(2*E_1);
> Eenpl:=2*3.14159*int(eta*r,r=r_n..r_1);
> Energy:= Eenel + Eenpl;
> Work:=3.14159*p_n*u_n*(R_n+r_n)/2;
> FF:=evalf(Energy - Work):
> y_c:=solve(FF,u_n); u_n:=y_c; W:=Work;
> r_n:=R_n+u_n;r_0:=R_0+u_0;  u_n:='u_n':
> print('[r_0,r_1,r_n,g_1,g_2,Energy,Work]'=[r_0,r_1,r_n,g_1c,g_2c,Energy,W]);
> sigma_rP:=-g_1c*(r_0^2/r^2-1)+g_2c*(r_1^2/r^2-1-2*ln(r_1/r)):
> sigma_tP:=g_1c*(r_0^2/r^2+1)-g_2c*(r_1^2/r^2-1+2*ln(r_1/r)):
> sigma_zP:=4*nu_2*g_2c*ln(r/r_1)+q*g_1c:
> sigma_rE:=-g_1c*(r_0^2/r^2-1):
> sigma_tE:=g_1c*(r_0^2/r^2+1):
> sigma_zE:=q*g_1c:
> g_3:=r_n^2*p_n/(r_0^2-r_n^2):
> usigma_rP:=g_3*(r_0^2/r^2-1):usigma_tP:=-g_3*(r_0^2/r^2+1):usigma_zP:=-q*g_3:
> usigma_rE:=g_3*(r_0^2/r^2-1):usigma_tE:=-g_3*(r_0^2/r^2+1):usigma_zE:=-q*g_3:
> rsigma_rP:=sigma_rP+usigma_rP:rsigma_tP:=sigma_tP+usigma_tP:
> rsigma_zP:=sigma_zP+usigma_zP:
> rsigma_rE:=sigma_rE+usigma_rE:rsigma_tE:=sigma_tE+usigma_tE:
> rsigma_zE:=sigma_zE+usigma_zE:
> urE:=(usigma_rP-nu_1*usigma_tP-nu_1*usigma_zP)/E_1;
> utE:=(usigma_tP-nu_1*usigma_rP-nu_1*usigma_zP)/E_1;
> uzE:=(usigma_zP-nu_1*usigma_tP-nu_1*usigma_rP)/E_1;
> rP:=(sigma_rP-nu_2*sigma_tP-nu_2*sigma_zP)/E_2;
> tP:=(sigma_tP-nu_2*sigma_rP-nu_2*sigma_zP)/E_2;
> zP:=(sigma_zP-nu_2*sigma_rP-nu_2*sigma_tP)/E_2;
> rE:=(sigma_rE-nu_1*sigma_tE-nu_1*sigma_zE)/E_1;
> tE:=(sigma_tE-nu_1*sigma_rE-nu_1*sigma_zE)/E_1;
> zE:=(sigma_zE-nu_1*sigma_tE-nu_1*sigma_rE)/E_1;
```

```
> r:=r_1:
> rP_1:=rP;tP_1:=tP;zP_1:=zP;rE_1:=rE;tE_1:=tE;zE_1:=zE;
> r:='r':
> e_rP:=rP-rP_1+rE_1+urE;e_tP:=tP-tP_1+tE_1+utE;e_zP:=zP-zP_1+zE_1+uzE;
> e_rE:=rE+urE;e_tE:=tE+utE;e_zE:=zE+uzE;
> p_e:=plot([e_rE,e_tE,e_zE],r=r_1..R_0):p_p:=plot([e_rP,e_tP,e_zP],r=R_n..r_1):
> display({p_e,p_p});
```

Deformed Geometry

```
> for i from 1 to 5 do
> g_1:=x^2*S_Y/sqrt(3*r_0^4+(1-q)^2*x^4):
> g_2:=g_1*(1+nu_p)*E_2*r_0^2/(2*(1-nu_2^2)*E_p*x^2):
> f:=g_1*(r_0^2-r_n^2)-g_2*((x^2-r_n^2)-2*r_n^2*ln(x/r_n))-p_n*r_n^2:
> r_1:=fsolve(f,x): x:=r_1: g_1c:=g_1:g_2c:=g_2: x:='x':
> '[g_1c,g_2c,r_1]'=[g_1c,g_2c,r_1];
> Eenel:=3.14159*g_1c^2*(1+nu_1)*(r_0^2-r_1^2)/E_1*(r_0^2/r_1^2+(1-2*nu_1));
> sigma_rP:=-g_1c*(r_0^2/r^2-1)+g_2c*(r_1^2/r^2-1-2*ln(r_1/r)):
> sigma_tP:=g_1c*(r_0^2/r^2+1)-g_2c*(r_1^2/r^2-1+2*ln(r_1/r)):
> sigma_zP:=4*nu_2*g_2c*ln(r/r_1)+q*g_1c:
> sigma_rE:=-g_1c*(r_0^2/r^2-1):
> sigma_tE:=g_1c*(r_0^2/r^2+1):
> sigma_zE:=q*g_1c:
> etE:=(sigma_tE-nu_1*sigma_rE-nu_1*sigma_zE)/E_1:
> r:=r_0:etE0:=etE: r:='r':
> u_0:=r_0*etE0;
> sijsij_P:=sigma_rP^2+sigma_tP^2+sigma_zP^2:
> skk_P:=sigma_rP+sigma_tP+sigma_zP:
> sijsij_E:=sigma_rE^2+sigma_tE^2+sigma_zE^2:
> skk_E:=sigma_rE+sigma_tE+sigma_zE:
> r:=r_1:sijsij_P1:=sijsij_P:skk_P1:=skk_P:sijsij_E1:=sijsij_E:skk_E1:=skk_E:r:='r':
```

```
> eta:=((1+nu_2)*sijsij_P-nu_2*skk_P^2)/(2*E_2)-((1+nu_2)*sijsij_P1-
nu_2*skk_P1^2)/(2*E_2)+((1+nu_1)*sijsij_E1-nu_1*skk_E1^2)/(2*E_1);
> Eenpl:=2*3.14159*int(eta*r,r=r_n..r_1);
> Energy:= Eenel + Eenpl;
> Work:=3.14159*p_n*u_n*(R_n+r_n)/2;
> FF:=evalf(Energy - Work):
> y_c:=solve(FF,u_n); u_n:=y_c; W:=Work;
> r_n:=R_n+u_n;r_0:=R_0+u_0;  u_n:='u_n':
> print('[r_0,r_1,r_n,g_1,g_2,Energy,Work]'=[r_0,r_1,r_n,g_1c,g_2c,Energy,W]);
> od:
> sigma_rP:=-g_1c*(r_0^2/r^2-1)+g_2c*(r_1^2/r^2-1-2*ln(r_1/r)):
> sigma_tP:=g_1c*(r_0^2/r^2+1)-g_2c*(r_1^2/r^2-1+2*ln(r_1/r)):
> sigma_zP:=4*nu_2*g_2c*ln(r/r_1)+q*g_1c:
> sigma_rE:=-g_1c*(r_0^2/r^2-1):
> sigma_tE:=g_1c*(r_0^2/r^2+1):
> sigma_zE:=q*g_1c:
> g_3:=r_n^2*p_n/(r_0^2-r_n^2):
> usigma_rP:=g_3*(r_0^2/r^2-1):usigma_tP:=-g_3*(r_0^2/r^2+1):usigma_zP:=-q*g_3:
> usigma_rE:=g_3*(r_0^2/r^2-1):usigma_tE:=-g_3*(r_0^2/r^2+1):usigma_zE:=-q*g_3:
> rsigma_rP:=sigma_rP+usigma_rP:rsigma_tP:=sigma_tP+usigma_tP:
> rsigma_zP:=sigma_zP+usigma_zP:
> rsigma_rE:=sigma_rE+usigma_rE:rsigma_tE:=sigma_tE+usigma_tE:
> rsigma_zE:=sigma_zE+usigma_zE:
> urE:=(usigma_rP-nu_1*usigma_tP-nu_1*usigma_zP)/E_1;
> utE:=(usigma_tP-nu_1*usigma_rP-nu_1*usigma_zP)/E_1;
> uzE:=(usigma_zP-nu_1*usigma_tP-nu_1*usigma_rP)/E_1;
> rP:=(sigma_rP-nu_2*sigma_tP-nu_2*sigma_zP)/E_2;
> tP:=(sigma_tP-nu_2*sigma_rP-nu_2*sigma_zP)/E_2;
> zP:=(sigma_zP-nu_2*sigma_rP-nu_2*sigma_tP)/E_2;
> rE:=(sigma_rE-nu_1*sigma_tE-nu_1*sigma_zE)/E_1;
> tE:=(sigma_tE-nu_1*sigma_rE-nu_1*sigma_zE)/E_1;
```

```
> zE:=(sigma_zE-nu_1*sigma_tE-nu_1*sigma_rE)/E_1;
> r:=r_1:
> rP_1:=rP;tP_1:=tP;zP_1:=zP;rE_1:=rE;tE_1:=tE;zE_1:=zE;
> r:='r':
> e_rP:=rP-rP_1+rE_1+urE;e_tP:=tP-tP_1+tE_1+utE;e_zP:=zP-zP_1+zE_1+uzE;
> e_rE:=rE+urE;e_tE:=tE+utE;e_zE:=zE+uzE;
> p_em:=plot([e_rE,e_tE,e_zE],r=r_1..r_0):p_pm:=plot([e_rP,e_tP,e_zP],r=r_n..r_1):
> display({p_e,p_p,p_em,p_pm});

> err:=0.001:
> c:=0:step_p:=(r_1-r_n)/8:step_e:=(r_0-r_1)/8:
> for r from r_n by step_p to r_1+err do
> c:=c+1:r:=r:
> rad[c]:=r:
> lprint(rad[c]);
> od:
> r_11:=r_1+step_e:
> for r from r_11 by step_e to r_0+err do
> c:=c+1:r:=r:
> rad[c]:=r:
> lprint(rad[c]);
> od:

> c:=0:step_p:=(r_1-r_n)/8:step_e:=(r_0-r_1)/8:
> for r from r_n by step_p to r_1+err do
> c:=c+1:r:=r:e_rP := rP-rP_1+rE_1+urE:
> rad[c]:=r:e_rP[c]:=e_rP:
> lprint(e_rP[c]);
> od:
> r_11:=r_1+step_e:
> for r from r_11 by step_e to r_0+err do
```

```
> c:=c+1:r:=r:e_rE := rE+urE:
> rad[c]:=r:e_rE[c]:=e_rE:
> lprint(e_rE[c]);
> od:

> c:=0:step_p:=(r_1-r_n)/8:step_e:=(r_0-r_1)/8:
> for r from r_n by step_p to r_1+err do
> c:=c+1:r:=r:e_tP := tP-tP_1+tE_1+utE:
> rad[c]:=r:e_tP[c]:=e_tP:
> lprint(e_tP[c]);
> od:
> r_11:=r_1+step_e:
> for r from r_11 by step_e to r_0+err do
> c:=c+1:r:=r:e_tE := tE+utE:
> rad[c]:=r:e_tE[c]:=e_tE:
> lprint(e_tE[c]);
> od:

> c:=0:step_p:=(r_1-r_n)/8:step_e:=(r_0-r_1)/8:
> for r from r_n by step_p to r_1+err do
> c:=c+1:r:=r:e_zP := zP-zP_1+zE_1+uzE:
> rad[c]:=r:e_zP[c]:=e_zP:
> lprint(e_zP[c]);
> od:
> r_11:=r_1+step_e:
> for r from r_11 by step_e to r_0+err do
> c:=c+1:r:=r:e_zE:=zE+uzE:
> rad[c]:=r:e_zE[c]:=e_zE:
> lprint(e_zE[c]);
> od:
```

A.7 Maple 6 Program for Shakedown Pressure Estimation – Deformed Geometry

Formulation Based on Virtual Work Principle

General Procedure for Closed Ends, Plane Strain, and Plane Stress Conditions

In Plane Stress, q=0; in Plane Strain, q = 2*nu; in Closed Ends, q = 1.

Plane Strain in This Example

```
> restart: Digits:=10:with(linalg): with(plots):
> S_Y:=30000;
> E_1:=30*10^6;
> E_2:=E_1/100;
> E_p:=1/((1/E_2)-(1/E_1)):
> nu_1:=0.3: nu_p:=0.5: nu_2:=E_2*((nu_1/E_1)+(0.5/E_p )):
> R_0:=9.1: R_n:=4.0:  r_0:=R_0: r_n:=R_n: t:=r_0/r_n: T:=R_0/R_n:
> 'E_1'=E_1,'E_2'=E_2,'E_p'=E_p,'p_n'=p_n;
> q:=2*nu_1;
> for i from 1 to 10 do
> g_1:=x^2*S_Y/sqrt(3*r_0^4+(1-q)^2*x^4):
> g_2:=g_1*(1+nu_p)*E_2*r_0^2/(2*(1-nu_2^2)*E_p*x^2):
> p_n:=g_1*(r_0^2-r_n^2)/r_n^2-g_2*((x^2-r_n^2)/r_n^2-2*ln(x/r_n)):
> sigma_rP:=-g_1*(r_0^2/r^2-1)+g_2*(x^2/r^2-1-2*ln(x/r)):
> sigma_tP:=g_1*(r_0^2/r^2+1)-g_2*(x^2/r^2-1+2*ln(x/r)):
> sigma_zP:=4*nu_2*g_2*ln(r/x)+q*g_1:
> sigma_rE:=-g_1*(r_0^2/r^2-1):
> sigma_tE:=g_1*(r_0^2/r^2+1):
> sigma_zE:=q*g_1:
> g_3:=r_n^2*p_n/(r_0^2-r_n^2):
> usigma_rP:=g_3*(r_0^2/r^2-1):usigma_tP:=-g_3*(r_0^2/r^2+1):usigma_zP:=-q*g_3:
> usigma_rE:=g_3*(r_0^2/r^2-1):usigma_tE:=-g_3*(r_0^2/r^2+1):usigma_zE:=-q*g_3:
> rsigma_rP:=sigma_rP+usigma_rP:rsigma_tP:=sigma_tP+usigma_tP:
> rsigma_zP:=sigma_zP+usigma_zP:
```

```
> rsigma_rE:=sigma_rE+usigma_rE:rsigma_tE:=sigma_tE+usigma_tE:
> rsigma_zE:=sigma_zE+usigma_zE:
> sigma_eqp:=sqrt(.5*((sigma_rP-sigma_tP)^2+(sigma_rP-sigma_zP)^2+(sigma_tP-
sigma_zP)^2)):
> rsigma_eqp:=sqrt(.5*((rsigma_rP-rsigma_tP)^2+(rsigma_rP-rsigma_zP)^2
+(rsigma_tP-rsigma_zP)^2)):
> r:=r_n:sigma_eqpn:=sigma_eqp:rsigma_eqpn:=rsigma_eqp:r:='r':
> r_sd:=fsolve(sigma_eqpn+rsigma_eqpn=2*S_Y,x,x=r_n..r_0);
> x:=r_sd:p_sd:=p_n;x:='x':r_1:=r_sd:
> g_1:=r_1^2*S_Y/sqrt(3*r_0^4+(1-q)^2*r_1^4);
> g_2:=g_1*(1+nu_p)*E_2*r_0^2/(2*(1-nu_2^2)*E_p*r_1^2);
> g_1c:=g_1:g_2c:=g_2:
> '[g_1c,g_2c,r_1]'=[g_1c,g_2c,r_1];
> Eenel:=3.14159*g_1c^2*(1+nu_1)*(r_0^2-r_1^2)/E_1*(r_0^2/r_1^2+(1-2*nu_1));
> sigma_rP:=-g_1c*(r_0^2/r^2-1)+g_2c*(r_1^2/r^2-1-2*ln(r_1/r));
> sigma_tP:=g_1c*(r_0^2/r^2+1)-g_2c*(r_1^2/r^2-1+2*ln(r_1/r));
> sigma_zP:=4*nu_2*g_2c*ln(r/r_1)+q*g_1c;
> sigma_rE:=-g_1c*(r_0^2/r^2-1); sigma_tE:=g_1c*(r_0^2/r^2+1); sigma_zE:=q*g_1c;
> > etE:=(sigma_tE-nu_1*sigma_rE-nu_1*sigma_zE)/E_1;
> r:=r_0:etE0:=etE: r:='r': u_0:=r_0*etE0;
> sijsij_P:=sigma_rP^2+sigma_tP^2+sigma_zP^2:
> skk_P:=sigma_rP+sigma_tP+sigma_zP:
> sijsij_E:=sigma_rE^2+sigma_tE^2+sigma_zE^2:
> skk_E:=sigma_rE+sigma_tE+sigma_zE:
> r:=r_1:sijsij_P1:=sijsij_P:skk_P1:=skk_P:sijsij_E1:=sijsij_E:skk_E1:=skk_E:r:='r':
> eta:=((1+nu_2)*sijsij_P-nu_2*skk_P^2)/(2*E_2)-((1+nu_2)*sijsij_P1-
nu_2*skk_P1^2)/(2*E_2)+((1+nu_1)*sijsij_E1-nu_1*skk_E1^2)/(2*E_1):
> Eenpl:=2*3.14159*int(eta*r,r=r_n..r_1);
> Energy:= Eenel + Eenpl;
> Work:=3.14159*p_sd*u_n*(R_n+r_n)/2;
> FF:=evalf(Energy - Work):
```

```
> y_c:=solve(FF,u_n); u_n:=y_c; W:=Work;
> r_n:=R_n+u_n;r_0:=R_0+u_0;  u_n:='u_n':
> print('[r_0,r_1,r_n,g_1,g_2,Energy,Work,Shakedown_Pressure]'
=[r_0,r_1,r_n,g_1c,g_2c,Energy,W,p_sd]);
> od:
```

A.8 Maple 6 Program for Shakedown Pressure Estimation – Undeformed Geometry

General Procedure for Closed Ends, Plane Strain, and Plane Stress Conditions
In Plane Stress, q=0; in Plane Strain, q = 2*nu; in Closed Ends, q = 1.
Plane Strain in This Example

```
> restart: Digits:=10:with(linalg): with(plots):
> S_Y:=30000;
> E_1:=30*10^6;
> E_2:=E_1/100;
> E_p:=1/((1/E_2)-(1/E_1)):
> nu_1:=0.3: nu_p:=0.5: nu_2:=E_2*((nu_1/E_1)+(0.5/E_p )):
> R_0:=12.0: R_n:=4.0:  r_0:=R_0: r_n:=R_n: t:=r_0/r_n: T:=R_0/R_n:
> 'E_1'=E_1,'E_2'=E_2,'E_p'=E_p,'p_n'=p_n;
> q:=2*nu_1;
> g_1:=r_1^2*S_Y/sqrt(3*r_0^4+(1-q)^2*r_1^4):
> g_2:=g_1*(1+nu_p)*E_2*r_0^2/(2*(1-nu_2^2)*E_p*r_1^2):
> p_n:=g_1*(r_0^2-r_n^2)/r_n^2-g_2*((r_1^2-r_n^2)/r_n^2-2*ln(r_1/r_n)):
> sigma_rP:=-g_1*(r_0^2/r^2-1)+g_2*(r_1^2/r^2-1-2*ln(r_1/r)):
> sigma_tP:=g_1*(r_0^2/r^2+1)-g_2*(r_1^2/r^2-1+2*ln(r_1/r)):
> sigma_zP:=4*nu_2*g_2*ln(r/r_1)+q*g_1:
> sigma_rE:=-g_1*(r_0^2/r^2-1):
> sigma_tE:=g_1*(r_0^2/r^2+1):
> sigma_zE:=q*g_1:
> g_3:=r_n^2*p_n/(r_0^2-r_n^2):
```

```
> usigma_rP:=g_3*(r_0^2/r^2-1):usigma_tP:=-g_3*(r_0^2/r^2+1):usigma_zP:=-q*g_3:
> usigma_rE:=g_3*(r_0^2/r^2-1):usigma_tE:=-g_3*(r_0^2/r^2+1):usigma_zE:=-q*g_3:
> rsigma_rP:=sigma_rP+usigma_rP:rsigma_tP:=sigma_tP+usigma_tP:
> rsigma_zP:=sigma_zP+usigma_zP:
> rsigma_rE:=sigma_rE+usigma_rE:rsigma_tE:=sigma_tE+usigma_tE:
> rsigma_zE:=sigma_zE+usigma_zE:
> sigma_eqp:=sqrt(.5*((sigma_rP-sigma_tP)^2+(sigma_rP-sigma_zP)^2+(sigma_tP-
sigma_zP)^2)):
> rsigma_eqp:=sqrt(.5*((rsigma_rP-rsigma_tP)^2+(rsigma_rP-
rsigma_zP)^2+(rsigma_tP-rsigma_zP)^2)):
> r:=r_n:sigma_eqpn:=sigma_eqp:rsigma_eqpn:=rsigma_eqp:r:='r':
> r_sd:=fsolve(sigma_eqpn+rsigma_eqpn=2*S_Y,r_1,r_1=r_n..r_0);
> r_1:=r_sd:p_sd:=p_n;
```

A.9 Maple 6 Program for Plastic Collapse Load Estimation – Deformed Geometry

General Procedure for Closed Ends, Plane Strain, and Plane Stress Conditions
Formulation Based on Virtual Work Principle
In Plane Stress, q=0; in Plane Strain, q = 2*nu; in Closed Ends, q = 1.
Closed End in This Example

```
> restart: Digits:=10:with(linalg): with(plots):
> S_Y:=30000;
> E_1:=30*10^6;
> E_2:=E_1/100;
> E_p:=1/((1/E_2)-(1/E_1)):
> nu_1:=0.3: nu_p:=0.5: nu_2:=E_2*((nu_1/E_1)+(0.5/E_p )):
> R_0:=16.8: R_n:=4.0:  r_0:=R_0: r_n:=R_n: t:=r_0/r_n: T:=R_0/R_n: p_0:=0:
> 'E_1'=E_1,'E_2'=E_2,'E_p'=E_p,'p_n'=p_n;
> q:=1;
> for p_n from 51530 by 2 to 100000 do
```

```
> for i from 1 to 10 do
> g_1:=x^2*S_Y/sqrt(3*r_0^4+(1-q)^2*x^4):
> g_2:=g_1*(1+nu_p)*E_2*r_0^2/(2*(1-nu_2^2)*E_p*x^2):
> f:=g_1*(r_0^2-r_n^2)-g_2*((x^2-r_n^2)-2*r_n^2*ln(x/r_n))-p_n*r_n^2:
> r_1:=fsolve(f,x): x:=r_1: g_1c:=g_1:g_2c:=g_2: x:='x':
> '[g_1c,g_2c,r_1]'=[g_1c,g_2c,r_1];
> Eenel:=3.14159*g_1c^2*(1+nu_1)*(r_0^2-r_1^2)/E_1*(r_0^2/r_1^2+(1-2*nu_1));
> sigma_rP:=-g_1c*(r_0^2/r^2-1)+g_2c*(r_1^2/r^2-1-2*ln(r_1/r)):
> sigma_tP:=g_1c*(r_0^2/r^2+1)-g_2c*(r_1^2/r^2-1+2*ln(r_1/r)):
> sigma_zP:=4*nu_2*g_2c*ln(r/r_1)+q*g_1c:
> sigma_rE:=-g_1c*(r_0^2/r^2-1):
> sigma_tE:=g_1c*(r_0^2/r^2+1):
> sigma_zE:=q*g_1c:
> etE:=(sigma_tE-nu_1*sigma_rE-nu_1*sigma_zE)/E_1:
> r:=r_0:etE0:=etE: r:='r': u_0:=r_0*etE0;
> sijsij_P:=sigma_rP^2+sigma_tP^2+sigma_zP^2:
> skk_P:=sigma_rP+sigma_tP+sigma_zP:
> sijsij_E:=sigma_rE^2+sigma_tE^2+sigma_zE^2:
> skk_E:=sigma_rE+sigma_tE+sigma_zE:
> r:=r_1:sijsij_P1:=sijsij_P:skk_P1:=skk_P:sijsij_E1:=sijsij_E:skk_E1:=skk_E:r:='r':
> eta:=((1+nu_2)*sijsij_P-nu_2*skk_P^2)/(2*E_2)-((1+nu_2)*sijsij_P1-
nu_2*skk_P1^2)/(2*E_2)+((1+nu_1)*sijsij_E1-nu_1*skk_E1^2)/(2*E_1);
> Eenpl:=2*3.14159*int(eta*r,r=r_n..r_1);
> Energy:= Eenel + Eenpl;
> Work:=3.14159*p_n*u_n*r_n;
> FF:=evalf(Energy - Work):
> y_c:=solve(FF,u_n); u_n:=y_c; W:=Work;
> r_n:=R_n+u_n;r_0:=R_0+u_0;  u_n:='u_n':
> print('[r_0,r_1,r_n,Energy,Work,p_n]'=[r_0,r_1,r_n,Energy,W,p_n]);
> od:
> if (r_0-r_1)<0.001 then break;
```

```
> fi;
> od:
> print('[u_0,r_1,u_n,g_1,g_2,Energy,Work]'=[u_0,r_1,y_c,g_1c,g_2c,Energy,W]);
> 'Limit_Load'=p_n;
```

A.10 Maple 6 Program for Plastic Collapse Load Estimation – Undeformed Geometry

General Procedure for Closed Ends, Plane Strain, and Plane Stress Conditions
In Plane Stress, q=0; in Plane Strain, q = 2*nu; in Closed Ends, q = 1.
Closed End in This Example

```
> restart: Digits:=10:with(linalg): with(plots):
> S_Y:=30000;
> E_1:=30*10^6;
> E_2:=E_1/100;
> E_p:=1/((1/E_2)-(1/E_1)):
> nu_1:=0.3: nu_p:=0.5: nu_2:=E_2*((nu_1/E_1)+(0.5/E_p )):
> R_0:=16.8: R_n:=4.0:  r_0:=R_0: r_n:=R_n: t:=r_0/r_n: T:=R_0/R_n: p_0:=0:
> 'E_1'=E_1,'E_2'=E_2,'E_p'=E_p,'p_n'=p_n; q:=1;
> for p_n from 52500 to 100000 do
> g_1:=x^2*S_Y/sqrt(3*r_0^4+(1-q)^2*x^4):
> g_2:=g_1*(1+nu_p)*E_2*r_0^2/(2*(1-nu_2^2)*E_p*x^2):
> f:=g_1*(r_0^2-r_n^2)-g_2*((x^2-r_n^2)-2*r_n^2*ln(x/r_n))-p_n*r_n^2:
> r_1:=fsolve(f,x): x:=r_1: g_1c:=g_1:g_2c:=g_2: x:='x':
> '[g_1c,g_2c,r_1]'=[g_1c,g_2c,r_1];
> print('[r_0,r_1,r_n,p_n]'=[r_0,r_1,r_n,p_n]);
> if (R_0-r_1)<0.01 then break;
> fi;
> od:
> 'Limit_Load'=p_n;
```

APPENDIX B: ANSYS Programs For Inelastic Analyses

This appendix lists the ANSYS routines and macros for implementing the inelastic analysis on thick walled cylinders subject to high internal pressure with large deformation or small deformation.

B.1 ANSYS Commands for Inelastic Analysis in Large Deformation

```
/BATCH, LIST
/TITLE, ELASTIC PLASTIC ANAYSIS OF LARGE DEFORMATION
/FILNAM,CYLINDER
/CONFIG,NRES,10000
/PREP7
RO=20
RN=4
ET,1,42,,,1
MP,EX,1,30E6
MP,NUXY,1,0.3
!DEFINE A BILINEAR HARDENING PLASTICITY CURVE USING KINH
TB,KINH,1,1,2
TBPT,,0.001,30000
TBPT,,0.1,59700
!SET THE AXLES LABELS FOR THE STRESS-STAIN CURVE PLOT
/AXLAB,X,STRAIN
/AXLAB,Y,TRUE STRESS (PSI.)
TBPL,KINH,1
!MODELLING
K,1,RN
K,2,RO
K,3,RO,.4
```

```
K,4,RN,.4
A,1,2,3,4
ESIZE,0.4
AMESH,ALL
/SOLU
D,ALL,UY,0
NLGEOM,ON
!NULL LOAD TO GIVE GRAPH STARTING AT ZERO
TIME,1E-6
LSWRIT
P_INT=30000
TIME,P_INT
KBC,0
DELTIM,5,1,20
AUTOTS,ON
PRED,ON
NSEL,S,LOC,X,RN
SFL,4,PRES,P_INT
NSEL,ALL
LSWRIT
OUTRES,ALL,ALL
SOLVE
FINI
/POST1
SET,LAST
ETABLE,STRS_R,S,X
ETABLE,STRS_T,S,Y
ETABLE,STRS_Z,S,Z
ETABLE,STRN_R,EPTO,X
ETABLE,STRN_T,EPTO,Y
ETABLE,STRN_Z,EPTO,Z
```

```
ETABLE,EQV_S,S,EQV
ETABLE,EQV_NE,EPEL,EQV
ETABLE,EQV_NP,EPPL,EQV
ETABLE,ENER,SENE
ETABLE,VOL,VOLU
*GET,MAXI,ELEM,0,COUNT
*CFOPEN,NONLIN20
TENER=0
*DO,KK,1,MAXI
*GET,SS,ELEM,KK,ETAB,EQV_S
*GET,SNE,ELEM,KK,ETAB,EQV_NE
*GET,SNP,ELEM,KK,ETAB,EQV_NP
*GET,SX,ELEM,KK,ETAB,STRS_R
*GET,SY,ELEM,KK,ETAB,STRS_T
*GET,SZ,ELEM,KK,ETAB,STRS_Z
*GET,SNX,ELEM,KK,ETAB,STRN_R
*GET,SNY,ELEM,KK,ETAB,STRN_T
*GET,SNZ,ELEM,KK,ETAB,STRN_Z
*GET,ENERD,ELEM,KK,ETAB,ENER
*GET,VOLUME,ELEM,KK,ETAB,VOL
TENER=TENER+ENERD*2.5
FTENER=TENER
SN=SNE/1.3+SNP/1.5
*VWRITE,KK,SS,SN,SX,SY,SZ,SNX,SNY,SNZ,FTENER
(X,F6.1,E15.8,3X,E15.8,3X,E15.8,3X,E15.8,3X,E15.8,3X,E15.8,3X,E15.8,3X,E15.8,3X
,E15.8,3X)
*ENDDO
*CFCLOS

FINISH
```

B.2 ANSYS Commands for Inelastic Analysis of Small Deformation Theory

```
/BATCH, LIST
/TITLE, ELASTIC PLASTIC ANAYSIS OF SMALL DEFORMATION
/FILNAM,CYLINDER
/CONFIG,NRES,10000

/PREP7
RO=20
RN=4
ET,1,42,,,1
MP,EX,1,30E6
MP,NUXY,1,0.3
!DEFINE A BILINEAR HARDENING PLASTICITY CURVE USING KINH
TB,KINH,1,1,2
TBPT,,0.001,30000
TBPT,,0.1,59700
!SET THE AXLES LABELS FOR THE STRESS-STAIN CURVE PLOT
/AXLAB,X,STRAIN
/AXLAB,Y,TRUE STRESS (PSI.)
TBPL,KINH,1
!MODELLING
K,1,RN
K,2,RO
K,3,RO,.4
K,4,RN,.4
A,1,2,3,4
ESIZE,0.4
AMESH,ALL
```

```
/SOLU
D,ALL,UY,0
!NULL LOAD TO GIVE GRAPH STARTING AT ZERO
TIME,1E-6
LSWRIT
P_INT=30000
TIME,P_INT
KBC,0
DELTIM,5,1,20
AUTOTS,ON
PRED,ON
NSEL,S,LOC,X,RN
SFL,4,PRES,P_INT
NSEL,ALL
LSWRIT
OUTRES,ALL,ALL
SOLVE
FINI

/POST1
SET,LAST
ETABLE,STRS_R,S,X
ETABLE,STRS_T,S,Y
ETABLE,STRS_Z,S,Z
ETABLE,STRN_R,EPTO,X
ETABLE,STRN_T,EPTO,Y
ETABLE,STRN_Z,EPTO,Z
ETABLE,EQV_S,S,EQV
ETABLE,EQV_NE,EPEL,EQV
ETABLE,EQV_NP,EPPL,EQV
ETABLE,ENER,SENE
```

```
ETABLE,VOL,VOLU
*GET,MAXI,ELEM,0,COUNT
*CFOPEN,NONLIN20
TENER=0
*DO,KK,1,MAXI
*GET,SS,ELEM,KK,ETAB,EQV_S
*GET,SNE,ELEM,KK,ETAB,EQV_NE
*GET,SNP,ELEM,KK,ETAB,EQV_NP
*GET,SX,ELEM,KK,ETAB,STRS_R
*GET,SY,ELEM,KK,ETAB,STRS_T
*GET,SZ,ELEM,KK,ETAB,STRS_Z
*GET,SNX,ELEM,KK,ETAB,STRN_R
*GET,SNY,ELEM,KK,ETAB,STRN_T
*GET,SNZ,ELEM,KK,ETAB,STRN_Z
*GET,ENERD,ELEM,KK,ETAB,ENER
*GET,VOLUME,ELEM,KK,ETAB,VOL
TENER=TENER+ENERD*2.5
FTENER=TENER
SN=SNE/1.3+SNP/1.5
*VWRITE,KK,SS,SN,SX,SY,SZ,SNX,SNY,SNZ,FTENER
(X,F6.1,E15.8,3X,E15.8,3X,E15.8,3X,E15.8,3X,E15.8,3X,E15.8,3X,E15.8,3X,E15.8,3X
,E15.8,3X)
*ENDDO
*CFCLOS

FINISH
```

B.3 ANSYS Commands for Autofrettage of Thick Walled Cylinders of Large Deformation Formulation

```
/BATCH,LIST
/TITLE, AUTOFRETTAGE OF THICK WALLED CYLINDERS
/FILNAM,CLOSEEND
/CONFIG,NRES,10000
/PREP7
RO=20
RN=4
ET,1,42,,,1
MP,EX,1,30E6
MP,NUXY,1,0.3
TB,KINH,1,1,2
TBPT,,0.001,30000
TBPT,,0.1,59700
/AXLAB,X,STRAIN
/AXLAB,Y,TRUE STRESS (PSI.)
TBPL,KINH,1
K,1,RN
K,2,RO
K,3,RO,0.4
K,4,RN,0.4
A,1,2,3,4
ESIZE,0.4
AMESH,ALL

/SOLU
D,ALL,UY,0
NLGEOM,ON
TIME,1E-6
```

```
LSWRIT
P_INT=25000
TIME,P_INT
KBC,0
DELTIM,5,1,20
P_T=P_INT*(RN**2)/(RO**2-RN**2)
AUTOTS,ON
PRED,ON
NSEL,S,LOC,X,RN
SFL,4,PRES,P_INT
SFL,3,PRES,-P_T
NSEL,ALL
LSWRIT
OUTRES,ALL,ALL
SOLVE
P_INT=0 !UNLOAD TO ZERO PRESSURE
P_T=P_INT*(RN**2)/(RO**2-RN**2)
SFL,4,PRES,P_INT
SFL,3,PRES,-P_T
LSWRIT
OUTRES,ALL,ALL
SOLVE
FINI

/POST1
SET,LAST
ETABLE,STRS_R,S,X
ETABLE,STRS_T,S,Y
ETABLE,STRS_Z,S,Z
ETABLE,STRN_R,EPTO,X
ETABLE,STRN_T,EPTO,Y
```

```
ETABLE,STRN_Z,EPTO,Z
ETABLE,EQV_S,S,EQV
ETABLE,EQV_NE,EPEL,EQV
ETABLE,EQV_NP,EPPL,EQV
ETABLE,ENER,SENE
ETABLE,VOL,VOLU
*GET,MAXI,ELEM,0,COUNT
*CFOPEN,NONLIN20
TENER=0
*DO,KK,1,MAXI
*GET,SS,ELEM,KK,ETAB,EQV_S
*GET,SNE,ELEM,KK,ETAB,EQV_NE
*GET,SNP,ELEM,KK,ETAB,EQV_NP
*GET,SX,ELEM,KK,ETAB,STRS_R
*GET,SY,ELEM,KK,ETAB,STRS_T
*GET,SZ,ELEM,KK,ETAB,STRS_Z
*GET,SNX,ELEM,KK,ETAB,STRN_R
*GET,SNY,ELEM,KK,ETAB,STRN_T
*GET,SNZ,ELEM,KK,ETAB,STRN_Z
*GET,ENERD,ELEM,KK,ETAB,ENER
*GET,VOLUME,ELEM,KK,ETAB,VOL
TENER=TENER+ENERD
FTENER=TENER
SN=SNE/1.3+SNP/1.5
*VWRITE,KK,SS,SN,SX,SZ,SY,SNX,SNZ,SNY,FTENER
(X,F6.1,E15.8,3X,E15.8,3X,E15.8,3X,E15.8,3X,E15.8,3X,E15.8,3X,E15.8,3X,E15.8,3X
,E15.8,3X)
*ENDDO
*CFCLOS

FINISH
```

B.4 ANSYS Commands for Autofrettage of Thick Walled Cylinders of Small Deformation Formulation

```
/BATCH,LIST
/TITLE, AUTOFRETTAGE OF THICK WALLED CYLINDERS
/FILNAM,CLOSEEND
/CONFIG,NRES,10000
/PREP7
RO=20
RN=4
ET,1,42,,,1
MP,EX,1,30E6
MP,NUXY,1,0.3
TB,KINH,1,1,2
TBPT,,0.001,30000
TBPT,,0.1,59700
/AXLAB,X,STRAIN
/AXLAB,Y,TRUE STRESS (PSI.)
TBPL,KINH,1
K,1,RN
K,2,RO
K,3,RO,0.4
K,4,RN,0.4
A,1,2,3,4
ESIZE,0.4
AMESH,ALL

/SOLU
D,ALL,UY,0
TIME,1E-6
LSWRIT
```

```
P_INT=25000
TIME,P_INT
KBC,0
DELTIM,5,1,20
P_T=P_INT*(RN**2)/(RO**2-RN**2)
AUTOTS,ON
PRED,ON
NSEL,S,LOC,X,RN
SFL,4,PRES,P_INT
SFL,3,PRES,-P_T
NSEL,ALL
LSWRIT
OUTRES,ALL,ALL
SOLVE
P_INT=0 !UNLOAD TO ZERO PRESSURE
P_T=P_INT*(RN**2)/(RO**2-RN**2)
SFL,4,PRES,P_INT
SFL,3,PRES,-P_T
LSWRIT
OUTRES,ALL,ALL
SOLVE
FINI

/POST1
SET,LAST
ETABLE,STRS_R,S,X
ETABLE,STRS_T,S,Y
ETABLE,STRS_Z,S,Z
ETABLE,STRN_R,EPTO,X
ETABLE,STRN_T,EPTO,Y
ETABLE,STRN_Z,EPTO,Z
```

```
ETABLE,EQV_S,S,EQV
ETABLE,EQV_NE,EPEL,EQV
ETABLE,EQV_NP,EPPL,EQV
ETABLE,ENER,SENE
ETABLE,VOL,VOLU
*GET,MAXI,ELEM,0,COUNT
*CFOPEN,NONLIN20
TENER=0
*DO,KK,1,MAXI
*GET,SS,ELEM,KK,ETAB,EQV_S
*GET,SNE,ELEM,KK,ETAB,EQV_NE
*GET,SNP,ELEM,KK,ETAB,EQV_NP
*GET,SX,ELEM,KK,ETAB,STRS_R
*GET,SY,ELEM,KK,ETAB,STRS_T
*GET,SZ,ELEM,KK,ETAB,STRS_Z
*GET,SNX,ELEM,KK,ETAB,STRN_R
*GET,SNY,ELEM,KK,ETAB,STRN_T
*GET,SNZ,ELEM,KK,ETAB,STRN_Z
*GET,ENERD,ELEM,KK,ETAB,ENER
*GET,VOLUME,ELEM,KK,ETAB,VOL
TENER=TENER+ENERD
FTENER=TENER
SN=SNE/1.3+SNP/1.5
*VWRITE,KK,SS,SN,SX,SZ,SY,SNX,SNZ,SNY,FTENER
(X,F6.1,E15.8,3X,E15.8,3X,E15.8,3X,E15.8,3X,E15.8,3X,E15.8,3X,E15.8,3X,E15.8,3X
,E15.8,3X)
*ENDDO
*CFCLOS

FINISH
```

B.5 ANSYS Commands for Plastic Collapse Load Estimations of Thick Walled Cylinders in Large Deformation

```
/BATCH,LIST
/TITLE, ELASTIC PLASTIC ANAYSIS OF THICK WALLED CYLINDER
SUBJECTED TO INTERNAL PRESSURE
/FILNAM,CYLINDER
/CONFIG,NRES,10000

/PREP7
RO=8
RN=4
ET,1,42,,,1
MP,EX,1,30E6
MP,NUXY,1,0.3
!DEFINE A BILINEAR HARDENING PLASTICITY CURVE USING KINH
TB,KINH,1,1,2
TBPT,,0.001,30000
TBPT,,0.004,30090
!SET THE AXLES LABELS FOR THE STRESS-STAIN CURVE PLOT
/AXLAB,X,STRAIN
/AXLAB,Y,TRUE STRESS (PSI.)
TBPL,KINH,1

!MODELLING
K,1,RN
K,2,RO
K,3,RO,.4
K,4,RN,.4
A,1,2,3,4
ESIZE,.4
```

```
AMESH,ALL

/SOLU
D,ALL,UY,0
NLGEOM,ON
!NULL LOAD TO GIVE GRAPH STARTING AT ZERO
TIME,1E-6
LSWRIT
P_INT=60000
TIME,P_INT
KBC,0
DELTIM,5,1,20
AUTOTS,ON
PRED,ON
NSEL,S,LOC,X,RN
SFL,4,PRES,P_INT
SFL,3,PRES,-(P_INT*RN**2)/(RO**2-RN**2)
NSEL,ALL
LSWRIT
OUTRES,ALL,LAST
SOLVE

FINI
```

B.6 ANSYS Commands for Plastic Collapse Load Estimations of Thick Walled Cylinders in Small Deformation

```
/BATCH,LIST
/TITLE, ELASTIC PLASTIC ANAYSIS OF THICK WALLED CYLINDER
SUBJECTED TO INTERNAL PRESSURE
/FILNAM,CYLINDER
/CONFIG,NRES,10000

/PREP7
RO=8
RN=4
ET,1,42,,,1
MP,EX,1,30E6
MP,NUXY,1,0.3
!DEFINE A BILINEAR HARDENING PLASTICITY CURVE USING KINH
TB,KINH,1,1,2
TBPT,,0.001,30000
TBPT,,0.004,30090
!SET THE AXLES LABELS FOR THE STRESS-STAIN CURVE PLOT
/AXLAB,X,STRAIN
/AXLAB,Y,TRUE STRESS (PSI.)
TBPL,KINH,1

!MODELLING
K,1,RN
K,2,RO
K,3,RO,.4
K,4,RN,.4
A,1,2,3,4
ESIZE,.4
```

```
AMESH,ALL

/SOLU
D,ALL,UY,0
!NULL LOAD TO GIVE GRAPH STARTING AT ZERO
TIME,1E-6
LSWRIT
P_INT=60000
TIME,P_INT
KBC,0
DELTIM,5,1,20
AUTOTS,ON
PRED,ON
NSEL,S,LOC,X,RN
SFL,4,PRES,P_INT
SFL,3,PRES,-(P_INT*RN**2)/(RO**2-RN**2)
NSEL,ALL
LSWRIT
OUTRES,ALL,LAST
SOLVE

FINI
```

B.7 ANSYS Macros for J-Integral Calculation of Thick Walled Cylinders with Circumferential Flaw (Large Deformation)

```
/BATCH,LIST
/TITLE,2D AXISYMMETRIC CIRCUMFERENTIAL CRACKED SPECIMEN
!LARGE DEFORMATON NONLINEAR ANALYS
/FILNAM,CYLINDER
/CONFIG,NRES,10000

/PREP7
*SET,YM,30E6
*SET,NU,0.3
*SET,WT,4
*SET,RN,4
*SET,CK,2
*SET,HT,4
*SET,RO,(RN+WT)
ET,1,82,0,0,1
MP,EX,1,YM
MP,NUXY,1,NU
TB,KINH,1,1,2
TBPT,,0.001,30000
TBPT,,0.1,35940
/AXLAB,X,STRAIN
/AXLAB,Y,TRUE STRESS (PSI.)
TBPL,KINH,1
!MODELING
K,1,(RN+CK),0
K,2,RO,0
K,3,RO,HT
K,4,RN,HT
```

```
K,5,RN,0
L,1,2
L,2,3
LESIZE,2,,,8
L,3,4
LESIZE,3,,,6
L,4,5
LESIZE,4,,,10,0.2
L,5,1
ESIZE,,6
KSCON,1,0.15*CK,1,8
AL,1,2,3,4,5
AMESH,1
OUTPR,ALL
FINI

/SOLU
ANTYPE,0
NLGEOM,ON
NROPT,FULL,,OFF
OUTRES,ALL,ALL
NCNV,1,20
NSEL,S,LOC,X,0
NSEL,R,LOC,Y,0
D,ALL,UX,0
NSEL,ALL
DL,1,1,SYMM
NSEL,S,LOC,Y,HT
D,ALL,ROTX,0
D,ALL,ROTY,0
NSEL,ALL
```

```
*DO,I,0,20000,200
PI=100+1*I
SFL,3,PRES,-(PI*RN**2)/(RO**2-RN**2)
SFL,4,PRES,PI
SAVE
SOLVE
*ENDDO
FINI

/POST1
! J-INTE MACRO FILE TO CALCULATE THE J-INTEGRAL
ETABLE,ENER,SENE
ETABLE,VOL,VOLU
SEXP,W,ENER,VOL,1,-1
PATH,TEST,4
PPATH,1,71
PPATH,2,151
PPATH,3,127
PPATH,4,14
PDEF,W,ETAB,W
PCALC,INTG,J,W,YG
*GET,JA,PATH,0,LAST,J
PDEF,CLEAR
PVECT,NORM,NX,NY,NZ
PDEF,SX,S,X
PDEF,SY,S,Y
PDEF,SXY,S,XY
PCALC,MULT,TX1,SX,NX
PCALC,MULT,TX2,SXY,NY
PCALC,ADD,TX,TX1,TX2
PCALC,MULT,TY1,SXY,NX
```

```
PCALC,MULT,TY2,SY,NY
PCALC,ADD,TY,TY1,TY2
*GET,DX,PATH,0,LAST,S
DX=DX/100
PCALC,ADD,XG,XG,,,,-DX/2
PDEF,UX1,U,X
PDEF,UY1,U,Y
PCALC,ADD,XG,XG,,,,DX
PDEF,UX2,U,X
PDEF,UY2,U,Y
PCALC,ADD,XG,XG,,,,-DX/2
C=(1/DX)
PCALC,ADD,C1,UX2,UX1,C,-C
PCALC,ADD,C2,UY2,UY1,C,-C
PCALC,MULT,C1,TX,C1
PCALC,MULT,C2,TY,C2
PCALC,ADD,C1,C1,C2
PCALC,INTG,J,C1,S
*GET,JB,PATH,0,LAST,J
JINT=(2*(JA-JB))
PDEF,CLEAR

FINI
```

B.8 ANSYS Macros for J-Integral Calculation of Thick Walled Cylinders with Circumferential Flaw (Small Deformation)

```
/BATCH,LIST
/TITLE,2D AXISYMMETRIC CIRCUMFERENTIAL CRACKED SPECIMEN
!CIRCUMFERENTIAL FLAW NONLINEAR ANALYS – SMALL DEFORMATION
/FILNAM,CYLINDER
/CONFIG,NRES,10000

/PREP7
*SET,YM,30E6
*SET,NU,0.3
*SET,WT,4
*SET,RN,4
*SET,CK,2
*SET,HT,4
*SET,RO,(RN+WT)
ET,1,82,0,0,1
MP,EX,1,YM
MP,NUXY,1,NU
TB,KINH,1,1,2
TBPT,,0.001,30000
TBPT,,0.1,35940
/AXLAB,X,STRAIN
/AXLAB,Y,TRUE STRESS (PSI.)
TBPL,KINH,1
!MODELING
K,1,(RN+CK),0
K,2,RO,0
K,3,RO,HT
K,4,RN,HT
```

```
K,5,RN,0
L,1,2
L,2,3
LESIZE,2,,,8
L,3,4
LESIZE,3,,,6
L,4,5
LESIZE,4,,,10,0.2
L,5,1
ESIZE,,6
KSCON,1,0.15*CK,1,8
AL,1,2,3,4,5
AMESH,1
OUTPR,ALL
FINI

/SOLU
ANTYPE,0
NROPT,FULL,,OFF
OUTRES,ALL,ALL
NCNV,1,20
NSEL,S,LOC,X,0
NSEL,R,LOC,Y,0
D,ALL,UX,0
NSEL,ALL
DL,1,1,SYMM
NSEL,S,LOC,Y,HT
D,ALL,ROTX,0
D,ALL,ROTY,0
NSEL,ALL
*DO,I,0,20000,200
```

```
PI=100+1*I
SFL,3,PRES,-(PI*RN**2)/(RO**2-RN**2)
SFL,4,PRES,PI
SAVE
SOLVE
*ENDDO
FINI

/POST1
! J-INTE MACRO FILE TO CALCULATE THE J-INTEGRAL
ETABLE,ENER,SENE
ETABLE,VOL,VOLU
SEXP,W,ENER,VOL,1,-1
PATH,TEST,4
PPATH,1,71
PPATH,2,151
PPATH,3,127
PPATH,4,14
PDEF,W,ETAB,W
PCALC,INTG,J,W,YG
*GET,JA,PATH,0,LAST,J
PDEF,CLEAR
PVECT,NORM,NX,NY,NZ
PDEF,SX,S,X
PDEF,SY,S,Y
PDEF,SXY,S,XY
PCALC,MULT,TX1,SX,NX
PCALC,MULT,TX2,SXY,NY
PCALC,ADD,TX,TX1,TX2
PCALC,MULT,TY1,SXY,NX
PCALC,MULT,TY2,SY,NY
```

```
PCALC,ADD,TY,TY1,TY2
*GET,DX,PATH,0,LAST,S
DX=DX/100
PCALC,ADD,XG,XG,,,,-DX/2
PDEF,UX1,U,X
PDEF,UY1,U,Y
PCALC,ADD,XG,XG,,,,DX
PDEF,UX2,U,X
PDEF,UY2,U,Y
PCALC,ADD,XG,XG,,,,-DX/2
C=(1/DX)
PCALC,ADD,C1,UX2,UX1,C,-C
PCALC,ADD,C2,UY2,UY1,C,-C
PCALC,MULT,C1,TX,C1
PCALC,MULT,C2,TY,C2
PCALC,ADD,C1,C1,C2
PCALC,INTG,J,C1,S
*GET,JB,PATH,0,LAST,J
JINT=(2*(JA-JB))
PDEF,CLEAR

FINI
```